Cation-Mediated Interaction Between DNA and Anionic Lipid Surfaces: Experimental and Simulation Study

Germán Luque Caballero

Biocolloid and Fluid Physics Group

University of Granada

A PhD dissertation supervised by:

Alberto Martín Molina

Prof. titular de Física Aplicada

Julia Maldonado Valderrama

Investigadora Ramón y Cajal

Manuel Quesada Pérez

Prof. titular de Física

El doctorando Germán Luque Caballero y los directores de la tesis Alberto Martín Molina, Julia Maldonado Valderrama y Manuel Quesada Pérez garantizamos, al firmar esta tesis doctoral, que el trabajo ha sido realizado por el doctorando bajo la dirección de los directores de la tesis y hasta donde nuestro conocimiento alcanza, en la realización del trabajo, se han respetado los derechos de otros autores a ser citados, cuando se han utilizado sus resultados o publicaciones.

En Granada, a lunes 16 de junio de 2014

Director/es de la Tesis   Doctorando

Fdo.: Alberto Martín Molina   Fdo.: Germán Luque Caballero

Fdo.: Julia Maldonado Valderrama

Fdo: Manuel Quesada Pérez

CONTENTS

Abbreviations

AFM: Atomic force microscopy

BAM: Brewster angle microscopy

bp: Base pair

CG: Coarse grain

CHOL: Cholesterol

CHO-K1: Chinese hamster ovary-K1

CM: Center of mass

COG: Center of gravity

ctDNA: Calf thymus DNA

DCP: Dicetylphosphate

DDAB: Dimethyldioctadecylammonium bromide

DLPC: 1,2-dilauroyl-*sn*-glycero-3-phosphocholine

DMPC: 1,2-dimyristoyl-*sn*-glycero-3-phosphocholine

DMPE: 1,2-dimyristoylphosphatidylethanolamine

DMPS: 1,2-dimyristoyl-*sn*-glycero-3-phospho-L-serine

DNA: Deoxyribonucleic acid

DODAB: Dioctadecyldimethylammonium bromide

DOPC: 1,2-dioleoyl-*sn*-glycero-3-phosphocholine

DOPE: 1,2-dioleoyl-sn-glycero-3-phosphatidylethanolamine

DOPG: 1,2-dioleoyl-*sn*-glycero-3-phospho-(1'-*rac*-glycerol)

DOPS: 1,2-dioleoyl-*sn*-glycero-3-phospho-L-serine

DPPA: 1,2-dipalmitoyl-*sn*-glycero-3-phosphate

DPPC: 1,2-dipalmitoyl-*sn*-glycero-3-phosphocholine

DPPS: 1,2-dipalmitoyl-*sn*-glycero-3-phospho-L-serine

DPPG: 1,2-dipalmitoyl-*sn*-glycero-3-phospho-(1'-*rac*-glycerol)

DSC: Differential scanning calorimetry

DSPC: 1,2-distearoyl-*sn*-glycero-3-phosphocholine

dsDNA: Double stranded DNA

dsRNA: Double stranded RNA

EdBr: Ethidium bromide

EDTA: Ethylenediaminetetraacetic acid

EGTA: Ethyleneglycol-bis(β-aminoethyl)ether-N,N,N',N'-tetraacetic acid

EPM: External potential method

FENE: Finite extensible nonlinear elastic

HM: Heating method

HNC/MSA: Hypernetted-chain/mean-spherical-approximation

IRRA: Infrared reflection-absorption

IRRAS: Infrared reflection-absorption spectroscopy

LB: Langmuir-Blodgett

LC: Liquid condensed

L/D: total phospholipid-DNA base pair ratio

LE: Liquid expanded

LJ: Lennard Jones

M^{2+}: Metal divalent cation

M^{3+}: Metal trivalent cation

MX_3: [3:1] electrolyte

MC: Monte Carlo

MD: Molecular dynamics

MG: Malachite green

MLV: Multilamellar vesicles

N-C12-DOPE: N-dodecanoyldioleoylphosphatidylethanolamine

NLDFT: Nonlocal density functional theory

PA: Polyanion

PB: Poisson-Boltzmann

PC: Phosphatidylcholine

PCS: Photon correlation spectroscopy

PM-IRRAS: Pulse modulated-IRRAS

POPA: 1-palmitoyl-2-oleoyl-phosphatidyl-adenosine

POPC: 1-palmitoyl-2-oleoyl-sn-glycero-3-phosphocholine

POPU: 1-palmitoyl-2-oleoylphosphatidyl-uridine

PS: Phosphatidylserine

QCM-D: Dissipative quartz crystal microbalance

RNA: Ribonucleic acid

SAXS: Small angle x-ray scattering

SHG: Second harmonic generation

siRNA: Short interfering RNA

SOPS: 1-stearoyl-2-oleoyl-sn-glycero-3-phospho-L-serine

ssDNA: Single stranded DNA

ssRNA: Single stranded RNA

SUV: Small unilamellar vesicles

TBE: Tris-Borate-EDTA electrophoresis buffer (0.9 M Tris-Borate, 20 mM EDTA)

TEM: Transmission Electron Microscopy

tRNA: Transfer RNA

RMS: Root mean square roughness

SPM: Scanning probe microscopy

UV: Ultraviolet

VMD: Visual molecular dynamics

VSFG: Vibration sum frequency generation

Symbols

A: Area per molecule

A_{260}: Absorbance at λ = 260 nm

A_{280}: Absorbance at λ = 280 nm

c: MX_3 concentration

c_{DNA}: DNA concentration

d: LJ parameter of length

d_i: diameter of species i

e: elementary charge

F: Helmholtz free energy

F_{min}: F minimum

$|F_{min}|$: Absolute value of F_{min}

f: PA charge in -e units (number of charged beads per PA chain)

g_M: Counterion distribution function

g_X: Coion distribution function

I: Ionic strength

k_{bond}: elastic harmonic bond constant

k': FENE bond constant

L: simulation cell height (z-axis)

l: light path

N_A: Avogadro number

N_{ad}: Number of mean adsorbed monomers

N_{bead}: Number of monomers in the PA chain (polymerization degree)

P(z): Probability density to find the CM of the PA at a distance z

R: Reflectivity of the film−covered surface

R_0: Reflectivity of the bare subphase

R_i: radius of particle i

$R-A$: Reflectance–absorbance

$R_{G_{xy}}$: Radius of gyration projection onto the xy-plane

R_{G_z}: Radius of gyration projection in the z-axis

r: Center-to-center distance between a given pair of particles

r_0: Equilibrium bond length

$\vec{r}_i$: Position vector of particle i

r_c: LJ cut-off distance

r_{max}: FENE maximum bond distance

s: Standard deviation

T_m: Melting temperature (lipid phase transition)

u_{bond}: Bond potential for PA monomers

u_{elec}: Pairwise electrostatic potential

u_{HS}: Potential for hard spheres

W: Simulation cell width (x and y-axis)

$W(z)$: Window potential

Z_i: Valence of species i

ε_0: Gibbs elasticity

ϵ_0: Vacuum permittivity

ϵ_{260}: Molar extinction coefficient

ϵ_r: Relative permittivity

λ: Wavelength

λ_B: Bjerrum length

λ_D: Debye length

λ_{em}: Emission wavelength

λ_{ex}: Excitation wavelength

λ_L: Linear charge density

ν_{as}: Asymmetric stretching

ν_{as}: Symmetric stretching

Ξ: electrostatic coupling parameter

ξ: LJ energy parameter

π: Surface pressure

$\rho(z)$: Surface charge density at a distance z inside the simulation cell

σ_{int}: Integrated charge density

σ_0: Surface charge density

$|\sigma_0|$: Absolute value of σ_0

ψ_{ext}: External potential outside the simulation cell

ABSTRACT

The object of this survey is the interaction between polyanions and negatively charged membranes as mediated by multivalent cations. This phenomenon appears in the formation of anionic lipoplexes, which are mesoscopic assemblies formed from negatively charged liposomes and polynucleotides in the presence of multivalent cations. The interest in this sort of systems is due to its capability to transport genetic material inside the cell, allowing access to a therapeutic target at a molecular level. Their main advantage over other kinds of vectors used in gene therapy is that, since they are formed by lipids occurring in the cell membrane, their toxicity is much lower. The basic research we address in this project about the nature of the interactions involved in anionic lipoplexes is essential to understand the mechanisms underlying their formation, stability and function. Thus, in the present work we carry out a characterization of the membrane-cation-polyanion system through a combination of experimental and theoretical approaches.

The manuscript begins with an introduction where we summarize the state of the art of the biophysics of anionic lipoplexes. Firstly, we list the results about the structure and function of a variety of systems prepared in solution. Next, we introduce the study of complexation at the air-water interface as an experimental model to look into the influence of other factors such as lateral packing. Finally, we describe the application of theoretical models to predict the factors governing the formation and structure of this kind of complexes. Later on, we formulate the aims of this research project in agreement with the approaches mentioned in the introduction.

In the methodology section, we detail the experimental and

simulation protocols used. In particular, we have set up the Langmuir-Blodgett technique for film deposition and atomic force microscopy imaging of the structures at the interface, in our laboratory. We have performed infrared reflexion-absorption spectroscopy measurements during a short training stay in the Max Planck Institute for Colloids and Interfaces in Potsdam (Germany). We have also programmed the source code used in coarse grain simulations. We have carried out fluorescence spectroscopy measurements through a collaboration in the Physical Chemistry Department in the University of Granada.

Afterward, we thoroughly discuss the results obtained and the publications to which they have given rise are listed in the annex. We have organized result presentation from the strategy employed to study the complexation. First, we show the results obtained from the characterization of the interaction at the air-solution interface, visualizing the resulting structures and identifying the functional groups involved; then, we evaluate DNA encapsulation capability in solution and, in the end, we show the results concerning the theoretical study of the role of electrostatic interactions in complex formation and stability.

Finally, we enunciate the conclusions based on the results of this work. In this way, we have learned that interactions of different nature combine to form anionic lipoplexes. Especially, surface effects derived from the lateral packing modulate the morphology of the structures formed at the interface, while electrostatic interactions affect in a decisive way to complex stability. After assessment of the work done, we consider that, based on the knowledge gained in this research we begin

to understand the mechanisms involved in DNA/anionic lipid complexation. However,it is necessary to improve the approaches chosen here in combination with other strategies, in order to elucidate the group of interactions that take place in these complex systems. Only by understanding the fundamentals of formation, stability and function of anionic lipoplexes, we may be able to rationally design optimized formulations for a biomedical performance.

RESUMEN

El objeto de este estudio es la interacción entre polianiones y membranas cargadas negativamente mediada por cationes multivalentes. Este fenómeno se pone de manifiesto en la formación de lipoplejos aniónicos, que son agregados mesoscópicos formados a partir de liposomas con carga negativa y polinucleótidos en presencia de cationes multivalentes. El interés en este tipo de sistemas se debe a su capacidad para transportar material genético al interior celular, permitiendo el acceso a una diana terapéutica a nivel molecular. Su principal ventaja frente a otro tipo de vectores usados en terapia génica es que, al estar formados por lípidos presentes en la membrana celular, su toxicidad es mucho menor. La investigación básica que nos planteamos con este proyecto sobre la naturaleza de las interacciones presentes en los lipoplejos aniónicos es esencial para comprender los mecanismos responsables de su formación, estabilidad y función. Así, en el presente trabajo realizamos una caracterización del sistema membrana-catión-polianión combinando enfoques experimentales y teóricos.

El manuscrito comienza con una introducción donde se resume el estado del arte de la biofísica de lipoplejos aniónicos. En primer lugar, se recopilan los resultados relacionados con la estructura y función de una variedad de sistemas preparados en disolución. Seguidamente, presentamos el estudio de la complejación en la interfase aire-agua como un modelo experimental para indagar en la influencia de otros factores como el empaquetamiento lateral. Finalmente, describimos la aplicación de modelos teóricos para predecir los factores que gobiernan la formación y la estructura de este tipo de complejos. Más adelante,

planteamos los objetivos del proyecto de investigación de acuerdo a los enfoques mencionados en la introducción.

En la sección de metodología, detallamos los protocolos experimentales y de simulación empleados. En particular, la deposición de películas por el método de Langmuir-Blodgett y la visualización por microscopía de fuerzas atómicas de las estructuras presentes en la interfase se ha puesto a punto en nuestro laboratorio. Las medidas de espectroscopía de reflexión-absorción de infrarrojo se realizaron durante una estancia de formación en el Instituto Max Planck de Coloides e Interfases en Potsdam (Alemania). También se ha desarrollado el código fuente de los programas utilizados para llevar a cabo las simulaciones computacionales sobre modelos de grano grueso. Las medidas de espectroscopía de fluorescencia se realizaron a través de una colaboración en los laboratorios del Departamento de Química-Física de la Universidad de Granada.

A continuación, discutimos ampliamente los resultados obtenidos, y las publicaciones a las que han dado lugar se recogen en un anexo. La presentación de los resultados se organiza en función de la estrategia utilizada para estudiar la complejación. Primero, presentamos los resultados procedentes de la caracterización de la interacción en la interfase aire-disolución, visualizando las estructuras resultantes e identificando los grupos funcionales implicados; después, evaluamos la capacidad de encapsulamiento de ADN en disolución y por último, mostramos los resultados del estudio teórico sobre el papel de las interacciones electrostáticas en la formación y estabilidad de los

complejos.

Finalmente, enunciamos las conclusiones en función de los resultados del trabajo. Así, hemos demostrado que interacciones de distinta naturaleza concurren en la formación de los lipoplejos aniónicos. En particular, los efectos superficiales derivados del empaquetamiento lateral modulan la morfología de las estructuras que se forman en la interfase, mientras que las interacciones electrostáticas afectan de manera decisiva a la estabilidad de los complejos. Tras valorar el trabajo realizado, consideramos que a partir del conocimiento adquirido en esta investigación es necesaria una caracterización más amplia, profundizando en los enfoques escogidos en combinación con otras estrategias, permitiendo desentrañar el conjunto de interacciones que intervienen en estos sistemas complejos. La comprensión de aspectos básicos de la formación, estabilidad y función de los lipoplejos aniónicos será de gran ayuda para el diseño de fórmulas optimizadas para prestaciones biomédicas.

CHAPTER 1: INTRODUCTION

1.1. BACKGROUND. FROM CATIONIC TO ANIONIC LIPOPLEXES.

Lipoplexes are mesoscopic complexes generated from the spontaneous reaction of liposomes with nucleic acids (DNA or RNA). Their capability to encapsulate genetic material make them good candidates as non-viric gene delivery vectors. In fact, lipoplex characterization and development have been motivated by its application in gene therapy. Briefly, gene therapy consists in introducing genetic material in damaged cells (target cells) either to repair or replace damages in the cellular genome or to silence the expression of certain sequences and thus to treat many inherited or acquired human diseases. Implementation of this biomedical approach requires efficient and biocompatible vectors as gene vehicles for transfection (introduction of foreign genetic material inside the cell). Vectors derived from virus have shown high transfection rates, but they have shown problems as side-effects, immune response, limited capacity to transport DNA, recombination and high cost[16,46,52,53,72,162]. In order to overcome these drawbacks, alternative non-viric vectors are being synthesized and optimized.

Since the early 60s, the research aims to combine the DNA with chemical substances which are able to electrically neutralize, complexate and condensate the DNA[21,39,70,119]. Since the early 1980s, chemical transfection methods, based on liposome vectors (lipoplexes), emerge as an alternative to overcome the lack of efficiency found in the rest of chemical methods[40]. However, despite great progresses in

relation to the use of lipoplexes in gene therapy, the use of these gene vehicles is still in an early stage principally due to their low transfection capacity with regard to the viral vectors. Nonetheless, as predicted Danilo D. Lasic (1952-2000), pioneer of the application of liposomes in medicine, a good understanding of the physicochemical properties of the lipoplexes contributes significantly to the increase in their rates of transfection[70].

Depending on the electric charge sign of the liposomes used to complex the nucleic acid, we differentiate two different sorts of lipoplexes: i) cationic lipoplexes, prepared from the direct interaction between cationic liposomes and DNA; ii) anionic lipoplexes, in which the the interaction between negatively charged liposomes and DNA is mediated by multivalent cations. Both sorts of lipoplexes usually contain also helper zwitterionic lipids that dilute the surface charge density and improve transfection efficiency[60,137]. Concerning cationic lipoplexes, these complex the DNA giving rise to a great variety of structures where the cationic lipid bilayers appear as the polycations with the capability to compact the DNA and to form a supramolecular assembly with applications in gene delivery[64,117,127,137,142,163]. These complexes facilitate the transfection owing to the similarity between the cell membrane and the bilayer lipid membrane which yields endocytosis (process whereby cells absorb material from the outside). However, cationic liposomes induce a large number of adverse effects for DNA delivery. For instance, the use of cationic liposomes to deliver nucleic acids to cells is inappropriate due to the lack of efficiency in the transfection, the

instability of storage, the potential toxicity of the cationic lipid in a cellular environment, etc.[29,41,42,51,68,78,84,118] Cationic lipoplexes can be inactivated in the presence of serum and they are not likely to maintain their stability upon intravenous injection as a consequence of the presence of high concentrations of negatively charged plasma proteins and circulating blood cells[51,84]. Regarding the toxicity, experimental studies have shown that they cause cytotoxicity in both, *in-vitro* and *in-vivo*[29,41,42,68,78,118]. For instance, Filion and Philips studied cationic lipoplexes based on 1,2-diacyl-3-trimethylammonium propane or DDAB as cationic lipids in combination with the zwitterionic lipid DOPE as a helper lipid[41] (frequently used to form cationic lipoplexes[4,110,111,131]). In particular, these authors evaluated, among other things, the toxicity of different DOPE-cationic lipoplexes towards phagocytic macrophages and non-phagocytic T-lymphocytes. According to their results, this kind of cationic lipoplexes resulted extremely toxic. As a consequence, they claimed that alternatives to cationic liposomes for gene therapy should be considered in order to avoid dose-limiting and adverse effects[41,42]. With the same spirit, Patil *et al*. studied delivery of plasmid DNA in mammalian cell cultures using anionic lipoplexes formed by mixtures of DOPE and anionic DOPG lipids[118]. According to their results, toxicity of lipoplexes prepared from naturally occurring anionic and zwitterionic phospholipids revealed lower than the commercial cationic lipoplex Lipofectamine®. Later, Lv *et al*. reported a very complete review with respect to the toxicity of cationic lipids and polymers in gene delivery in which a relationship of toxicity and structure of diverse cationic compounds was

provided[78].

Recent investigations have revealed the complexation of anionic liposomes with DNA (anionic lipoplexes) as an alternative to classical cationic lipoplexes due to their lower cytotoxicity[44,60,61,74,99,100,104-107,109,118,120,140,141,145,167]. However, since both anionic lipids and DNA are negatively charged, cations are required as bridges between them. In this sense, monovalent cations are inappropriate due to their poor binding affinity with lipid headgroups[37]. Instead, multivalent metal cations, principally Ca^{2+}, have been employed to form anionic lipoplexes[44,60,61,65,104,105,109,118,120]. Precisely, this thesis is devoted to analyze in depth the experimental and computer simulation results concerning the complexation procedure of anionic lipoplexes as well as the interactions at the surface between anionic lipid monolayers and DNA mediated by cations. Given that, at some stage of the transfection process, the interfacial properties of these compounds are involved; their surface properties are of major importance for understanding the penetration (adsorption) mechanism of DNA and for identifying the conformational changes involved in the membrane. In this regard, Langmuir monolayers are a versatile and well established characterization method which allows elucidating structural and mechanical properties of lipid surfaces. Furthermore, Langmuir monolayers serve as substrate to complementary techniques such as SPM[108], BAM[90], fluorescence imaging[135,144], IRRAS[50], VSFG[144], SHG[62], etc. These allow visualization of the interfacial material and provide further structural details rendering Langmuir monolayers a very

attractive experimental method to study the interaction of DNA with lipids.

In addition, theoretical models and computer simulations related to the adsorption of DNA onto likely charged surfaces mediated by cations have been employed to elucidate the nature of the interactions responsible of anionic lipoplex formation and to predict its structure, as well. In particular, coarse grain (CG) models, in which several atoms are grouped together into effective interaction sites, appear as a satisfactory tool to study many phenomena that lie within the mesoscopic spatio-temporal scale. In a biological context, examples of such phenomena are protein–protein interactions, lipid–protein interactions, and membrane–membrane interactions[146]. In fact, CG models implemented by Monte Carlo (MC) simulations have been previously used to describe theoretically the physical properties of cationic and zwitterionic lipid–DNA complexes[34,35]. For the case of polyelectrolytes, Dias and Pais reported a complete review in which they discussed results from computer simulations based on CG polyion models applied to the conformation of polyanions (PAs) as well as their condensation in bulk, induced by multivalent ions and oppositely charged polycations. They also studied the PA condensation in responsive charged surfaces. However, the case of adsorption of such polyions onto likely charged surfaces mediated by multivalent cations was not reported[22].

Beyond the CG models, conventional all-atomic Molecular Dynamics (MD) simulation is a well-established technique in order to

simulate the structure and dynamics of soft matter in general, and of biomolecular systems in particular[136]. Approaches derived from CG models are correct in many situations but can become inaccurate for the so-called *last nanometer* phenomena[36]. These are interfacial processes with length scales of the order of the nanometer, whose description requires the inclusion of atomistic detail of the lipids. Examples of these phenomena are ion binding[38,87,88,160], membrane adhesion, the sequestering of lipids by other biomolecules[75] and membrane crystallization[122]. However, the high computational cost makes this simulation technique difficult to implement to the cation-mediated DNA adsorption onto phospholipid films. Faraudo and Martín-Molina have reported the first results in this field, showing the role of Ca^{2+} in mediating the interaction between a PS membrane and DNA[36]. Importantly, they describe a mechanism of the DNA adsorption based on amino groups exposition outer the membrane and their higher availability to form ion pairs with DNA phosphate groups, upon Ca^{2+} adsorption onto the PS membrane.

Alternatively to simulations, compaction of DNA by cationic liposomes has been also theoretically analyzed by a phenomenological theory put forward by Nguyen and Shklovskii[115]. This theory provides phase diagrams that contain information about the liposome and DNA concentration necessary to have either anionic or cationic isolated lipoplexes or also clusters of lipoplexes[111,117,131]. Unfortunately, quantitative predictions for chemical contributions (hydrogen bonding, solvation effects...) cannot be readily established from chemical

structure or physical property considerations. The only direct way to estimate the strength of these chemical contributions seems to be from the adsorption behavior at high salt concentrations, where the electrostatic contributions are gradually expected to become less important. Also, numerical calculations of the mean-field electrostatic free energy of a zwitterionic lipid monolayer–DNA complex support experimental observations where DNA adsorbs onto zwitterionic lipid monolayers in the presence of divalent cations[10,93].

To sum up, combination of different approaches is required to go in depth in the understanding of anionic lipoplexes. Research about the nature of the driving forces leading to anionic lipoplex formation and nucleic acid release upon cell uptake may allow designing valuable formulations from the biomedical point of view. This idea is schemed in fig. 1.1, where complementary methods such as *in vitro* assays (transfection efficiency, cytotoxicity); physicochemical measurements of anionic lipoplexes in solution (or in bulk); study of cation-mediated DNA binding to lipid films at interfaces and theory, including simulation techniques are combined to extend the biophysical characterization towards the formulation tuning in the anionic lipoplex preparation to achieve a successful biomedical performance.

In the next sections, we review the state of the art of biophysical characterization of anionic lipoplexes. We first discuss experimental evidence about anionic lipoplex formation in bulk and then, we review the current literature about phospholipid monolayer/M^{2+}/DNA complexation at the air-water interface. Later on, we deep into lipoplex models and simulation with both CG and all-atomic approaches.
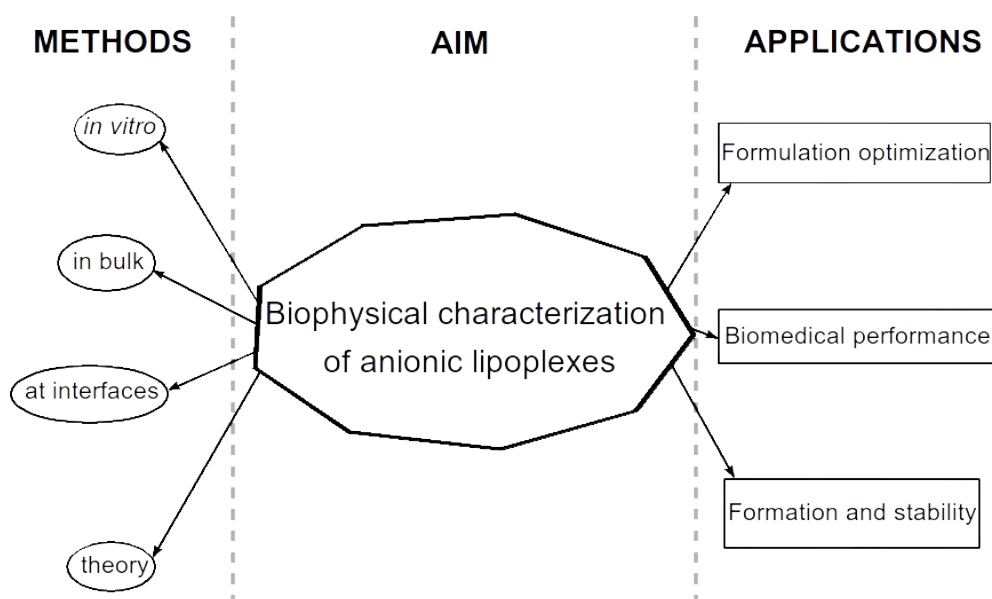

Figure 1.1. Mind map about different approaches to describe anionic lipoplex biophysical properties, creating basic knowledge to design adequate formulations for their biomedical performance.

1.2. EXPERIMENTAL EVIDENCE

1.2.1. Anionic lipoplexes. Formulation and transfection efficiency.

As mentioned above, anionic lipoplexes become an alternative to classical cationic lipoplexes due to their lower cytotoxicity. In this sense, the group of Prof. Mozafari pioneered the use of anionic lipoplexes since the early 90s (see references [103-109] and references cited therein). This group has specialized in the preparation and optimization of anionic lipoplexes reporting new strategies to incorporate polynucleotides to anionic liposomes by the mediation of divalent cations. For example, they have characterized the aggregation behavior of PC/DCP/CHOL SUV and MLV liposomes in the presence of both DNA and Ca^{2+} cations at the same time, deducing the formation of lipoplexes at Ca^{2+} concentrations higher than 10 mM[104,109]. In addition, Mozafari *et al*. have developed a scalable and safe method to prepare non-toxic anionic lipoplexes based on an original heating procedure so-called *Heating Method* (HM), in which no volatile organic solvent or detergent is used[107]. Therein, the authors indicated that HM-liposomes were completely non-toxic in human bronchial epithelial cells (16HBE14o-), whereas conventional liposomes prepared by the usual thin-film method revealed significant levels of toxicity[103,107]. They successfully used these lipoplexes to transfer plasmic DNA (pcDNA3.1/His B/lacZ) to this cell line[106]. Moreover, this group is skilled in the morphological characterization of the structure of the resulting complexes by diverse

techniques of microscopy, e.g. TEM micrographs of anionic lipoplexes revealed a fusogenic character of Ca^{2+}/DNA when added to DPPC/DCP/CHOL 7:2:1 liposomes (fig. 1.2)[106,108]. As a consequence, the investigation performed by this group has inspired other researchers in the use of anionic lipoplexes for applications in gene therapy and thus, the number of experimental studies has grown vertiginously in the last decade.
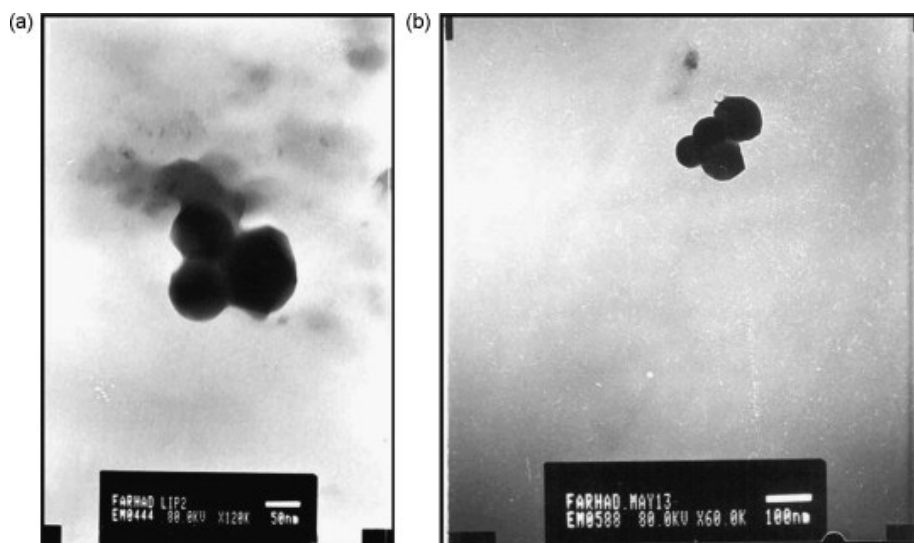
Figure 1.2. TEM micrographs of anionic lipoplexes. Three or four semi-fused vesicles are observed. Anionic liposomes were made of DPPC/DCP/CHOL in a 7:2:1 molar ratio; $CaCl_2$ was at 50 mM and plasmid DNA was added in a total lipid-DNA 7:1 mass ratio. Reprinted with permission from ref. [106]. Copyright (2007) Elsevier.

For instance, Patil *et al*. performed a biophysical characterization of DOPE/DOPG/Ca^{2+}/DNA lipoplexes[120]. They used electrokinetic techniques to demonstrate that Ca^{2+} interaction with plasmid DNA also induces restructuring of DNA that facilitates the transfection. Furthermore, they used circular dichroism and fluorescence

spectroscopy techniques to show how a plasmid DNA underwent a conformational transition due to compaction and condensation upon Ca^{2+}-mediated complexation with anionic liposomes. In addition, they proved that these structural changes were different to those found in cationic lipoplexes or in complexes Ca^{2+}/DNA. As a consequence they concluded that DNA cellular uptake, intracellular trafficking and transfection of anionic lipoplexes may involve different and more suitable pathways compared with other DNA delivery systems[120]. Patil *et al*. also carried out studies concerning DOPE/DOPG/Ca^{2+}/DNA anionic lipoplexes for plasmid DNA delivery into mammalian cells *in-vitro*[4,118]. The resulting transfection and toxicity assays were evaluated in CHO-K1 cells achieving an efficient delivery of plasmid DNA with anionic lipoplexes[118]. In this way, these authors demonstrated that biophysical characterization of anionic lipoplexes can be used to identify formulation conditions and electrochemical properties for achieving optimal transfections[120]. Afterward, this idea was followed by Srinivasan and Burgess, who also used DOPE/DOPG liposomes to study the role of Na^+, Mg^{2+} and Ca^{2+} at different lipid-DNA ratios to transfer plasmid DNA in CHO-K1 cells[145]. Hence, they carried out a biophysical characterization of the resulting lipoplexes by using techniques of particle size (DLS), zeta potential, gel electrophoresis and TEM to optimize the formulation for these anionic lipoplexes. As a result, they obtained 78 % transfection efficiency and 93 % cell viability for the optimized system: DOPE/DOPG 4:1 (mol/mol); 15-20 mM Ca^{2+}; and 15-20 µg total phospholipid for complexation with 0.8 µg plasmid DNA.

Interestingly, the authors demonstrated that the transfection efficiency of anionic lipoplexes is similar or higher than with cationic lipoplexes but the cellular toxicity was substantially smaller when anionic liposomes were used[145].

More recently, Kapoor *et al*., using DOPE/DOPG liposomes again, have demonstrated that physicochemical attributes of anionic lipoplexes can be used to estimate *in-vitro* activity of anionic lipid-based ternary siRNA complexes and understand their morphology correlating the lipoplex assemblies with biological activity[60]. They determined the amount of siRNA complexated within anionic lipoplexes by analyzing the amount of siRNA released upon EDTA treatment; additionally, they calculated the amount of siRNA encapsulated inside anionic lipoplexes from the difference between the siRNA released upon treatment with TX-100 surfactant and EDTA (encapsulated + complexated) and with EDTA (complexated). Based on their experimental characterization, they proposed a model representing the lipid/siRNA association within the anionic lipoplexes as a function of the anionic lipid/siRNA charge ratio that proves the existence of a synergistic role of lipids and Ca^{2+} in associating with siRNA to form anionic lipoplexes. At low anionic lipid/siRNA ratios, the whole siRNA loading of anionic lipoplexes is due to Ca^{2+}-complexation. In contrast, at high anionic lipid/siRNA ratios, Ca^{2+} primarily contributes to siRNA complexation whereas DOPE lipids contribute to siRNA encapsulation. From measurements of the biological activity of DOPG/DOPE/Ca^{2+}/siRNA in terms of silencing efficiency in breast cancer cells (MDA-MB-231), the authors deduced that it was

complexation and not encapsulation what favored silencing efficiency. Finally, the formulation was optimized at the anionic lipid/Ca^{2+}/siRNA charge ratio of 1.3/2.5/1, showing a maximum silencing efficiency owing to the high siRNA loading and the retention of the loaded siRNA in the presence of serum[60]. The excess of Ca^{2+} in the optimized formulation highlights the role of the cation in the biological performance of anionic lipoplexes.

With the aim of further understanding the structural aspects of anionic lipoplexes, Liang *et al*. investigated the structure and interactions of anionic lipoplexes in the presence of different divalent metal cations such as Mg^{2+}, Ca^{2+}, Co^{2+}, Cd^{2+}, Mn^{2+} and Zn^{2+} by performing SAXS experiments and confocal microscopy[74]. According to them, anionic lipoplexes self-assemble into a lamellar structure at low charge densities of the lipid membrane (fig. 1.3A). This lamellar assembly consisted of alternating layers of like-charged DNA and anionic membranes bound together with divalent cations. As the membrane charge density increased, they observed how the DNA was expelled from the complex and a sandwich-like structure resulted among lipid membrane sheets and divalent cations (fig. 1.3B). This transition between the two structures was also induced by increasing the concentration of divalent cations. Moreover, the system forms an inverted hexagonal phase comprised of a hexagonal array of divalent cation-coated DNA strands wrapped by anionic lipid monolayers (fig. 1.3C). In addition, it was reported that divalent cations (especially Zn^{2+}) could also coordinate nonelectrostatically with lipid molecules and

modify the resulting structure[74]. Later, Khiati *et al*. performed also SAXS studies of novel anionic nucleotide based lipids for DNA delivery and expression[61]. According to them, the structure of the complexes is strongly dependent on the formulation being the transfection enhanced by inverted hexagonal structures. In cooperation with the structural aspects of anionic lipoplexes, the equilibrium constants for the binary complexes Ca^{2+}-lipid, Ca^{2+}-DNA and DNA-lipid provide the basis for the electrotransfer of gene-DNA into biological cells and tissue[44].
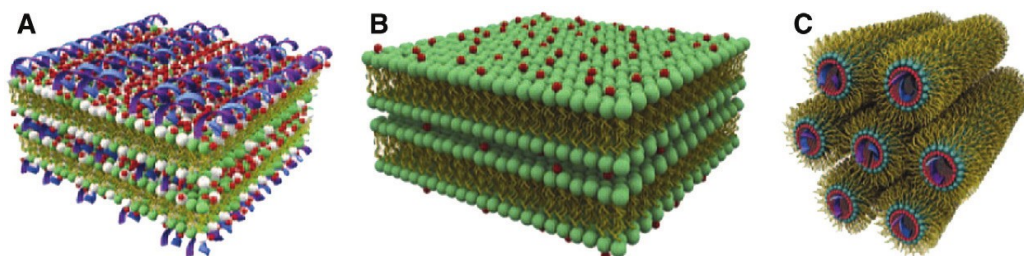

Figure 1.3. Schematic pictures of self-organized structures of anionic lipoplexes mediated by divalent cations. (A) Condensed DNA–ion–membrane lamellar structure with alternating layers of DNA and anionic membranes glued together by divalent cations. (B) Condensed ion–membrane lamellar structure in which charged membranes stacks are held together by divalent cations. (C) 2D inverted hexagonal structure in which hexagonal arrays of divalent cations coated DNA strands wrapped in the anionic membrane monolayer tubes. Lipoplex model with DNA wrapped into phospholipid inverted micelles. Reprinted with permission from ref. [74]. Copyright (2005) National Academy of Sciences, U.S.A.

Concerning the interaction between lipids and nucleic acids, Michanek *et al*. studied the interaction of tRNA or DNA with zwitterionic and anionic phospholipids by means of DSC and QCM-D[97]. Therein the authors showed that the length of the nucleic acids is one of the crucial factors in determining how association influences the lipid phase behavior of DMPC/DMPS liposomes, and lipid demixing was observed for the shorter nucleic acids. In addition, the interaction was weak,

reversible and invariant to the presence of 2 mM Ca^{2+}. In view of these results, the authors suggested a nonelectrostatic origin in the tRNA/bilayer interaction, presumably due to the interaction between the unpaired bases in tRNA with the hydrophobic part of the membrane. Additionally, Suga et al characterized the interaction of ssRNA with POPC/CHOL liposomes in the absence of multivalent cations, showing the complexation of ssRNA onto the liposome surface and mostly preserving its conformation[148].

In summary, experimental pieces of evidence of diverse anionic lipoplexes prove that the transfection efficiency of anionic complexes is similar or higher than that of cationic lipoplexes but the cellular toxicity is proved to be significantly lower when anionic liposomes are used. The transfection efficiency of anionic lipoplexes depends on the optimal formulation of the complexes, which is a function, in turn, of the structure of the lipid-cation-DNA ternary system as well as the lipid-cation, cation-DNA and DNA-lipid binding. These experimental facts are summarized in table 1.

Lipids	Lipid assemblies	Cations	Type of DNA-based Therapeutic	Ref.
N-C12-DOPE/DOPC (70:30)	Liposomes	spermine^{4+}	plasmid DNA pZeoLacZ	[140]
DCP:PC:CHOL (2:7:1)	MLV	Ca^{2+}	genomic DNA from wheat seedlings	[104,109]
DCP/PC/CHOL (2:7:1)	MLV	Ca^{2+}	plasmid DNA pCMV-GFP	[103]
DCP/PC/CHOL (2:7:1)	MLV	Ca^{2+}	plasmid DNA pcDNA3.1/His B/lacZ	[106]
DOPG/DOPE (17:83)	MLV	Ca^{2+}	plasmid DNA pCMV-GFP	[118,120]
DOPG/DOPE (1:1-1:9)	MLV	Ca^{2+}, Mg^{2+}, Na^+	plasmid DNA pEGFP-N3	[145]
DOPG/DOPE (variable)	ULV	Ca^{2+}	siRNA	[60]
DOPG/DOPC (variable)	MLV	Mg^{2+}, Ca^{2+}, Co^{2+}, Cd^{2+}, Mn^{2+}, Zn^{2+}	λ-phage DNA calf timus DNA	[74]
DOPG/DOPE (variable) DPPA/DOPE (variable)	ULV	Ca^{2+}	plasmid DNA pEGFP	[61]
PS/POPC (1:2)	ULV	Ca^{2+}	calf timus DNA	[44]
POPA	Bilayers	-	polynucleotide acid (polyU)	[99]
POPA, POPU, POPG	MLV, ULV	-	polynucleotide acids (polyA, polyU)	[100]
DMPS/DMPC (1:2)	ULV	Na^+, Ca^{2+}	tRNA and ssDNA	[97]

Table 1. Summary of experimental systems based on anionic lipoplexes. Reprinted with permission from ref. [85]. Copyright (2014) Elsevier.

1.2.2. Cation-mediated DNA adsorption onto anionic lipid films. The role of lateral packing.

The objective of investigating the interaction of DNA with anionic lipids by Langmuir monolayers is to enlighten the mechanism of formation of anionic lipoplexes as related to its transfection efficiency exposed above (table 1). In order to address this issue effectively, separate investigations into the nature of the interactions between the various components involved in the complexation (DNA, lipid molecules and cations) should be accomplished. As it has been discussed, anionic lipids require multivalent cations to mediate attractions to negatively-charged DNA through direct electrostatic *bridging* interactions. But also, multivalent cations can coordinate non-electrostatically with lipid molecules and modify its structure and mechanical properties. Hence, it is important to start investigating the physics governing the effect of cations on the properties of anionic monolayers in order to address later the interaction of DNA with anionic lipid monolayers and achieve a coherent understanding of the resulting structures. Lipid monolayers at the air-water interface hence allow studying these interactions by looking into the modification of the area per lipid molecule and hence the compression state and molecular packing of the monolayer.

One of the first works dealing with anionic lipid monolayers was done back in the 80's by Ohki and Düzgünes[116] who use an original experimental approach which mimics the process of membrane fusion

by looking into the adsorption of liposomes onto a monolayer comprised of the same lipids. These authors evaluated the surface tension of the system (PC and PS) as the liposomes penetrate into the monolayer as a function of concentration and type of the divalent cations present in the subphase (Ca^{2+}, Mg^{2+} and Mn^{2+}), thus examining the mechanism of the ion-induced membrane fusion in model membrane systems. As a result, the liposomes penetrate significantly into the monolayer only in the presence of a critical concentration of cations in the subphase and this mechanism is similar for both zwitterionic (PC) and anionic (PS) lipids. According to Ohki and Düzgünes, the interaction of divalent cations with the phospholipid polar group causes a water exclusion effect from the membrane resulting in an increased hydrophobicity of the cation-lipid complex. This is an important piece of work suggesting, for the first time, that the interaction between divalent cations and anionic lipid monolayers cannot be regarded as purely electrostatics but affects decisively the surface properties of the system. In fact, more recently it has been shown that the presence of Ca^{2+} or Mg^{2+} induces very different aggregation behavior for PS liposomes as characterized by their fractal dimensions[133,134]. This ion-lipid specific interaction, has also been intensely studied by MD simulations for the case of Ca^{2+}, Mg^{2+} and La^{3+} cations interacting with PS lipid bilayers[87,88].

Recently, Sovago *et al*. authored a very interesting contribution addressing specifically the interaction of Ca^{2+} with anionic lipid DOPS and zwitterionic lipid DPPC by means of Langmuir monolayers in combination with VSFG. This work emphasizes the role of the surface

pressure on the calcium-induced changes of the lipid monolayer. Namely, Ca^{2+} induces the formation of lipid domains at low surface pressure (<5 mN/m), induces disorder at intermediate surface pressures (5-25 mN/m) and expands and simultaneously orders the lipid chains at the highest surface pressures (> 25 mN/m)[144]. Interestingly, the authors also report qualitatively similar effects on anionic and zwitterionic lipids. Hence, this work confirms the importance of solvent interactions in the systems envisaged by Ohki and Düzgünes[116].

The influence of the surface pressure on the interaction of cations with anionic lipids has been also reported for an organic cation (MG) and anionic DPPG monolayers[62]. Kim *et al*. show again distinct types of adsorption of MG depending on the initial phase of the monolayer. Combination with SHG, fluorescence microscopy and X-ray reflectivity illustrates the orientation of MG in each phase: vertical penetration into the DPPG monolayer at a fluid phase; vertically but oppositely paired orientations at a more condensed phase and parallel adsorption at the interface near the lipid headgroup region at a highly packed condensed phase.

More recently Ross *et al*. visualized the calcium induced domains in mixed DPPC/DPPS 4:1 Langmuir-Blodgett (LB) monolayers[135]. By means of a combination of imaging techniques, the authors demonstrate that these lipids are miscible in the absence of Ca^{2+} while they form DPPS rich domains upon addition of Ca^{2+} (fig. 1.4). This study concentrates on low-intermediate surface pressure values and

concludes that the presence of Ca^{2+} triggers phase separation of the monolayer[135]. In addition, the presence of Ca^{2+} was reported to alter the morphology of the domains in a DPPC/DOPS bilayer[129].
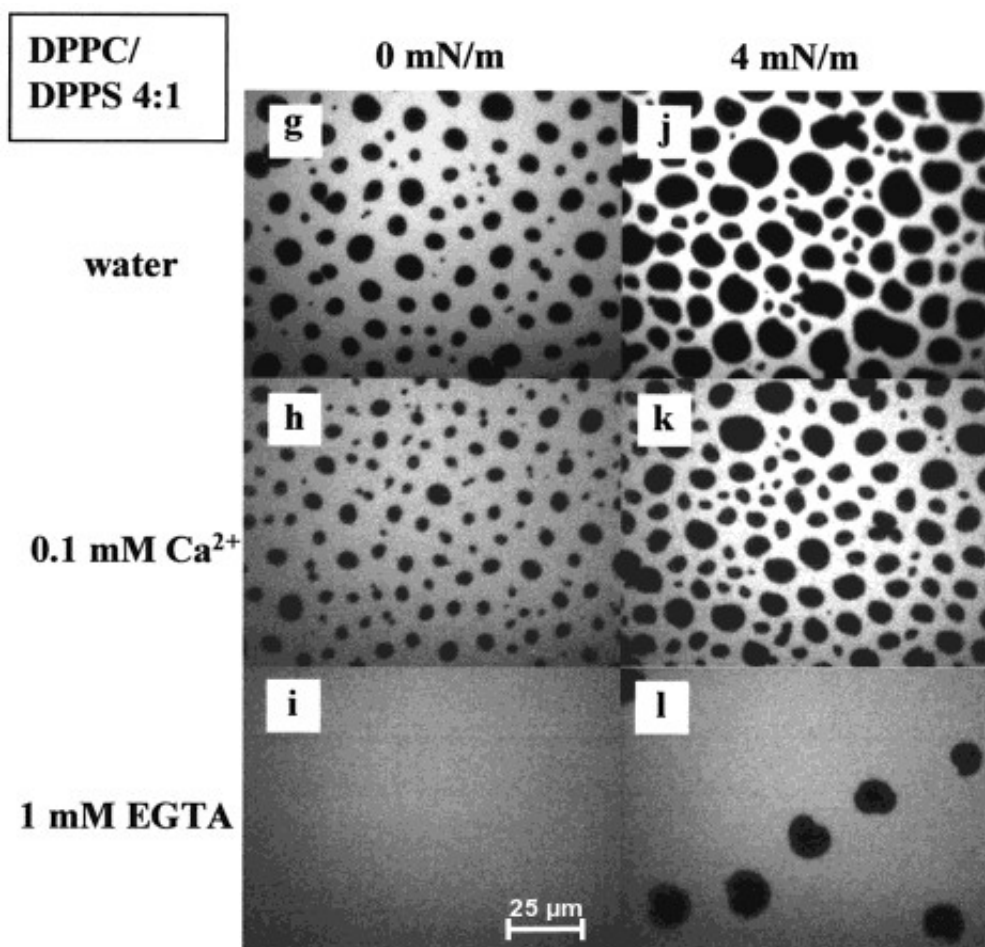
Figure 1.4. Fluorescence imaging of DPPC/DPPS 4:1 monolayers at low compression on different subphases. Formation of LC domains was observed on water or 0.1 mM Ca^{2+}, while only one phase was appreciated in the presence of the chelating agent EGTA. C promotes lipid demixing and formation of LC domains. Reprinted with permission from ref. [135]. Copyright (2001) American Chemical Society.

Hence, the analysis of the studies published so far concerning the

effect of cations on anionic lipid monolayers allows establishing some details of the possible scenario for the complexation. Apart from the electrostatics, the presence of cations affects crucially the hydrophobicity of the system, the molecular packing and the phase behavior of the monolayer. However, experimental investigations remain to be done in order to fully elucidate the role of the structural position of the anionic group in the lipid molecule and the role of the molecular packing of the lipid in the monolayer in the interaction of lipid with cations and the induced morphological changes in the lipid surface. Yet, the surface pressure seems to play a vital role in the cation-lipid interactions allowing tuning the molecular packing on the monolayer.

Concerning the interaction of DNA with lipids, since these are electrically repelled, the attraction needs to be mediated by multivalent cations, and this is the reason why the physical state of the lipid-cation monolayer has been established first. Nevertheless, none of the works has shown so far how to apply these findings to then allocate DNA in the system. There is indeed very little work dealing with the interaction between DNA and anionic monolayers and the research in this direction remains in a very early stage.

Langmuir monolayers in combination with other experimental techniques have been used to characterize the lipid-DNA interaction in order to understand and improve cationic and zwitterionic lipoplexes[2,19,25,80,90]. Interestingly, and in the line of the previous speculations, Gromelski *et al*. reported that the interaction with DNA is

not only mediated by cations but also depends on the surface pressure of the lipid monolayer[50]. These authors showed that the DNA partially penetrates into the DMPE monolayer only at low surface pressures and in the presence of Ca^{2+} but is squeezed out at higher surface pressures even in the presence of Ca^{2+}. This again demonstrates the importance of the physical state of the lipid monolayer for establishing the conditions which favor the complexation of DNA with the lipid. The presence of Ca^{2+} is not enough to trigger the complexation but also the molecular packing (i.e. surface tension) needs to be considered.

Concerning the interaction in zwitterionic monolayer/M^{2+}/DNA, McLoughlin *et al*. characterized the M^{2+}-mediated DNA binding onto DPPC and DSPC monolayers at the air-water interface[90]. They described the formation of a DSPC/M^{2+}/ctDNA interfacial complex in terms of a π-A isotherm shift to higher molecular areas and an increase in the surface potential. The effect was ion-specific, being greater in the case of Ca^{2+} than Mg^{2+} and Ba^{2+}. In addition, BAM observations of DPPC/Ca^{2+}/ctDNA revealed elongated Liquid Condensed (LC) domains (fig. 1.5), pointing out a decrease in line tension. In addition, Michanek *et al*. extended the characterization with QCM-D measurements on zwitterionic lipid bilayers. They observed tRNA adsorption onto both fluid liquid-crystalline phase DOPC and solid gel phase DPPC bilayers, being this adsorption weak and reversible. Interestingly, the magnitude of the adsorption did not changed in the presence of Ca^{2+} (although the concentration was not specified), but it was higher with the unsaturated DOPC bilayer than the saturated DPPC bilayer, highlighting the role of

lateral packing in the adsorption. Regarding the interaction in the absence of multivalent cations, the authors also characterized the ssRNA binding to DPPC monolayers at the air-water interface[98]. Interestingly, the association took place only at low surface pressures. Neutron reflectometry measurements explained this finding because of the interaction of the ssRNA unpaired bases with the exposed hydrophobic chains in the Liquid Expanded (LE) phase. Accordingly, no interaction was observed between DPPC monolayers and dsRNA or dsDNA in the absence of multivalent cations. In addition, only ssRNA transformed LE-LC domain morphology, forming fractal-like interconnected structures.

One of the few works showing specifically adsorption of DNA onto anionic lipid monolayers is the work done by Frantescu *et al*. with PS/POPC 1:2[44]. These authors report an increase of the area per lipid in the presence of DNA+Ca^{2+} in the subphase (fig. 1.6). In this way, the authors provide evidence of the binding of DNA to anionic lipids mediated by Ca^{2+}. Interestingly, in contrast to DMPE monolayers[50], the DNA complexation with PS/POPC 1:2 mediated by Ca^{2+} remains regardless of the surface coverage of the monolayer. Whereas DNA is expelled in DMPE monolayer at high surface pressures, for PS/POPC the lipid remains in a liquid-expanded state during all the compression. Hence, an important conclusion arising from these studies is that unsaturated chain phospholipids which reach the collapse directly from liquid-expanded phase never reach enough condensation to squeeze out the DNA in the presence of Ca^{2+}.
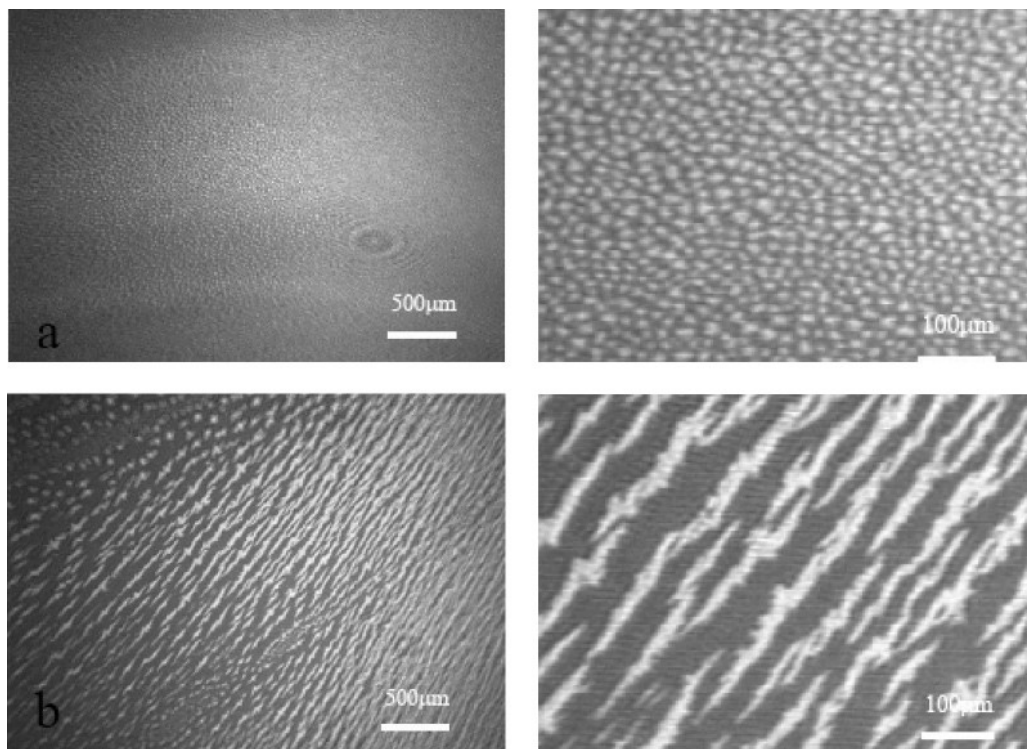
Figure 1.5. BAM images of DPPC monolayers on a) 5 mM $CaCl_2$ and b) 5 mM $CaCl_2$ + 0.1 mg/ml ctDNA. Molecular area was fixed at 60 Å^2. Formation of DPPC/Ca^{2+}/DNA ternary complexes resulted in an elongation of LC domains. Reprinted with permission from ref. [90]. Copyright (2005) American Chemical Society.

Moreover, LB transfer of these films provides a solid support for applying SPM Tools[82]. Once again, this technique has been applied for imaging positively charged amphiphile monolayers at the air-DNA solution interface[1,14,15]. Much less studied is the case of anionic monolayers with the exception of Dubrovin *et al.* who reported that polyadenylic acid (polyA) interfacial adsorption on stearic acid monolayers, with negative surface charge density, took place in the presence of Na^+ or Mg^{2+} cations[30]. They use LB-AFM technique to monitor the increase in the number of polyA fibers attached to the

stearic acid monolayer as a function of increasing concentrations of NaCl. Since they observed no polyA adsorption in the presence of both 1 M NaCl and the chelating agent EDTA at the concentration of 10 mM, they concluded that the divalent cations, which are present as minor components in the monovalent salts, were essential to bridge the interaction between the stearic acid monolayer and the polyA[30].
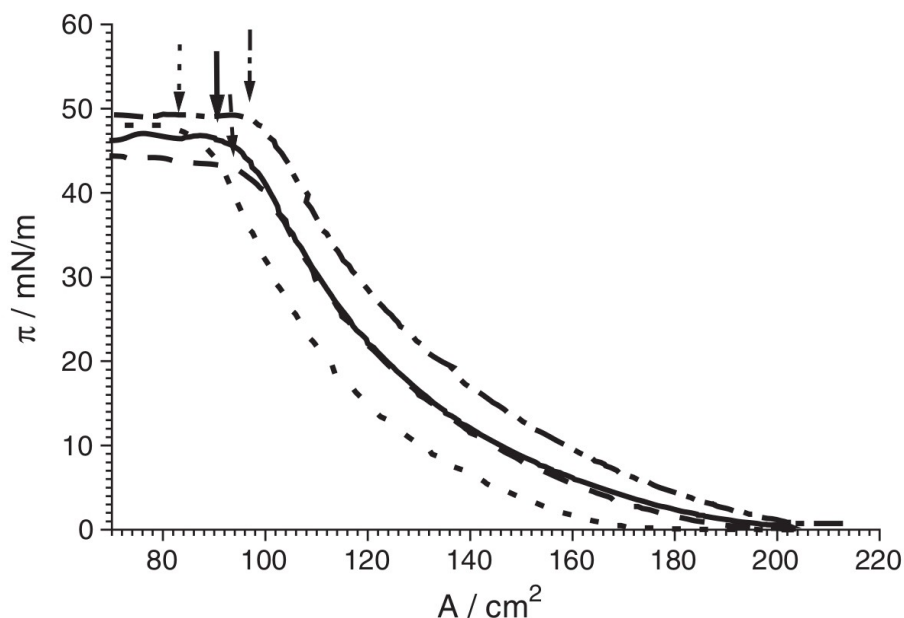
Figure 1.6. π-A isotherms of POPC/PS 1:2 (mol/mol) monolayers on different subphases: pure water (—); 0.5 mM Ca^{2+} (– –); 1 mM Ca^{2+} (- -) and 35 µM (bp) ctDNA + 1 mM Ca^{2+} (— -). A shift to higher molecular areas was observed when both Ca^{2+} and DNA were present in the subphase at the same time, pointing out the formation of POPC/PS 1:2/Ca^{2+}/DNA complexes at the air-water interface. Reprinted with permission from ref. [44]. Copyright (2006) Elsevier.

Results published so far importantly highlight the different interactions occurring in zwitterionic and anionic monolayers and we are beginning to understand how they influence the complexation with DNA

mediated by Ca^{2+}. Experimental works with Langmuir monolayers demonstrate the importance of cations in mediating the interaction between anionic lipids and DNA but also reveal the role of the nature of lipid and molecular packing as quantified by surface tension. The adsorption of DNA appears more stable for anionic systems but further investigation into this mechanism still needs to be undertaken in order to fully provide a clear explanation of the interactions taking place and validate this as a universal trend. To achieve this it seems crucial to combine it with more sophisticated techniques in order to unequivocally interpret the results. Furthermore, work on bilayers and numerical simulations (as those reviewed in next sections) need to be considered in order to realize the mechanism of nucleic acid transfer by liposome-DNA complexes.

In the present work, we extend the interfacial characterization of the phospholipid/Ca^{2+}/DNA complex. Two different anionic model monolayers have been employed in the characterization. On the one hand, we chose the DPPC/DPPS 4:1 system as a model of saturated monolayer to monitor the complexation and its effect in the phase transitions through π-A isotherms, which show the effect of molecular packing; Gibbs elasticity, following the evolution of the interfacial response to compression and LB-AFM imaging of the structures formed upon complexation. On the other hand, we have studied the role of the functional groups involved in the complexation from IRRAS measurements of unsaturated DOPC/DOPS 1:1 monolayers. These results will be discussed in detail in section 4.1.

1.3. MODELING AND SIMULATIONS

Before analyzing the mechanism underlying the formation of anionic lipoplexes, modeling the zwitterionic monolayer/M^{2+}/DNA system is essential to understand the role of divalent metal cations in its interactions with zwitterionic lipids and DNA. The formulation of a general theory about the DNA adsorption onto zwitterionic monolayers in the presence of divalent cations would be helpful to correlate such results, determine the driving force and the conditions that favor the formation of the monolayer/M^{2+}/DNA complexes and describe their structural features. In this sense, Mengistu *et al*. have developed a theoretical approach based on the classical Poisson-Boltzmann (PB) formalism to look into the role of divalent cations in the formation of a monolayer/M^{2+}/DNA complex[93]. To this aim, they represented the DNA with charged rods. The zwitterionic headgroups in the monolayer were modeled as electric dipoles. The dipole movement was limited by two constraints: *i)* The negative charge was fixed on the interface plane; *ii)* the distance between the positive and negative charges was constant (fig. 1.7). They calculated the increment in the free energy associated with the adsorption of the DNA rod onto the zwitterionic monolayer, showing that this magnitude decreased with increasing concentrations of either monovalent or divalent cations, and being more sensitive to the divalent ones. Hence, the addition of divalent cations made the DNA binding on the zwitterionic monolayer more stable. Moreover, the adsorption process took place with redistribution of divalent cations from

the DNA to the anionic moieties in the lipid headgroups. Consequently, the formation of the monolayer/M^{2+}/DNA complex seems to be governed by the electrostatic interactions. This model was recently extended to account for the change in the surface pressure induced by the M^{2+}-mediated DNA adsorption on the zwitterionic monolayer[10]. In this case, the authors focused on the second order tilt transition, which is observed experimentally at lower surface pressures when both M^{2+} and DNA are present in the subphase[50]. This downshift in the tilt transition surface pressure was qualitatively predicted by the model, indicating that the DNA-induced M^{2+} penetration into the headgroup region resulted in a lateral condensation in the monolayer. Although this theory explains satisfactorily the M^{2+}-mediated DNA adsorption onto zwitterionic monolayers, the implications of the introduction of an excess of negatively charged moieties in the monolayer have not been analyzed yet.
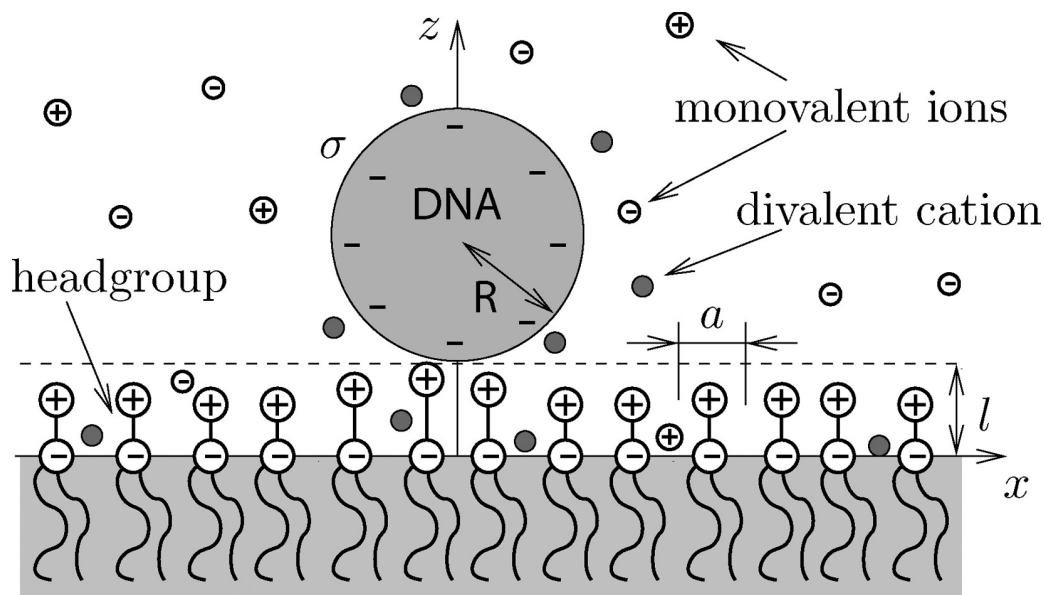
Figure 1.7. Model of DNA interacting with a zwitterionic monolayer. Zwitterionic headgroups are represented with electric dipoles in which the negative charge is fixed on the interface plane and the positive charge can freely pivot as long as the dipole length is kept constant. A homogeneously negatively charged rod stands for DNA. In addition, monovalent ions and divalent cations are considered. Adsorption free energy was more favorable in the presence of divalent cations. Reprinted with permission from ref. [93]. Copyright (2009) American Chemical Society.

The interactions of DNA with a negatively charged surface are not intuitive and have been therefore less studied. Waltkins *et al*. modeled ssDNA tethered to a hydroxylalkane-coated gold substrate, which is negatively charged in aqueous media[161]. To determine both the DNA conformation and the adsorption on the surface at different salt concentrations, they balanced the contributions to the folding free energy due to electrostatic interactions and excluded volume effects as well, concluding that the surface attachment stabilized the folded state respect to the unfolded state at high ionic strengths. In addition, the work of Waltkins *et al*. demonstrates that the presence of cations can

govern the DNA interfacial adsorption on negatively charged surfaces. In any case, the systematic search for the conditions in which metal cation mediated DNA binding to anionic monolayers can be appropriately addressed with simulation methods. The advantage of this approach is the possibility to test a wide range of cases by varying parameters such as the surface charge density, the length and geometry of the DNA and the valence and concentration of the metal cations. In addition, simulations can easily account for ionic correlations neglected by classical approaches (such as the PB theory).

The accuracy of a certain simulation to predict the mechanism of the DNA adsorption to a charged plane and the structural features of the monolayer/M^{2+}/DNA complex depends strongly on the model chosen for each of the different components of this system and the interactions applied among them. Accordingly, two well-differentiated sorts of models can be used: CG models, which imply a simplification of the charged objects involved (polyelectrolyte, surface and ions), and all atomistic models, which take into account the interaction among all the atoms in the system, including water molecules. The former is ideal to explore a vast range of conditions in a reasonable time and the latter offers us better precision, structural and conformational information and the effect of the solvent too, but the computational cost is much higher. Although both models provide valuable information, we cannot forget that they are approximations that could not reproduce reality perfectly. On one hand, a large number of effects derived from the molecular nature of the solvent and macromolecules are not included in CG models. On the

other hand, all-atomic models consider all the atoms present in the relevant chemical species and include also their bonds, however chemical reactions, titration, electron transfer and in general processes which require a quantum description are typically ignored. At this point, it is important to remark also that both procedures consider model systems for the charged interface which are far from the complexity of a real cell membrane. For instance, homogeneous membranes composed only by phospholipids are considered in all-atomic models whereas real membranes have also several types of proteins and also protein channels. Accordingly many of the phenomena that take place in the cell membrane cannot be properly studied by using the cited models. In addition, effects derived from a global curvature of the mono/bi-layer have not specifically studied in the present work. Undoubtedly this feature is an interesting subject with important implications since the elastic bending constants of lipid assemblies determine a variety of membrane-associated physical and functional properties such as the membrane vesicle shape, the structure and formation of interlamellar attachments and non-lamellar lipid phases, and may also play an important role in membrane fusion[83].

Once the models are proposed, a suitable methodology to solve them is required. One possibility is to use approximate theories or to employ simulation techniques which are, in principle, exact[45]. According with the literature reviewed, both MC and MD simulations are employed to solve the CG models, while MD is usually preferred in simulations on all-atomic models. Hypothesis and approximations associated to each

simulation method are described in the next sections. In particular, we first describe the basis and performance of some CG models below whereas the all atomistic simulations are treated in the next section.

1.3.1. Coarse grain models. The role of electrostatic interactions.

In many cases, CG models consist in a bead-spring representation where hard charged spheres are used to build the system to be simulated. For instance, the salt ions are represented by spheres with the same electric charge and the equivalent radius. The electrostatic interactions are usually computed by using a Coulomb potential:

$$u_{elec}(r_{ij}) = \frac{q_i q_j}{4\pi\epsilon_0\epsilon_r r}, \qquad r \geq R_i + R_j \tag{1}$$

where q_i and q_j are the electric charges of the particles i and j respectively, R_i and R_j are their radius, r is the distance between them, ϵ_0 is the vacuum electric permittivity and ϵ_r the relative electric permittivity of the solution. Usually, eq. 1 is expressed as:

$$u_{elec}(r_{ij}) = \frac{Z_i Z_j k_B T \lambda_B}{r}, \qquad r \geq R_i + R_j \tag{2}$$

where Z_i and Z_j are valences of the particles i and j respectively, k_B is the Boltzmann constant, T is the absolute temperature and λ_B is the Bjerrum length, which is defined as the distance between two monovalent particles at which the pairwise electrostatic potential is equal to the thermal energy ($k_B T$):

$$\lambda_B = \frac{e^2}{4\pi\epsilon_0\epsilon_r k_B T} \tag{3}$$

where e is the elemental charge.

Ions are allowed to move freely throughout the simulation cell, and excluded volume effects are usually introduced with either a hard sphere term or a LJ term (particularly when derivatives of the interaction energy are required):

$$u_{HS}(r) = \begin{cases} \infty & r \leq R_i + R_j \\ 0 & r > R_i + R_j \end{cases} \tag{4}$$

$$u_{LJ}(r) = \begin{cases} 4\xi\left[\left(\dfrac{d}{r}\right)^{12} - \left(\dfrac{d}{r}\right)^{6} + \dfrac{1}{4}\right] & r \leq r_c \\ 0 & r > r_c \end{cases} \tag{5}$$

where ξ is the depth of the potential well, $d = R_i + R_j$. The LJ potential is cut-off at $r_c = 2^{1/6}d$ yielding a purely repulsive interaction. Potentials described with eqs. (9), (2), (4) and (5) are not only applicable to the salt ions, but to all sorts of beads present in the system.

Negative net charge is also present in one of the faces of the simulation cell to mimic the headgroup side of the lipid monolayer. The simplest representation consists of a plane with uniform surface charge density, but when features such as corrugation, discrete charges and the presence of both negatively and positively charged groups on the interface need to be taken into account, then the surface charge can be introduced with charged beads embedded in the wall[11]. The sign of the

charge of each embedded bead can be positive or negative but the number of the latter must be greater than the former to ensure the plane has a negative net charge. In addition, these embedded beads can be fixed or they move along the plane to model the effect of the lateral diffusion.

The last item of the model to be described is the DNA. In a CG representation, its structure is usually simplified as a flexible chain of negatively charged beads. The diameter and the equilibrium separation distance between two adjacent beads in the DNA string slightly depend on the sort of interaction that is defined to keep the string cohesion. According to the literature reviewed, two different sorts of bond potentials can be applied. On the one hand, the elastic harmonic bond potential connects each pair of adjacent beads by a spring[22-24]:

$$u_{bond}(r) = \frac{1}{2} k_{bond}(r - r_0)^2 \qquad (6)$$

where k_{bond} is the bond constant and r_0 is the equilibrium distance between the two adjacent beads. k_{bond} and r_0 can be adjusted to match the DNA bond properties.

On the other hand, when the DNA polyelectrolyte is described as a sequence of beads connected with nonlinear springs, a finite extensible nonlinear elastic potential (FENE) is applied[20]:

$$u_{FENE}(r) = -\frac{1}{2} k' r_0^2 \ln\left(1 - \frac{r^2}{r_{max}^2}\right) \qquad (7)$$

where k' is the bond constant and r_{max} is the maximum bond distance. k' and r_{max} can be adjusted to match the DNA bond properties.

Similarly, the flexibility properties of the DNA are modulated by an angular potential:

$$u_{ang}(\alpha) = \frac{1}{2} k_{ang} (\alpha - \alpha_0)^2 \tag{8}$$

where k_{ang} is the bending constant, α is the angle formed by three adjacent beads and α_0 is the equilibrium angle. Again, k_{ang} and α_{eq} can be adjusted to match the DNA bending properties.

Dias *et al*. applied the CG model to search for the conditions that lead to a negatively charged polyelectrolyte to condensate under different geometries[22]. They run MC simulations to separately study, on the one hand, the PA condensation by metal cations in bulk and, on the other hand, the binding on a charged surface without any added salt. Although these cases cannot represent the formation of the anionic monolayer/M^{2+}/DNA, they should be considered as important precedents because the simulation methods and the factors governing condensation described in their works may inspire future computational research on the anionic monolayer/M^{2+}/DNA system. This is the reason why we would like to review the most remarkable findings reported by these authors about the effect of lateral diffusion and the PA geometry on the adsorption on a charged surface.

Lateral diffusion in lipid monolayers that contain both positively

and negatively charged headgroups make them to behave as responsive surfaces, since they undergo a reorganization of the surface charge to accommodate the PA. In fact, mobile charged bead embedded surfaces adsorb a higher number of monomers from both flexible and semiflexible polyanions than fixed ones independently on the surface net charge (fig. 1.8)[24]. This finding suggests that the membrane fluidity could be essential for the mechanisms of formation of lipoplexes and transfection efficiency. In addition, the same authors reported recently differences in interfacial adsorption due to circular or linear polyanions[23]; the former adsorbed more strongly on both fluid and frozen interfaces with respect to the latter. This effect was stronger for PA binding onto weakly and positively charged surfaces. However, when the fluid surfaces lacked of net charge the circular PA totally desorbed while the linear one retained a certain degree of adsorption. This difference between the simulation results observed for linear and circular polyanions points out that, when electrostatic interactions are low enough, the PA-responsive surface interaction is governed by a delicate balance between the entropy of the surface groups and that of the PA.

It should be mentioned, however, that the surveys about adsorption on responsive surfaces published by Dias *et al*. were carried out exclusively in the presence of monovalent counterions. In addition, they only considered the minimum number of counterions required for electroneutrality. For simulations about anionic lipoplexes, however, it would be desirable to account for the presence of multivalent cations and anions.

Similar bead-spring models have also been applied to study the DNA properties in solution with MD simulations[20,28,57,147,168] and some variations have been proposed to address the problem with different geometries. Since lipoplexes are bulk systems formed as a result of the interaction of DNA with liposomes, which are spherical colloids, models of charged curved surfaces are likely to be helpful in lipoplex modeling. This challenge has been tackled by Carnal *et al*.[12] They have run MC simulations with one negatively charged polyelectrolyte condensing on a positively charged spherical nanoparticle. They were able to determine the influence of parameters affecting the adsorption, such as the surface charge density of the nanoparticle, the valence of the salt and the pH, but nanoparticles with negative net charge were not considered. This work could be applicable to the cationic lipoplex early stage formation modeling and could be modified to study the anionic liposome/M^{2+}/DNA interaction.
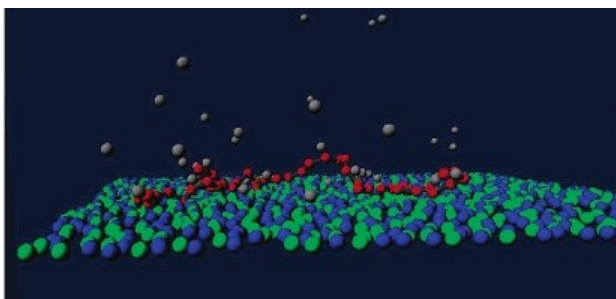

Figure 1.8. CG model of a polyanion (red) interacting with a responsive surface composed of positive (green) and negative groups (blue) with lateral diffusion inside the plane. Monovalent counterions are added to ensure electroneutrality (grey). Reprinted with permission from ref. [24]. Copyright (2005) American Chemical Society.

CG approaches can be formulated to predict the structure of lipoplexes. For instance, Farago *et al.* proved that CG models can

capture the self-assembly of cationic lipid-DNA complexes[34,35]. In fact, they found excellent agreement with x-ray diffraction experimental data for the dependence of the spacing between DNA chains on the cationic lipid concentration. At high charge densities, they observed that the increasing electrostatic pressure exerted on the membranes leads to pore opening, through which the DNA may be released from the complex. Also, zwitterionic phospholipid/M^{2+}/DNA self-assembly has been observed *in silico* at different length scales. On the one hand, at short range, Tresset *et al*. performed MC simulations to gain insight into the effect of different cations in the formation of lipoplexes from zwitterionic phospholipids[151,152]. In this case, a homogeneously charged rod represented DNA, while phospholipid molecules were modeled with three beads: two of them lacked of electric charge and represented the hydrophobic tail and the other one held an electric dipolar moment and represented the zwitterionic headgroup. At equilibrium, the phospholipid molecules formed inverted micelles, being the multivalent cations placed in the space between the DNA rod and the phospholipid headgroups, as has been experimentally measured by SAXS. On the other hand, more recently, the same author proposed these inverted micelles as building blocks to simulate the structure of the assemblies at the supramolecular level[153,154]. In this manner, such inverted micelles are now modeled as semiflexible tubes interacting with one another through electrostatic interactions, hydrophobic force and excluded-volume repulsion. As a result, the tubes formed clusters whose morphology depended on size and rigidity of the tube. In solution, the cluster should be wrapped into a

lipid monolayer as shown in fig. 1.9, because the polar headgroup contact with the water molecules should be more favorable. To sum up, different simulation methods based on CG models comprise a powerful tool to deduce the structural properties of lipoplexes. However, the effect of anionic lipids alone or in combination with zwitterionic ones is still to be elucidated.
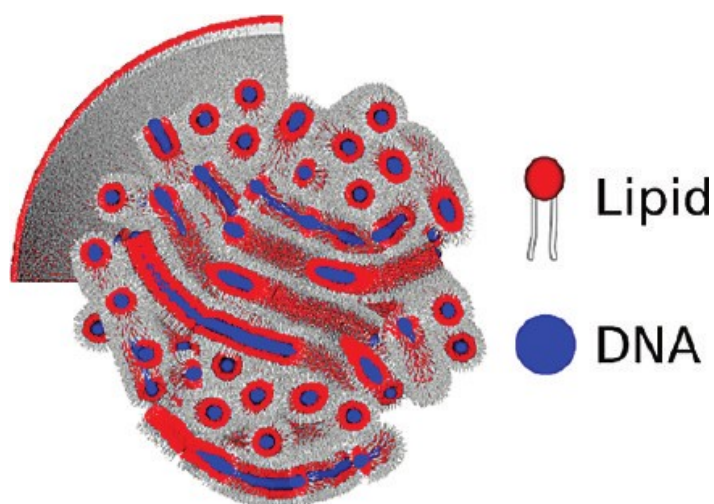

Figure 1.9. Lipoplex model with DNA wrapped into phospholipid inverted micelles. Reprinted with permission from ref. [153]. Copyright (2011) American Chemical Society.

In fact, only a few CG simulations have explicitly studied a related problem: the complexation of polyanions with like-charged surfaces in the presence of multivalent cations. Messina *et al.,* were pioneers in the field of the complexation between a negatively charged sphere and a long flexible PA in the presence of multivalent counterions but in a salt-free environment[95,96]. These authors considered different coupling regimes as well as the influence of the linear charge density (λ_L) of the PA chain by using MD simulations within the framework of a CG model.

To this end, they used the original definition of the *electrostatic coupling parameter* (Ξ) which uniquely describes different physical regimes that may be found for counterions of charge *q* at a planar charged wall with a surface charge density σ[114]. This parameter can be calculated as:

$$\Xi = 2\pi q^3 \lambda_B^2 \sigma \tag{9}$$

Under a strong Coulomb coupling regime (Ξ >> 1), structural ion correlations can lead to dominant attractive forces of mainly energetic origin between like-charged surfaces[112]. According to the findings obtained by Messina *et al.,* two important conclusions arise: on the one hand, the PA chain is always adsorbed as a flat structure under strong Coulomb coupling regime, and its conformation strongly depends on λ_L. On the other hand, upon reducing λ_L the chain tends to spread more and more over the particle surface. For typical electrostatic couplings of aqueous solution (Ξ < 1), complexation can be obtained with multivalent counterions for high enough values of λ_L, where the formation of loops was reported[94-96]. Jimenez-Ángeles *et al.* considered a simple model to study the attraction between two like-charged parallel rods immersed in an electrolyte solution[58]. Later Wang *et al.* used a nonlocal density functional theory (NLDFT) to conclude that the PA adsorption onto a like-charged plane requires the presence of salt containing multivalent counterions, being such attraction influenced by the surface charge density, the counterion valence and the salt concentration (fig. 1.10)[158].
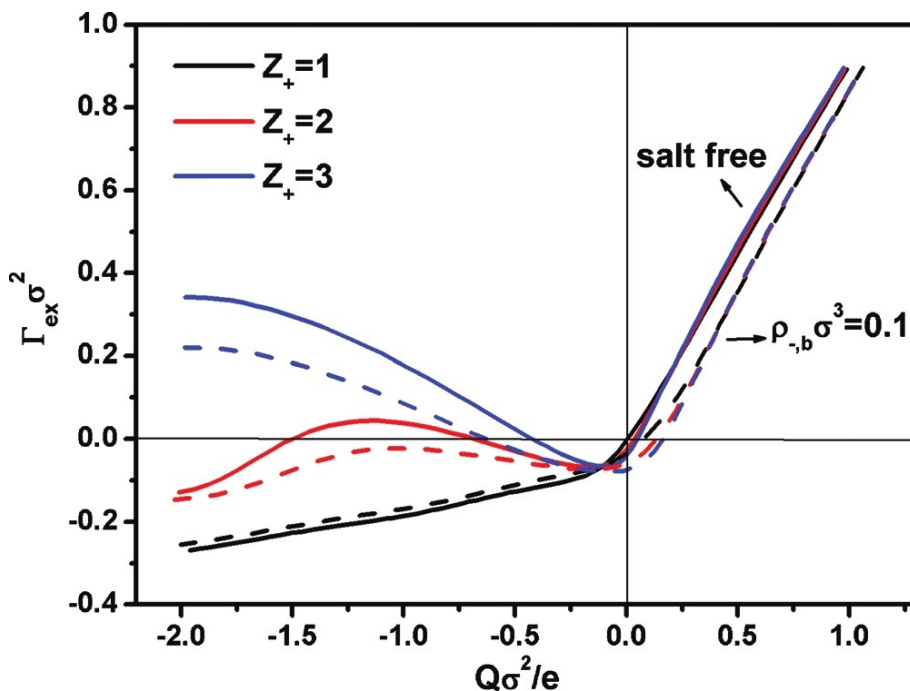
Figure 1.10. Surface excess of PA monomers as a function of surface charge density in the presence of monovalent (black), divalent (red) and trivalent (blue) cations in salt free conditions (solid lines) or with an excess of salt concentration (dashed lines), predicted by NLDFT theory. According to theoretical calculations, multivalent cations mediate PA adsorption onto like-charged surfaces. Reprinted with permission from ref. [158]. Copyright (2010) AIP Publishing LLC.

Furthermore, short-range specific interactions (solvent mediated, hydrogen bonding) and electrostatic correlations are not independent phenomena in the adsorption of polyanions onto like-charged surfaces. Rather, they are correlated and one effect reinforces the other[36,85]. Unfortunately, specific interactions are not always straightforwardly considered within the theoretical models and the interaction potential is frequently written into different and additive contributions of the different forces. For instance, Turesson *et al.* used a CG model to perform MC simulations to investigate the calcium-mediated PA adsorption onto a

like-charged surface[155]. Therein, surface charge was uniformly smeared on a plane. The authors concluded that a purely electrostatic adsorption is achieved but can be considerably increased if ion pairing effects between calcium and carboxylate monomers are taken into account. In line with these authors, a similar type of nonelectrostatic potential is considered by Jorge *et al.* in their study of DNA-PEI-Fe^{3+} complexes by using MC simulations as well[59]. Therein, this interaction energy is justified in terms of the specific chelation of Fe^{3+} by the PEI.

Concerning the M^{3+}-mediated PA adsorption onto like charged surfaces, we have implemented a MC simulation method within a CG model. We have extended the previous works characterizing the intensity of the adsorption in terms of Helmholtz free energy and we have also analyzed the role of the PA and surface charge, the concentration of salt containing trivalent cations and the M^{3+} diameter. These results will be discussed in detail in section 4.4.

1.3.2. All-atomic molecular-dynamics simulations. Mechanism of phospholipid/M^{2+}/DNA complex formation.

As was previously pointed out, the standard view of the interaction of electrolyte with interfaces is based on a simplified picture of the interface as a simple geometrical boundary with uniform charge (typically a charged plane)[33]. This standard view can be implemented for example by considering the PB classical theory of double layer electrostatics, usually employed not only for colloids but in general for

soft-matter systems and biomolecules. As long as the limitations of the PB theory became clear, more sophisticated theoretical approaches focused on the refinement of the description of the ions (ion size, polarizability,…) but retained an extremely simplified description of the interface as a boundary condition. In the case of complex systems such as lipids membranes, interactions are highly specific, i.e. depend strongly on the particular lipids and ions involved. Hence, at this scale, the hydration behavior of ions plays a major role, even for multivalent cations[38,87,88], in which interface-ion interaction was supposed to be mainly electrostatic. For example, experimental evidence (from turbidity measurements and other techniques) shows that similar divalent cations such as Ca^{2+} and Mg^{2+} induce different structural changes in phospholipid membranes and different membrane solvation, which in turn has substantial consequences in the interaction between membranes and their aggregation behavior[88,116,133,134]. Experimentally, it is also known that the binding of multivalent cations to negatively charged lipids is endothermic, and thus it is entropy driven[71,143]. This fact strongly suggests the existence of hydration effects as well as structural rearrangements in the membrane as the driving forces for ion binding, effects which cannot be captured by CG models.

The question is how to study theoretically all this complexity, relevant at the last nanometer scale near a lipid assembly. The continuous increase in computer power and the development of new algorithms for large-scale MD simulations has made possible its use as a kind of computational microscope to study molecular systems and

processes with atomic resolution. The development of force fields for lipids has allowed large scale atomistic simulations of lipid assemblies and their interactions with unprecedented resolution. Conceptually, the MD method is based on a classical description of the motion of atoms and molecules. Therefore, numerical solutions of the equations of movement are employed to display the motion of the molecular system[121]:

$$m_i \ddot{\vec{r}}_i = -\frac{\partial}{\partial \vec{r}_i} U_{total}\left(\vec{r}_1, \vec{r}_2, \ldots, \vec{r}_n\right) \qquad (10)$$

where, m_i, $\vec{r}_i$ and $\ddot{\vec{r}}_i$ are the mass, the position vector and the accelaration vector of the atom i and U_{total} is the total potential of the system:

$$U_{total} = U_{bond} + U_{angle} + U_{dihedral} + U_{VDW} + U_{Coulomb} \qquad (11)$$

where U_{bond}, U_{angle} and $U_{dihedral}$ are the summation of stretching, bending and torsion potentials of each molecule; U_{VDW} is the summation of Van der Waals intermolecular interaction between non-bonded atoms and $U_{Coulomb}$ is the electrostatic potential between charged atoms. A more detailed description of these potentials in MD simulations is given in ref. [121].

The information provided by all-atomic MD simulations is useful to predict the behavior and properties of matter from their molecular composition[33]. As an essential input, the MD technique requires a molecular model of the individual entities building up the system (all

atoms and bonds making up the molecules and a prescription for calculating atom-atom interactions). As an output, MD simulations provide equilibrium and transport properties of the system. More importantly, MD simulations give a detailed account of the different molecular contributions to the properties of the system and allow one to identify the molecular origin of the observed behavior. Of course, as any approach to a difficult problem, these simulations have their own difficulties. MD simulations of realistic models of lipid systems (with accurate atomic resolution) are far from easy. Also, the need for simulating large numbers of water molecules (in order to describe both interfacial phenomena but also bulk water and electrolyte) leads to the requirement of large amounts of computational power, which typically require the use of supercomputing facilities. In any case, MD results offer us many important insights which should be considered and incorporated in more general theories.

As it has been mentioned along the manuscript, the formation of anionic lipoplexes is achieved by the creation of a ternary complex between DNA and anionic liposomes using multivalent ion bridges. This feature has been shown in the extensive experimental evidence cited above as well as in the simulations on CG models presented in the previous section. However, the problem is still to be addressed from MD simulations with atomic resolution. Its capability to describe hydration effects as well as phospholipid restructuring in the bilayer upon multivalent cation adsorption[87,88] make this approach ideal to search for the nature of interactions beyond electrostatics responsible of anionic

lipoplex formation and stability. Before discussing the results concerning all-atomic description of anionic lipoplexes, some technical considerations as well as recent studies should be taken into account.

The DNA molecule is a strongly charged PA; with a typical charge of one electron every 0.17 nm of its length[48]. This large negative charge plays a major role in many biological and technological processes. For example, adhesion and desorption of DNA onto solid surfaces can be controlled by tuning the charge of the surface[32]. In these experiments, large adhesion forces are obtained in the case of a positive electrode, and the adhesive force over DNA is completely suppressed by turning the charge of the electrode to negative. Interestingly, the addition of low concentrations of Mg^{2+} cations (which are well known as condensing agents of DNA[48]) does not induce adhesion of DNA onto a negatively charged surface.

The interaction of DNA with lipid membranes presents a much higher complexity, due to the self-assembled nature of lipid bilayers. Obviously, negatively charged DNA easily associates strongly with cationic lipids[4,64,110,111,117,127,131,137,142,163]. As we have discussed in a previous section, the case of negatively charged membranes containing anionic lipids is more interesting not only for its fundamental interest, but also due to its potential interest for biocompatible DNA delivery systems for gene therapy. Diverse experimental pieces of evidence shown in section 1.2. suggested that the presence of anionic lipids, nucleic acids and multivalent cations do not assure the formation of anionic

lipoplexes, because these are complex systems in which multiple factors interact such as the nature of components, the concentration of cations, etc. Moreover, divalent cations are unable to invert the charge of a PS bilayer under reasonable concentrations (below the critical coagulation concentration) although they adsorb on PS membranes[88]. In other words, the PS membrane will remain with a net negative charge in the presence of cations. In any case, the binding of divalent cations onto PS membranes induces substantial conformational changes in the membrane and a complex (and highly inhomogeneous) charge distribution at the membrane surface, with positive patches coming from adsorbed cations and cationic amino groups also present in the anionic PS lipids. Amino groups are also known to interact strongly with DNA through ionic hydrogen bonds[32]. It is suggestive to think that these positive patches may act as putative binding sites for DNA in a negatively charged membrane.
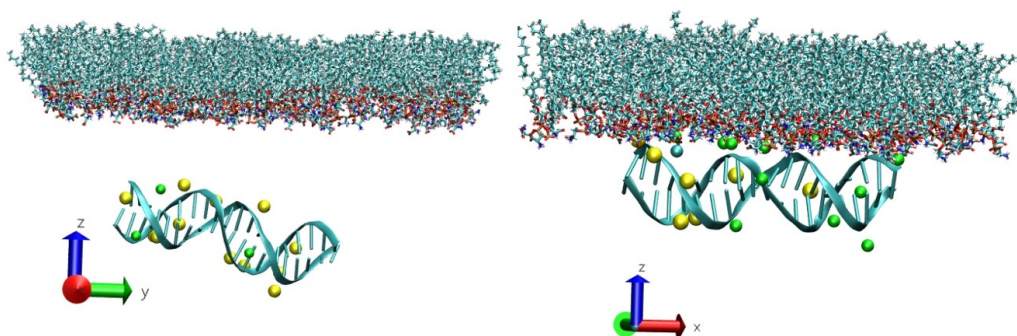
Figure 1.11. Snapshots of MD simulations of DNA and PS lipid interaction at two different simulation times. Left and right images correspond to labels (a) and (b) indicated in Fig. 7. Lipid molecules are shown as bonds (colours correspond to standard crystallographic conventions). DNA strands are shown schematically and cations close to DNA are shown as spheres with Van der Waals radius (green corresponds to Ca^{2+} and yellow to Na^+). Case (b) is slightly rotated (as compared with (a)) in order to show more clearly the bonds between lipids and DNA. Figure made with VMD[54]. Reprinted with permission from ref. [85]. Copyright (2014) Elsevier.

This possibility has been confirmed by recent MD simulations performed by Jordi Faraudo[36,85]. In these simulations, binding of a DNA molecule onto a pure PS monolayer is observed by hydrogen bonding between the phosphate groups of DNA and the amino groups of PS (see figs. 1.11 and 1.12). In addition, a small fragment of a DNA molecule is placed far from the PS monolayer (1.6 nm), in a solution containing low concentrations of $CaCl_2$. Na^+ counterions were added to balance the charge of DNA and Ca^{2+} counterions to balance the charge of the PS membrane. The PS monolayer has a strong negative charge of 1.15 e/nm². However this charge density is almost neutralized by adsorption of Ca^{2+}, which has a strong affinity to the surface as discussed in the previous section. The charge of DNA is also renormalized by adsorption of cations. Hence, the strong electrostatic repulsion between these two

negatively charged objects is greatly reduced due to both adsorption of cations and the efficient screening by divalent salt. In the simulations, the DNA molecule initially diffuses far from the surface, as seen during the first 15 ns of simulation in fig 1.12. However, the low repulsive barrier between the DNA (with its adsorbed counterions) and the PS membrane (also with adsorbed Ca^{2+}) can be surpassed by simple diffusive crossing, as seen in the jump between 15 and 20 ns in fig. 1.12. Once the DNA molecule is close to the surface, the DNA molecule approaches and patches onto the membrane containing positive charges (from lipid amino groups $-NH_3^+$ and adsorbed counterions) exposed to the solution. The atomistic detail given by the simulations reveals two different kinds of bonds between PS lipids and DNA molecules. In some of the bonds, Ca^{2+} cations participate as a bridge, linking a DNA phosphate with an acidic group of PS. However, the most frequent bond is a direct bond between the positively charged amino group of a PS lipid and a negatively charged phosphate of the DNA. In this case, also a Ca^{2+} is involved, but in this case indirectly. The PS lipids participating in these bonds have Ca^{2+} cations adsorbed at their negatively charged phosphate or carboxylic groups. Recall that, according to the results discussed in the previous section, PS lipids alter their conformations in the presence of divalent cations. In this new configuration, the positively charged amino groups (which interact strongly with DNA) become more exposed to the aqueous solution. In other words, adsorption of divalent cations by the membrane induces a structural change which makes possible the direct PS-DNA association.
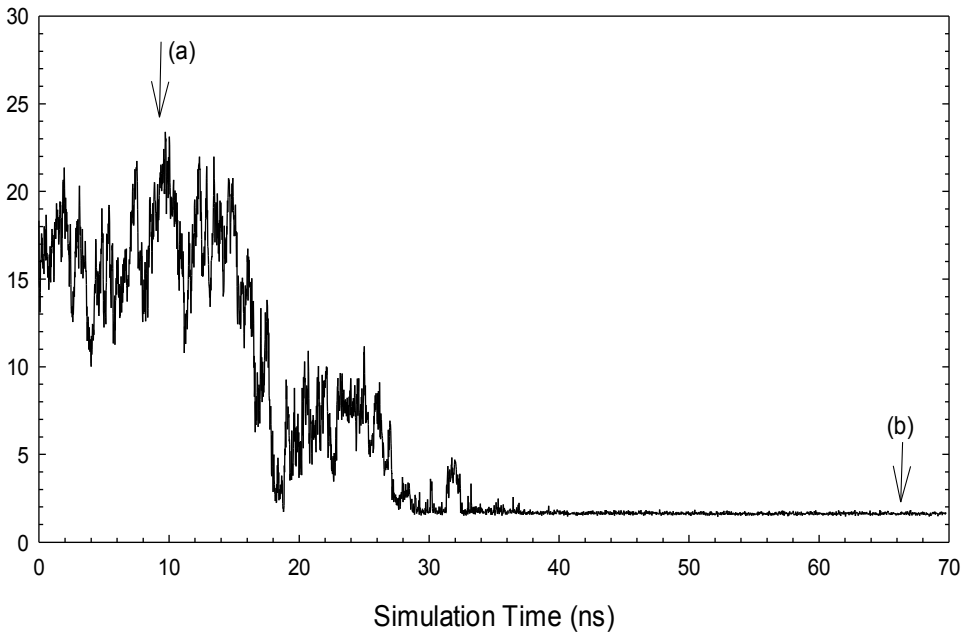
Figure 1.12. Distance between a DNA molecule in electrolyte solution and a PS lipid monolayer as a function of time during MD simulations. The distance is calculated as the closest distance between any atom of DNA and lipid molecules. The arrows indicate the time corresponding to the snapshots shown in fig. 11. Reprinted with permission from ref. [85]. Copyright (2014) Elsevier.

CHAPTER 2: OBJECTIVES

This thesis has been elaborated in the frame of the research project *'Physicochemical properties of mesoscopic complexes of biotechnological interest'* funded by Junta de Andalucía (P09-FQM-4698). Hence, the work presented here is devoted to part of the tasks scheduled there. As starting point, we have exposed in the introduction (section 1) the state of the art of the biophysics of anionic lipoplexes. We have explained two different experimental approaches: on the one hand, the preparation of complexes in solution and, on the other hand, the study of the complexation at the air-water interface. In addition, theoretical insights have been classified by the sort of model employed to describe the ternary system into coarse-grain and all-atomic. Taking this into account, the main objective of the thesis is to improve the current understanding of anionic lipoplex phenomenology by combining different experimental and theoretical strategies. The specific aims contemplated in this work are:

Regarding the formation of anionic lipoplexes in solution:

To demonstrate and characterize the formation of anionic lipoplexes in solution of different compositions, namely, as a function of the lipid-DNA ratio and the divalent cation concentration.

Regarding the cation-mediated binding of DNA onto negatively charged monolayers at the air-solution interface:

To determine the role of divalent cations in mediating the interaction between DNA and anionic monolayers at the air-solution interface.

To monitor the interaction as a function of lateral packing.

To visualize with AFM the resulting structures upon interfacial complexation.

To identify the moieties involved in the ternary complexes.

Regarding the theoretical description of the complexation:

To evaluate if the adsorption of polyanions onto like-charged surfaces mediated by trivalent cations can be predicted attending to purely electrostatic interactions.

To analyze the strength of the electrostatic attraction of polyanions onto like-charged surfaces mediated by trivalent cations as a function of the polyanion charge, the surface charge density, the cation concentration and the cation diameter.

In chapter 3, we explain in detail the experimental and simulation methods used in this survey in order to achieve these aims. We would like also to remark that we have implemented some of these procedures in our facilities as part of the research project, especially the film deposition by the Langmuir-Blodgett technique and programming the Monte Carlo simulation based in a coarse-grain model.

CHAPTER 3: METHODOLOGY

3.1. EXPERIMENTAL

3.1.1. MATERIALS

3.1.1.1. Phospholipids

Phospholipids are naturally occurring cell membrane constituents. Most phospholipids contain a glycerol 3-phosphate molecule (diglycerides); fatty acids form esters with the other two hydroxyl groups of the glycerol and the phosphate can also binds other polar groups (fig. 3.1).
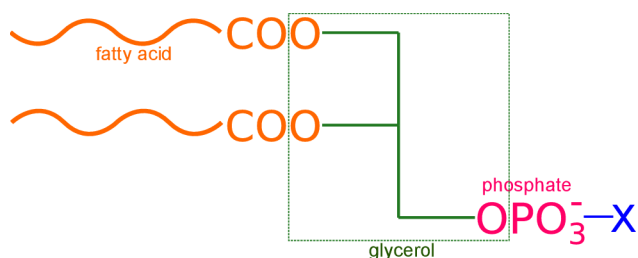

Figure 3.1. Phospholipid molecule. 3-carbon glycerol backbone (green), phosphate (fuchsia), X group bound to phosphate (blue) and fatty acids in the hydrophobic tail (orange).

As a result, these molecules have a hydrophobic tail and a polar head, that is to say, they are amphyphiles. Hence, they show high interfacial activity, with critical micellar concentrations at the nanomolar scale, and they have also the capability to form several emerging self assembled structures in solution, such as monolayers, bilayers and vesicles (fig. 3.2).

bilayer   liposome
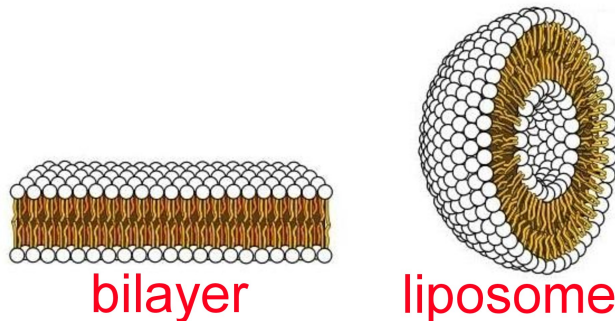
Figure 3.2. Phospholipid self assembled structures. Adapted from [166].

The above mentioned properties, as well as the biological function of phospholipids, are determined by the nature of the hydrophobic tail (fatty acids) and the polar headgroup. On the one hand, fatty acid alkyl chain length can influence the membrane thickness or it can introduce membrane singularities or defects when they are mixed with other lipids. Furthermore, the presence of *cis* double bonds in this alkyl chain disrupts the packaging among saturated chains, which has a significant effect in increasing the melting temperature at which the membrane phase transition, T_m between the solid and the fluid state takes place. On the other hand, the polar headgroup determines the phospholipid net charge and its dependence on pH. As a consequence, we distinguish anionic (negatively charged), cationic (positively charged), zwitterionic (with balanced positive and negative charges) and neutral (polar without charge) phospholipids. Moreover, the nature of the phospholipid headgroup also determines how the charges can stick together, the way they are exposed to the interface and their reaction to a change in the ambient conditions, like the presence of an interacting object, such as a colloid or a polyelectrolyte.

Table 2 displays the phospholipids used in this work. DPPC and DOPC are zwitterionic, while DPPS and DOPS are anionic. Attending to the sort of fatty acid substituents, DOPC and DOPS have monoinsaturated fatty acids, with melting temperatures considerably less than 0 ºC, so we will use them to prepare fluid films; on the contrary, DPPC and DPPS are saturated, with melting temperatures well over room temperature, so we will use them to prepare solid films at room temperature.
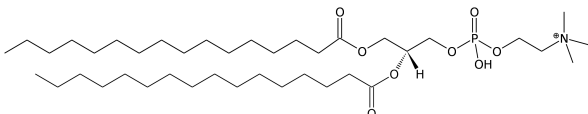
Structure	T_m (ºC)
dipalmitoylphosphatidylcholine (DPPC)	41
Dipalmitoylphosphatidylserine (DPPS)	54
Dioleoylphosphatidylcholine (DOPC)	-17
Dioleoylphosphatidylserine (DOPS)	-11
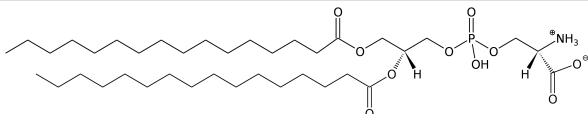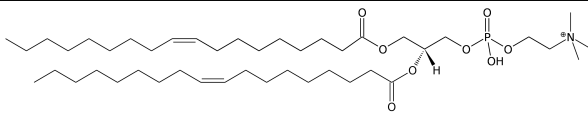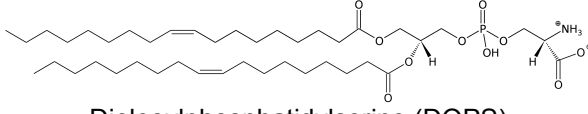
Table 2. Phospholipids used in this work. Structures, common names, abbreviations and transition temperatures (T_m) are given.

In addition, commercially available natural phospholipid extracts were also used. These samples are mixtures of phospholipids with the same headgroup but they have a variety of fatty acids in the hydrophobic tail. In this way, when we use the names phosphatidylcholine (PC) and phosphatidylserine (PS) without any specification of the fatty acids substituents, we will be referring to phospholipid extracts with those specific headgroups. PC was from egg yolk with POPC as predominant species; and PS was from bovine brain with SOPS as predominant species.

Phospholipids were purchased from Sigma-Aldrich as solid powder and they were carefully weighted after moisture removal in the desiccator and then dissolved in the required solvent: $CHCl_3$ in the case of DPPC, DOPC and PC; in $CHCl_3/CH_3OH$ 4:1 (v/v) in the case of DOPS and in $CHCl_3/CH_3OH$ 2:1 (v/v) in the case of DPPS and PS. Phospholipids were also supplied by Avanti Polar Lipids as solutions in $CHCl_3$ in the case of DPPC, DOPC, PC, DOPS and PS and solutions in $CHCl_3/CH_3OH/H_2O$ 65:35:8 in the case of DPPS. These phospholipid solutions were supplied in sealed ampoules with certificated analysis of concentration and purity.

3.1.1.2. Calf thymus DNA fragmentation and characterization

Double stranded DNA from calf thymus (ctDNA) was purchased from Sigma (> 98 % purity). This sort of genomic DNA was chosen for the experiments due to its high availability on a massive scale, which allowed us to prepare large amounts of solutions, required as subphase in the Langmuir balance. ctDNA has already been employed by other authors in the characterization of lipoplexes both in bulk[74,111,169] and at the air-water interface[44,49,90]. ctDNA stock solutions were prepared by mixing the DNA solid fibers with water at a 4 mg/ml concentration and stored at 4 ºC without any agitation for 3-4 days. After this time, the solution turned opalescent and viscous as the DNA fibers were totally dissolved.

DNA fragmentation

Commercially supplied ctDNA contains relatively large and highly polydisperse linear DNA fragments $(15-23) \cdot 10^3$ bp (according to manufacturer). In order to reduce the mean size of the DNA provided, it was fragmented. Several ctDNA fragmentation protocols are reviewed in [69]. The sonication method was preferred rather than enzyme restriction treatment because of its efficiency to produce a limited size range from genomic DNA. In addition, this method reduces costs and avoids further purification protocols to remove protein residues. Despite being more time-consuming than direct sonication with a tip immersed in the DNA solution, sonication in bath was chosen to softly fragment ctDNA to

prevent free radical generation which can result in DNA chemical modification. Accordingly, the ctDNA fragmentation protocol was carefully adapted and optimized from procedures described elsewhere[66,69,90].

50 ml of 4 mg/ml ctDNA stock solution were first introduced in a glass container. Oxygen removal was achieved with a nitrogen stream through a double head needle sealed with a septum. In this way, we avoid the formation of reactive oxygen species that can cause DNA damage upon the fragmentation process. The whole setup can be seen in fig. 3.3. The nitrogen flow was maintained for 30 min in the bath with water and ice before connecting the sonication. Once the sonication had started, the bath was periodically refilled with ice to keep the temperature near 0 °C and the solution was kept under the nitrogen stream until the fragmentation process was completed. The fragmented ctDNA was then stored in 10 ml aliquots at -20 °C until they were used. In addition, 50 µl of fragmented ctDNA stock solution were stored separately for gel electrophoresis and spectrophotometry characterization.
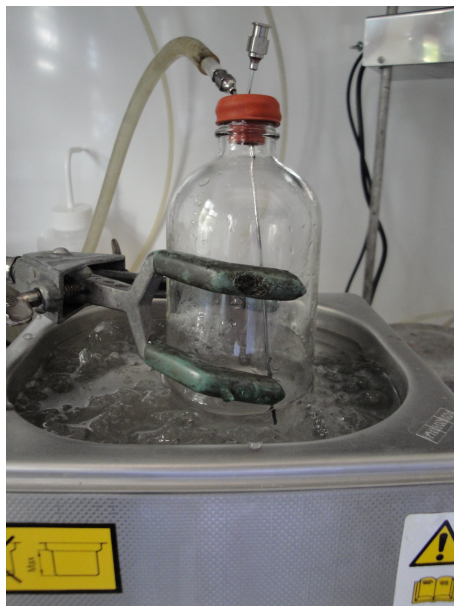
Figure 3.3. DNA fragmentation setup. The DNA solution is placed in a glass bottle and it is sonicated in sonicator bath under a nitrogen flow bubbled with a needle introduced through a septum.

In fig. 3.4, we show a time course of the DNA fragmentation. The sample at 0 h is unfragmented DNA. It contains so large DNA fragments that some of them did not migrate from the well. However, the size distribution moved towards lower values as sonication time was gradually increased. This size distribution stabilized at 10 h sonication time, ranging between $0.3 \cdot 10^3$ and $1.4 \cdot 10^3$ bp. This sonication time was fixed in all the DNA fragmentation assays conducted in this work.
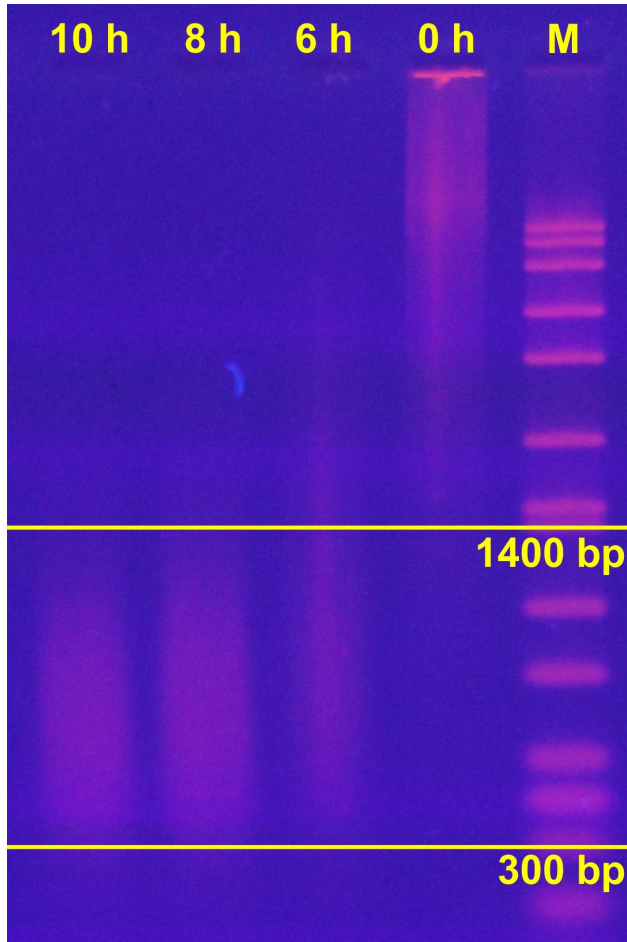
Figure 3.4. DNA fragmentation time course. From right to left: DNA size marker (M), unfragmented calf thymus DNA (0 h), DNA fragments after 6, 8 and 10 h sonication time. The DNA size range is marked for the sample at 10 h sonication time.

UV absorption spectroscopy

dsDNA solutions spectra usually display a maximum at λ = 260 nm due to aromatic nitrogen bases. Given that the molar extinction coefficient for dsDNA is well known at this wavelength at a certain conditions of pH, ionic strength and ambient temperature, the DNA concentration can be estimated. Moreover, the presence of proteins enhances the absorption at λ = 280 nm, due to the three aromatic amino acids. Therefore, ultraviolet absorption spectroscopy measurements at these two wavelengths were used to assess both the DNA purity and its concentration by using standard protocols[138].

- **Sample preparation**: Three samples were prepared by diluting fragmented 4 mg/ml ctDNA stock solution with buffer 10 mM Tris·HCl pH = 7.5 to the ctDNA concentrations 60, 30 and 15 µg/ml.

- **Absorbance measurements**: Absorbance measurements were carried out in a spectrophotometer with a quartz cuvette. First, the blank was registered with buffer. Then, measurements at two UV wavelengths, λ = 260 nm and λ = 280 nm were performed on the three samples.

- **DNA purity**: The absorbance at λ = 260 nm and λ = 280 nm ratio, A_{260}/A_{280} was calculated for the three samples. As long as this ratio is equal or less than 1.8, we consider that protein

contamination is negligible. All the DNA preparations used in this work have met the quality requirements of the cited test.

- **DNA concentration**: The exact DNA concentration was determined from the absorbance of the samples at λ = 260 nm, A_{260}. To this aim, the Lambert-Beer law is applied (eq. 12):

$$A_{260} = \epsilon_{260} \cdot l \cdot c_{DNA} \tag{12}$$

where ϵ_{260} = 50 ml·µg^{-1}·cm^{-1} is the dsDNA molar extinction coefficient at λ = 260 nm, l is the light path (standard 1 cm) and c_{DNA} is the DNA concentration, in µg/ml. From the exact DNA concentration in each sample, ctDNA stock solution concentration is determined multiplying by the corresponding dilution factors and the final ctDNA stock solution concentration is calculated as the average of the three values.

Agarose gel electrophoresis

Agarose gel electrophoresis was performed in order to characterize the size distribution after DNA fragmentation. The basis of this technique is the different migration rate of different size DNA fragments inside a porous gel under an electric field. Therefore, after the electrophoresis the short fragments migrate a further distance from the cathode to the anode, while the large ones are exposed to a higher resistance against the gel migrating a shorter distance as compared to the short fragments. As a result, DNA fragments are separated along the gel as a function of its size. The protocol is fully described in ref. [138].

- **Agarose gel preparation**: The appropriate amount of solid agarose was dissolved in TBE in mass concentration ranging from 1 to 3 % (m/m). Good resolution of the shortest DNA fragments was achieved with 3 % (m/m) agarose. The mixture was prepared in an Erlenmeyer flask and it was weighed over a platform before heating in the microwave at 10 – 20 s intervals with manual agitation after each interval until boiling. Care must be taken to avoid burning. We kept the heating intervals until the agarose is totally dissolved and the solution turns fully transparent. The flask was weighed again over the platform and pure water was added if necessary to recover the initial weight in order to compensate for evaporation. The solution was partially cooled under tap stream before pouring it into the gel cast. A comb was placed in the cast to create wells to load samples. Once cooled and solid, the comb was removed and the gel was transferred to the electrophoresis tank, where was immersed in electrophoresis buffer. The gel can be stored there until it is used as long as is submerged in electrophoresis buffer.

- **Sample preparation and loading**: ctDNA was diluted in pure water to 62.5 ng/µl and 16 µl of this ctDNA solution were mixed with 4 µl loading buffer. 10 µl of the prepared sample, containing 0.5 µg ctDNA, were carefully loaded in each well with a pipette. DNA marker was also loaded in one or two wells so that the separate DNA fragments can be ranged in base pairs.

- **Running**: A potential difference of 100 mV was applied for 1 – 2 h until the colored indicator was placed at a distance of 1 – 2 cm to the gel border.

- **Gel staining and visualization**: Once the electric power was switched off, the gel was removed from the tank and it was introduced in a recipient and submerged in GelRed® 3x (stock supplied at 10000x) solution and gently stirred in an orbital stirrer for 15 min. The gel was visualized and photographed right after under UV light source.

3.1.2. METHODS

3.1.2.1. Monolayers

π-area isotherms and Gibbs elasticity.

Phospholipid monolayers at the air/water surface were formed in a Langmuir trough of total area 244.5 cm^2, equipped with paper Wilhelmy plates pressure measuring system (KSV) with π sensitivity of 0.1 mN/m. The trough was first cleaned with 10% Micro-90$^®$ cleaning solution, isopropanol and then repeatedly rinsed with distilled and ultrapure water. The absence of surface active contaminants was verified by compressing the bare water subphase, obtaining values of π < 0.2 mN/m within the whole compression cycle. Then, 50 μl of phospholipid solution (0.5 mg/ml DPPC/DPPS 4:1 (mol/mol)) were carefully spread on the subphase by means of a microsyringe (Hamilton$^®$). After an evaporation time of 20 min, the surface pressure-area (π-A) is recorded upon symmetric uniaxial compression at constant rate of 3.75 cm^2/min. First, the π-A isotherm of the DPPC/DPPS 4:1 was measured on pure water. Then, the experiment is repeated using a 5 mM CaCl$_2$ solution as subphase and, later on, with a 0.1 mg/ml DNA solution. Finally, the effect of DNA and Ca^{2+} together was tested by spreading the DPPC/DPPS 4:1 on a subphase containing both 5 mM CaCl$_2$ and 0.1 mg/ml DNA at the same time, and recording the π-area isotherm. The whole experiment series (DPPC/DPPS 4:1 monolayer spread on water, Ca^{2+}, DNA and Ca^{2+}+DNA subphase) was carried out

on the same day with the same phospholipid solution in order to keep constant all the conditions. The reproducibility of the π-area isotherms of the DPPC/DPPS 4:1 monolayer spread on water or Ca^{2+}+DNA subphase was tested by independent measurements carried out in triplicate for independent samples. The whole setup was located in a transparent Plexiglas case to avoid air streams and dust deposition and to allow temperature control at 20.0 ± 0.1 ºC.

The surface Gibbs elasticity[5] of the monolayer was calculated directly from the π-A isotherms using equation 13:

$$\varepsilon_0 = -A \cdot \left(\frac{\partial \pi}{\partial A} \right)_T \qquad (13)$$

where ε_0 is the Gibbs elasticity, π is the surface pressure of the monolayer and A is the area per molecule.

Langmuir-Blodgett monolayers

Surface films were sampled by transferring material onto freshly cleaved mica (Agar Scientific) using the Langmuir-Blodgett (LB) technique at various selected surface pressures, as described elsewhere[102]. LB films were prepared by vertical dipping into the subphase at constant surface pressure (see fig. 3.5). This is automatically done by the KSV-LB software. The mica support was first immersed and then extracted from the subphase. The transfer rate was 5 mm/min for the monolayers prepared on either pure water or DNA subphases and 2 mm/min for the monolayers prepared on a subphase

containing DNA and $CaCl_2$. In this way, transfer ratios were 0 during the immersion while they were 1 for the extraction process, proving the film deposition at this stage. The samples collected were allowed to dry before imaging.
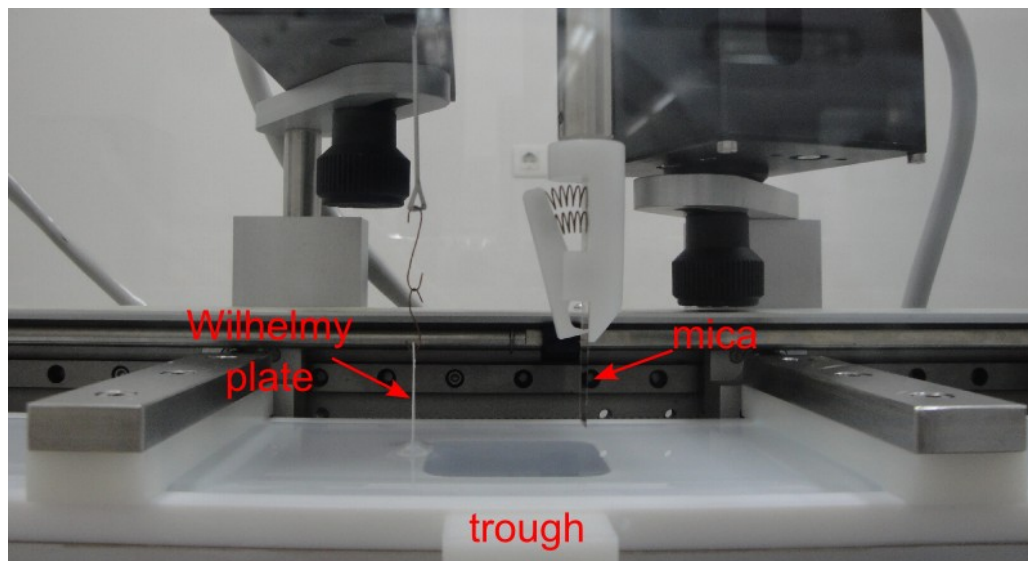
Figure 3.5. Langmuir-Blodgett film deposition setup in our laboratory.

Atomic Force Microscopy

Imaging of transferred LB films was carried out using an Atomic Force Microscope Nanoscope IV MultiMode in air (Digital Instruments). Images were obtained in tapping mode with a Si-dopped P(u) cantilever. The topography data were sampled in a grid of 512 × 512 points or 1024 x 1024 points. The imaging was carried out under ambient laboratory conditions. The structures seen following LB transfer of phospholipids correspond with those present at the air-water interface as has been

demonstrated using Brewster Angle Microscopy (BAM)[102]. Each sample was imaged in at least two different areas obtaining similar patterns. The reproducibility of the current experiments was tested by measurements in duplicate for the DPPC/DPPS 4:1 monolayers on pure water at 2 mN/m and on Ca^{2+}+DNA at 25 and 40 mN/m, obtaining similar patterns. AFM images were processed with open source software Gwyddion 2.22[165], which was used also to determine height distribution functions.

Infrared Reflection-Absorbption Spectroscopy

IRRAS measurements were carried out using an IFS 66 FT–IR spectrometer (Bruker) equipped with a nitrogen cooled MCT (mercury cadmium telluride) detector. The spectrometer is coupled to a Langmuir–film trough (R&K) placed in an external air–water reflection unit. A KRS–5–wire–grid polarizer is used to polarize the IR beam perpendicular to the incidence plane (s–polarized) and it is then focused on the water surface of the Langmuir trough. The incidence angle with respect to the surface normal was set to 40º and the reflected radiation was collected and measured at the same angle. The setup consisted of two troughs connected by little pipes to ensure the same liquid height and it is placed inside of a hermetically sealed compartment. Both troughs have a total volume of 120 ml and the surface pressure was measured by a filter paper Wilhelmy plate system.

Firstly, the absence of surface–active contaminants in the buffer was verified by recording the π–A compression isotherm and assuring

values of π<0.1 mN/m. Then, 50 μl of $5.4 \cdot 10^{-4}$ M of DOPS/DOPC solution were spread on the water surface in one trough (sample), whereas the other (reference) is filled with the pure subphase. 1 h was given for the equilibration and water vapor saturation and then the monolayer was compressed at the rate of 9 cm^2/min. Once π reached the values of 5 or 30 mN/m, the barrier motion was programmed to keep the pressure constant during IRRAS acquisition time. In order to eliminate the interference due to water vapor, measurements were performed by switching between the two troughs at regular intervals using a trough shuttle system. IRRAS data are reported in terms of reflectance–absorbance (R–A) vs. wavenumber. R–A is defined in equation 14:

$$R-A=-\log\left(\frac{R}{R_0}\right)$$

(14)

where R is the reflectivity of the film–covered surface and R_0 is the reflectivity of the bare subphase. The spectra were recorded with a spectral resolution of 8 cm^{-1}, a scanner speed of 20 kHz, accumulated using 400 scans and shifted to zero at 1157 cm^{-1}.

3.1.2.2. Lipoplexes

Preparation of liposomes

Liposomes were prepared by the extrusion method described elsewhere[131,132]. Firstly, PC/PS 1:1 (mol/mol) in $CHCl_3$/CH_3OH 2:1 (v/v) at the concentration of 10 mM total phospholipid were prepared. Then, the

solvent was evaporated under vacuum by rotary evaporation for 30 min and right after passed through a steady stream of nitrogen gas in order to remove any trace of solvent. Next, the dry films were brought back to the initial volume with buffer solution 40 mM HEPES pH 7.4 and it was left for hydration for 4 h with continuous rotation in a bath at 55 ºC at atmospheric pressure. This temperature was above the transition T_m of both lipids (see table 2). Alternating cycles of vigorous sonication and hydration were used if necessary to achieve the homogenization of the MLV solution as long as the total time of sonication did not exceed 5 min. Finally, SUV were formed by extruding the MLV solution, first 5 passes through 800 nm and then 5 passes through 200 nm pore size polycarbonate membranes. The extrusion was carried out using a Thermobarrel Lipex Extruder (Northern Lipids), that uses a N_2 current under pressure to force the solution through the membrane. The final liposome solution was stored in the fridge at 4−7 ºC. The monodispersity of the sample was tested by photon correlation spectroscopy (PCS), obtaining a mean particle size of 179 ± 6 nm and mean polydispersity of 0.36 ± 0.08.

GelRed exclusion fluorescence assay

The basis of this assay is to determine the lipoplex formation from the fluorescence intensity decrease of the DNA-GelRed® when DNA takes part in the phospholipid/Ca^{2+}/DNA complex and it is not accesible any more to the fluorescence probe GelRed®. In this way, the GelRed® was added after lipoplex formation and the fluorescence spectra were

compared with controls at the same concentration of DNA and $CaCl_2$. The procedure was adapted from the one reported elsewhere[131].

Lipoplexes were prepared by adding reagents in the following order: First, buffer HEPES 40 mM pH = 7.4 and PC/PS 1:1 (mol/mol) liposomes from a 10 mM total phospholipid stock solution; then, fragmented ctDNA at a final concentration 29.5 µg/ml, adjusted to have a good signal-noise ratio. The samples were stirred in the vortex and softly centrifuged before adding $CaCl_2$ and then they were immediately stirred in the vortex after the addition. Finally, GelRed® is added at a final concentration of 15x and the sample is stirred immediately before measurement. Any other control samples without $CaCl_2$ or liposomes were prepared by mixing the components in this order.

DNA-GelRed® excitation is possible at two different wavelengths: λ_{ex} = 264 nm, characteristic of DNA nitrogen bases and λ_{ex} = 525 nm, characteristic of GelRed®. Optimal signal-noise ratios were achieved at λ_{ex} = 525 nm, background signal of GelRed® bound to the liposomes is detected in the absence of DNA, though. On the contrary, fluorescence intensity at λ_{ex} = 264 nm was specific of the DNA-GelRed® complex. Fluorescence emission spectra were registered in the range from λ_{em} = 550 nm to λ_{em} = 700 nm. The maximum emission was located at λ_{em} = 608 nm, independently of λ_{ex}.

Fluorescence spectra were registered for each sample in a Cary Eclipse spectrofluorimeter (Varian). Control experiments were performed incubating the samples for different periods of time and we checked that

the lipoplex formation was quick, since fluorescence spectra were stable and reproducible 1 h after lipoplex formation.

3.2. MODELIZATION

3.2.1. Coarse Grain model

Simulations have been performed using a CG model whose main features are: i) PA chains were modeled by a bead–spring polymer model that has been described elsewhere in the literature[22,27]; ii) ions are explicitly considered; iii) the charged surface is assumed to be planar; iv) the solvent (water) is taken into account only through its dielectric permittivity (primitive model). Similar models have been employed by other authors[22,23,155].

The negatively charged PA chain is described as a sequence of certain number of hard spheres (beads), N_{bead}, connected with harmonic bonds. In this work N_{bead}=20. The number of charged beads per chain is *f*. The charge of the beads remains fixed (it is not transferred to one bead to another). It should be kept in mind, however, that the adsorption of a single PA chain onto a planar surface has been simulated in this work, as some authors have previously done[22,23]. It should be mentioned, however, that other authors have performed studies in which PA chains adsorb from a solution[155,158]. Although these two kinds of surveys may lead to similar conclusions, the explored situations, the employed techniques and the examined properties are not the same.

The simulation cell also contains trivalent cations and monovalent anions (in a fixed number given by the bulk electrolyte concentration) as well as excess of trivalent cations required to have an electroneutral

system. All of them are treated as hard spheres. The simulations of this work have been performed assuming that the surface charge is uniformly smeared out. An impenetrable charged wall is located at $z=0$ whereas at $z=L$ another impenetrable wall without charge is placed.

The short-range repulsion between any pair of particles (beads and ions) due to excluded volume effects is modeled by means of the usual potential for hard spheres (u_{HS}):

$$u_{HS}(r)=\begin{cases} \infty & r\leq(d_i+d_j)/2 \\ 0 & r>(d_i+d_j)/2 \end{cases} \tag{15}$$

where r is the center-to-center distance between a given pair of particles and d_i is the diameter of species i. The diameter of all the particles is 0.4 nm although a value of 0.8 nm was also used for ions. The adjacent beads of a given chain are connected by harmonic bonds, whose interaction potential is:

$$u_{bond}(r)=\frac{1}{2}k_{bond}(r-r_0)^2 \tag{16}$$

where k_{bond} is the elastic constant and r_0 is the equilibrium bond length. In this work, we have assumed that $r_0=0.5$ nm and $k_{bond}=0.4$ N/m. This k_{bond}-value has been widely used for polymer chain and networks[24,123,124,126]. All the charged species (charged monomers and ions) interact electrostatically through the Coulomb potential:

$$u_{elec}(r)=\frac{Z_i Z_j e^2}{4\pi\epsilon_0\epsilon_r r} \tag{17}$$

where Z_i is the valence of species i, e is the elementary charge and $\epsilon_0\epsilon_r$ is the permittivity of the solvent. The interaction energy of ion i with the uniformly charged surface is:

$$u(\vec{r}_i) = \frac{\sigma_0 Z_i e z_i}{2\epsilon_0 \epsilon_r} \tag{18}$$

where $\vec{r}_i$ is the position vector of particle i, z_i is its z-coordinate, and σ_0 is the surface charge density of the charged wall.

At this point, it should be mentioned that we have assumed the walls located at $z=0$ and $z=L$ have the same dielectric constant as the solvent. This assumption, also made by other authors, allows us to discard image charge effects associated to dielectric discontinuities. In the last decade, several authors have analyzed the influence of image charges on the electric double layer and polyelectrolyte adsorption under different conditions (see, for instance, the works by Wang *et al.* and Seijo *et al.* and the references cited therein)[139,159]. In any case, these effects are highly specific. For instance, they are expected to be different for a liposome, which involves two dielectric discontinuities and encapsulates an aqueous medium, and a solid substrate. Since we are rather interested in non-specific systems and general trends, image charge effects go beyond the scope of this work.

3.2.2. Monte Carlo simulations

The simulations were carried out in a canonical ensemble employing the standard Metropolis algorithm. Particles were confined in

a rectangular prism of dimensions $W \times W \times L$, which must be carefully chosen: both L and W must be much larger than the Debye length of the system λ_D, that is, the distance beyond electrostatic interactions are significantly screened. The Debye length is given by:

$$\lambda_D = \left(8 \pi \lambda_B I N_A\right)^{-\frac{1}{2}} \qquad (19)$$

where N_A is the Avogadro number and I the ionic strength. In addition, W was chosen to be of the order of L, as other authors have done[20,150]. Before performing simulations in the presence of the PA chain, it is advisable to check, particularly at high charge densities, that cationic and anionic profiles reach well defined and stable values far from the charged surface and do not exhibit noticeable and little reliable border effects near the neutral wall.

Periodic boundary conditions were used in the lateral directions (x and y). The long-range electrostatic interactions were handled using a classical method for the slab geometry put forward by Torrie and Valleau in the early 80s, which we will refer to as the *external potential method* (EPM)[150]. Each charged particle is allowed to interact with the others in the simulation cell according to the usual minimum image convention. The interaction with the charges outside the cell is considered through an external potential, $\psi_{ext}(z)$, which is calculated assuming that the ionic distribution profiles outside the cell are identical to those inside. If $\rho(z)$ is the charge density at z, the external potential can be calculated as:

$$\psi_{ext}(z) = \frac{1}{4\pi\epsilon_0\epsilon_r}\int_0^L \int_{\pm\frac{W}{2}}^{\pm\infty}\int_{\pm\frac{W}{2}}^{\pm\infty}\frac{\rho(z')}{\sqrt{(x')^2+(y')^2+(z'-z)^2}}dx'\,dy'\,dz \qquad (20)$$

This expression gives us the electrostatic potential generated by a set of infinite sheets of thickness dz' and surface charge density $\rho(z')dz'$ where a central square 'hole' (of dimensions $W\times W$) has been removed. The integration over x' and y' can be carried out analytically[139], whereas the integration over z' must be performed numerically since the function $\rho(z')$ is tabulated. The reader should note that this function must be updated during the simulation from the charge density profiles. This method for slab geometry is intuitive, easy to implement and extremely fast. In a previous work, the ionic profiles and electrostatic potentials obtained from EPM in the presence of divalent and trivalent counterions were compared to those obtained from the so-called Lekner-Sperb method[125]. In general, the agreement was quite good, which supports its reliability. In addition, simulations performed within this approximation were able to capture the behavior of electrophoretic mobility data of latex particles in the presence of divalent and multivalent counterions[86]. What is more, the existence of charge inversion was proved using a simple model in which only electrostatic interactions between ions and charged surface were considered[86]. We should also mention that there is a more refined method (inspired in the EPM) but also more time-consuming[9].

All the particles execute translational moves following the recommendations of other authors[17,18,24], two additional types of moves

were tried in the case of PA chain: i) translation of the entire chain; ii) slithering, where one of the end beads is moved to the opposite end of the chain. The translation of the entire chain is advisable because the movement of its center of mass might become extremely slow. Single particle moves were attempted 100 times more often than the other two types of moves. The acceptance ratio, which is the ratio between the accepted moves and the total number of moves in a simulation, was kept between 0.3 and 0.7, according to the rule-of-thumb for obtaining reasonable statistics. It should be also mentioned that maximum displacements permitted in trail moves for chain beads and ions must be different so that the acceptance ratio of each of these particles satisfies this rule-of-thumb. The systems were always equilibrated (at least during $2 \cdot 10^6$ moves) before collecting data for averaging. Our code was checked computing the number of adsorbed monomers onto an oppositely charged surface of +0.02 C/m^2 (in the presence of monovalent counterions). Dias *et al.* reported results for this case[22]. Although they considered discrete surface charges, good agreement was found (as expected if the surface charge density is large enough).

3.2.3. Helmholtz free energy

In this work the strength of the attraction between the surface and the polymer will be characterized through the Helmholtz free energy of the system formed by the surface, the PA chain and the electrolyte solution. In our case, we will examine different positions of the center of mass (CM) of the PA chain averaging on statistically representative configurations of the chain and the ionic cloud.

The free energy when the CM of the PA chain is located at a distance z from the charged surface can be computed as[13,45]:

$$F(z) = -k_B T \ln(P(z)) + F_0 \qquad (21)$$

where $P(z)$ is the probability density to find the CM of the PA at a distance z and F_0 is an undetermined constant. Here, F_0 will be adjusted so that $F(z)$ tends to 0 far from the surface. According to eq. 21, the straightforward determination of $F(z)$ requires to compute the number of times that different positions of the CM are visited during a MC trajectory. The histogram obtained from this analysis is proportional to $P(z)$ and its logarithm determines $F(z)$. In practice, however, we can find some problems. For instance, the movement of the CM of long PA chains might become extremely slow. Consequently, the displacement along the whole cell would require a prohibitive number of moves. In addition, some configurations could be rarely visited and relatively poor statistics will be acquired for them. Umbrella sampling methods help to avoid these difficulties[13,45]. It consists in the introduction of a bias potential that favors configurations that are rarely visited. A particular

and simple choice for this case is the window potential:

$$W(z) = \begin{cases} 0 & z_{min} < z < z_{max} \\ \infty & \text{otherwise} \end{cases} \tag{22}$$

where z_{min} and z_{max} are the lower and upper limits of the window, respectively. Note that this potential restricts the movement of the chain CM between z_{min} and z_{max} but the beads of the chain can individually visit the region out of these limits. The cell can be divided into certain number of windows like this one (in the z-direction). For each of these windows, a histogram is obtained. Fig. 3.6a shows an example of the free energy obtained in each window for the case $\sigma_0 = -0.20$ C/m^2, an electrolyte concentration of 30 mM and a PA chain with 5 elementary charges. As can be seen, this curve is not continuous. The reader should note that the free energy is determined in each window to within an additive constant, which is related to the normalization constant of the probability density in each window. After exploring the whole cell in this way, the complete free energy can be reconstructed recalling that this function must be continuous from one window to the next. This is equivalent to adjusting the additive constant from one window to the next. Fig. 3.6b shows the continuous curve obtained assuming that the adjacent windows have points in common. As can be seen, we have used overlapping windows, which facilitates the connection of the functions belonging to adjacent windows.
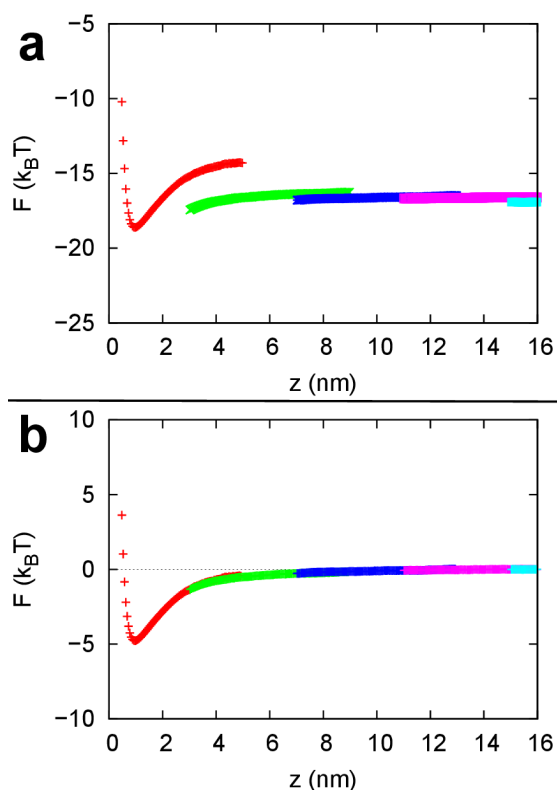
Figure 3.6. Helmholtz free energy (*F*) as a function of the distance of the center of mass of the PA to the charged surface (*z*) in each window for the case σ_0=-0.20 C/m^2, an electrolyte concentration of 30 mM and a PA chain with 5 elementary charges. (a) Raw data. (b) Continuous curve obtained assuming that the adjacent windows have points in common. Reprinted with permission from ref. [76]. Copyright (2014) AIP publishing LLC.

3.2.4. Radius of gyration

Although this work is not focused on conformational properties, it would be quite instructive to analyze how the conformation of the PA chain changes with the surface charge density (since this parameter has huge influence on adsorption, as discussed previously). The extension of the chain can be characterized by the radius of gyration, but we have preferred to calculate its projections parallel and perpendicular to the charged surface, respectively defined as[22]:

$$\langle R_{Gxy}^2 \rangle^{1/2} = \langle \frac{1}{N_{bead}} \sum_i \left[(x_i - x)^2 + (y_i - y)^2 \right] \rangle^{1/2} \tag{23}$$

$$\langle R_{Gz}^2 \rangle^{1/2} = \langle \frac{1}{N_{bead}} \sum_i (z_i - z)^2 \rangle^{1/2} \tag{24}$$

where x_i, y_i and z_i are the Cartesian coordinates of the center of particle i, x, y and z are the Cartesian coordinates of the CM of the chain, the summation runs over the beads of the chain, and ‹…› stands for ensemble average.

CHAPTER 4: RESULTS

4.1. INTERFACIAL CHARACTERIZATION

In this section we analyze the role of Ca^{2+} cations in mediating the interaction between the DNA and negatively charged phospholipid monolayers at the air-water interface. To this aim, we have applied a combination of techniques including π-A isotherms, Gibbs elasticity, AFM and IRRAS to monitor the state of the monolayer when Ca^{2+} and DNA are both present in the subphase. Additionally, control measurements with the separate components and in the absence of both of them were also performed. By so doing, we can determine if the DNA binding takes place only in the presence of Ca^{2+} cations and we can differentiate the effects due to the formation of a monolayer/Ca^{2+}/DNA complex from the possible alterations induced by the presence of the single components in bulk. In the sections below, we will characterize first the complexation with a saturated phospholipid monolayer (DPPC/DPPS 4:1) and, later on, with an unsaturated phospholipid monolayer (DOPC/DOPS 1:1). In the following sections we will specify the reasons underlying the choice of these phospholipid mixtures. Measurements at different π allow us to evaluate the possible interaction as a function of the phospholipid surface coverage and the influence of monolayer phases.

4.1.1. Complexation of DNA with DPPC/DPPS 4:1 mediated by Ca^{2+}: the role of surface pressure.

We have chosen a negatively-charged saturated phospholipid monolayer of DPPC and DPPS in a molar ratio 4:1 to develop an experimental protocol to determine the DNA binding onto the monolayer

mediated by Ca^{2+}. Since this lipid composition is well-known in the literature[135], we were not only able to validate our own measurements, but we also could enrich the discussion of the results when DNA or DNA+Ca^{2+} were used as subphase with the information about phase distribution and composition. In the following sections we present first the results of π-A isotherms as a function of the subphase composition: *i)* pure water, *ii)* Ca^{2+}, *iii)* DNA and *iv)* DNA+Ca^{2+}. Then, we analyze the effect of the formation of the monolayer/Ca^{2+}/DNA complex in the compressibility of the monolayer and the phase distribution through the Gibbs elasticity. Finally, we image the structures formed upon complexation at the air-water interface by AFM from Langmuir-Blodgett films prepared at different surface pressures.

4.1.1.1. π-A isotherm of phospholipid/Ca^{2+}/DNA monolayer.

Fig. 4.1 shows the π-A isotherms (surface pressure *versus* mean molecular area) obtained for DPPC/DPPS 4:1 spread on water, on subphases containing Ca^{2+}, DNA and Ca^{2+}+DNA. The mean molecular area per lipid molecule is obtained by dividing the surface area available between the barriers by the total amount of spread phospholipid. It can be seen that the isotherm remains invariable under the presence of Ca^{2+} alone while it is affected by the presence of DNA, alone or in combination with the Ca^{2+}, being the effect stronger when both components are present in the subphase. Let us discuss these isotherms (fig. 4.1) in more detail.

First, the π-A isotherm of DPPC/DPPS 4:1 spread on water

displays an irregular increase in surface pressure showing a number of distinct regions upon lateral compression (fig. 4.1). Following the general assignments for the phospholipid phases in the literature[79], these regions were assigned as gas-LE, LE, LE-LC, LC and collapse phases. The surface pressure lifted off at 90 ± 8 Å^2/molecule (mean value of three measurements) and entered a linear regime lasting until approximately 6.2 ± 0.6 mN/m when the isotherm exhibits a transition region for 6 < π < 10 mN/m, implying the coexistence of LE and LC phases. Further compression led to a LC phase characterized by a very steep increase of the surface pressure, and finally the isotherm reached a collapse pressure of 55 ± 1 mN/m (mean value of three measurements). The shape of the isotherms in fig. 4.1 are in good correlation with the π-A isotherm reported by Ross *et al.*[135] for the same lipid mixture.

Before addressing the effect of both Ca^{2+} cations and DNA at the same time, the effect of these substances on the monolayer was characterized separately. The π-A isotherms of the DPPC/DPPS 4:1 spread on either 5 mM $CaCl_2$ or 0.1 mg/ml DNA are also plotted in fig. 4.1. No significant changes with respect to the isotherm recorded on pure water were appreciated for the $CaCl_2$ and the slight differences between both isotherms are smaller than the experimental error. Furthermore, our findings confirm those reported by Ross *et al.*[135] who also show that the shape of the isotherm was unaffected by the presence of Ca^{2+} in the subphase. However, when a 0.1 mg/ml DNA solution is used as subphase, the isotherm is shifted to slightly higher

molecular areas with the lift off at the beginning of the compression (fig. 4.1). The displacement to higher molecular areas remains for the linear region and the first part of the LE-LC transition region but decays at higher compression states overlapping with the isotherm recorded on pure water for surface pressures above 15 mN/m.
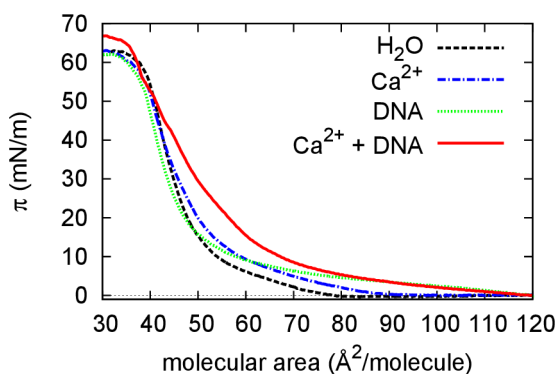

Figure 4.1. π-area isotherms of a DPPC/DPPS 4:1 monolayer on different subphases: a) pure water (black dashed line), b) 5 mM $CaCl_2$ (blue dash-dot line), c) 0.1 mg/ml DNA (green dotted line) and d) 5 mM $CaCl_2$ and 0.1 mg/ml DNA (red solid line). T = 20 °C. Reproduced from ref. [77] with permission from the Royal Society of Chemistry.

Conversely, the isotherm recorded for DPPC/DPPS 4:1 on a subphase containing DNA and Ca^{2+} displays various and significant differences with respect to the one spread on pure water (fig. 4.1). Firstly, the surface pressure starts to increase almost from the beginning of the compression. This already suggests the higher separation of the polar heads of the phospholipids at the surface. Secondly, the whole curve is displaced to higher molecular areas, not only at low surface pressures, but also at high surface pressures corresponding to the LC region. Also, the well defined LE-LC coexistence region (6 < π < 10

mN/m) is less clear in the case of DNA and Ca^{2+}. Instead, the surface pressure increases smoothly suggesting the existence of a pseudo liquid-expanded (LE) phase from the gas-LE coexistence or else a large coexistence LE-LC phase. Finally, at a surface pressure of 46 ± 7 mN/m, the slope changes abruptly and the isotherm overlaps with that recorded on a pure water subphase until collapse. The differences encountered in each of these separated regions are discussed in detail below.

Firstly, concerning the earlier lift off of the isotherm recorded in the presence of Ca^{2+} and DNA, it can also be appreciated that the surface pressure starts to increase linearly from the very beginning of the compression for the Ca^{2+}+DNA subphase. This enhanced compression sensitivity of the monolayer was also observed for the DNA subphase without Ca^{2+} (fig. 4.1), so it cannot be related with the presence of cations solely. Ross *et al.*[135] also observed a remarkable increase in the molecular area corresponding to the π lift off with the same monolayer and using as subphase a solution containing EGTA. They showed that, as a result of the EGTA cation removal, the miscibility of the two lipids increased, producing an increase in the total packing density. Since DNA is a negatively charged polyelectrolyte, it may produce a similar effect than the EGTA.

Secondly, regarding the shift to higher molecular areas, we can distinguish three regions in the isotherm recorded in the presence of Ca^{2+} and DNA. At low surface pressures the isotherm overlaps with the one recorded in the presence of DNA without Ca^{2+}. The displacement to

higher molecular areas remains during the whole LE-LC region until very high compression states where the isotherm overlaps with that recorded on pure water. Accordingly, the net expansion of the isotherm reveals that the average intermolecular distance between polar heads increases due to the migration of the DNA into the monolayer. This can be explained considering that Ca^{2+} plays the role of a bridge between the negatively charged phospholipid monolayer and the DNA, leading to the formation of a complex monolayer/Ca^{2+}/DNA. This effect has been recorded so far only for zwitterionic monolayers, which lack of net charge. Hence, Gromelski and Brezesinski prove the penetration of DNA into a DMPE monolayer by recording a shift to higher molecular areas of DMPE in the presence of DNA and Mg^{2+} cations[49]. Similarly, according to McLoughlin *et al.*[90], the Ca^{2+} is able to induce this sort of shift to higher molecular areas in a π-A isotherm for a zwitterionic monolayer (DPPC) in the presence of DNA. Concerning the behavior of ternary zwitterionic monolayer/cation/DNA complex, Mengistu *et al*. developed a theoretical approach based on the classical PB formalism to look into the role of divalent cations in the formation of such type of ternary complex[93]. Therein, the authors report that DNA adsorption process takes place accompanied by a redistribution of divalent cations from the DNA to the anionic moieties in the lipid headgroups, indicating that the DNA-induced cation penetration into the headgroup region resulted in a lateral condensation in the monolayer.

Accordingly, fig. 4.1 demonstrates for the first time the penetration of DNA into an anionic lipid monolayer of DPPC/DPPS mediated by

Ca^{2+}. Additionally, we may quantify the shift in molecular area units in table 3 obtaining similar values for the pure DPPC and the mixture DPPC/DPPS 4:1. Accordingly, the effect observed in the π-A isotherm appears mainly surface charge-independent. This finding should be taken into account in order to understand the molecular mechanism underlying this interaction, which cannot be understood from pure electrostatic effects.

π (mN/m)	ΔA (Å²/molecule)	
	DPPC	DPPC/DPPS 4:1
10.0 ± 0.1	9 ± 5	12 ± 3
20.0 ± 0.1	6 ± 4	8.5 ± 2.2
30.0 ± 0.1	3.3 ± 2.3	4.2 ± 1.7
40.0 ± 0.1	1.5 ± 1.5	1.3 ± 1.5

Table 3. Displacement of the π-A isotherm to higher mean molecular areas (ΔA) at different surface pressures for DPPC and DPPC/DPPS 4:1 Langmuir monolayers on a subphase containing 5 mM $CaCl_2$ and 0.1 mg/ml DNA with respect to the same monolayer on pure water. Reproduced from ref. [77] with permission from the Royal Society of Chemistry.

Finally, the overlap of the two isotherms seen at very high surface pressures (π > 52 mN/m) possibly implies that the DNA is being squeezed out of the monolayer at very high lateral packing. This sort of surface pressure–induced DNA detachment has so far only been reported for pure zwitterionic lipids[49,50] since, Frantescu *et al.*[44] did not find this overlapping tendency for POPC/PS 2:1/Ca^{2+}/DNA. The reason for this apparent controversy could be originated in the nature of the lipid monolayer, rather than in the net charge. The collapse for unsaturated

phospholipids is reached at significantly lower surface pressures than the saturated ones. Accordingly, the detachment of DNA from the former case is not observed because the steric instability induced by the double bonds provokes the collapse of the monolayer before reaching a sufficiently high surface pressure to squeeze out the DNA. Hence, unsaturated lipid monolayers never reach enough condensation to squeeze out the DNA. This is a very important finding that must be considered when designing lipoplexes with different anionic lipids.

4.1.1.2. Surface Gibbs elasticity.

Fig. 4.1 shows experimental evidence about structural changes induced by DNA in phospholipid monolayer in the presence of Ca^{2+}. To gain further structural insight into the conformation of the system we now look into the Gibbs elasticity of the monolayers, a property sensitive to molecular conformation[81]. Fig. 4.2 shows the Gibbs elasticity plot of the isotherms of DPPC/DPPS 4:1 monolayers spread on water or on a subphase containing DNA and Ca^{2+} from fig. 4.2. Given that only the π-A isotherm of the DPPC/DPPS 4:1/Ca^{2+}/DNA has given significant differences with the pure DPPC/DPPS 4:1 system, we only compare these two systems in fig. 4.2. Gibbs elasticity (ε_0) is the elastic modulus representing a rheological quantity related to the monolayer rigidity and to its capability to store elastic energy, which is defined by eq. 13. The compression of the monolayer is performed at sufficiently low rate assuring that the system is always in a stationary state and possible relaxation processes in the monolayer can be neglected. Hence, at this

compression rate and for insoluble monolayers, Gibbs elasticity plotted in fig. 4.2 provides generic information on the mechanical state of the monolayer.

In general, ε_0 increases upon lateral compression meaning that the higher the phospholipid packing density, the higher the resistance of the monolayer to deformation. However, this general tendency is altered by any phase transition event. The coexistence of different phases leads to a local minimum of ε_0 owing to a decreasing cohesion of the surface film, which is disrupted by the presence of the new phase[73]. The Gibbs elasticity increases again as the surface layer fills with the new phase and reaches a maximum at the maximum packing density in the new phase. A new transition within the monolayer would imply a new local decrease. Accordingly, the minima reflect phase coexistences in the monolayer whereas the maxima in the Gibbs elasticity plot are ascribed to the existence of an homogeneous cohesive layer.

For the DPPC/DPPS 4:1 spread on a pure water subphase (fig. 4.2), we can distinguish two ε_0 local maxima located at $\pi = 3 \pm 1$ and $\pi = 44 \pm 2$ mN/m (mean values of three measurements), respectively. The first corresponds to the elasticity of a monolayer in LE state ($\varepsilon_0 = 22 \pm 3$ mN/m) followed by the LE-LC transition in which the ε_0 decreases locally to a minimum. The second maximum provides the elasticity of the monolayer in LC state ($\varepsilon_0 = 239 \pm 17$ mN/m) followed by collapse of the monolayer (mean values of three measurements). Clearly, the rigidity of the monolayer is substantially higher at the LC state. After the second

maximum, ε_0 drops sharply indicating that the monolayer has broken down, with the formation of a variety of bidimensional and tridimensional structures.
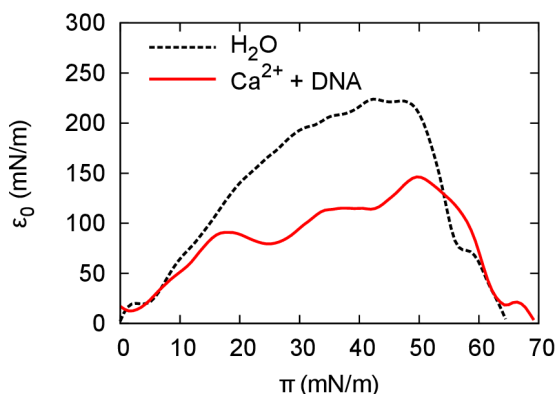
**Figure 4.2**. ε_0-π plots from a) and d) curves in fig. 1. DPPC/DPPS 4:1 monolayer on: pure water subphase (black dashed line), 5 mM CaCl$_2$ and 0.1 mg/ml DNA subphase (red solid line). T = 20 ºC. Reproduced from ref. [77] with permission from the Royal Society of Chemistry.

The evolution of ε_0 as a function of lateral packing suffers several changes in the presence of both Ca^{2+} and DNA in the subphase. In general, it appears importantly lower than the values corresponding to the pure water subphase. This means that the monolayer formed on the subphase containing both Ca^{2+} and DNA is more deformable than that recorded on a pure water subphase. Structural differences between DPPC/DPPS 4:1 and the DPPC/DPPS 4:1/Ca^{2+}/DNA systems were already inferred from fig. 4.1 at these surface pressures. We denoted this region (π < 52 mN/m) as pseudo LE or long LE-LC coexistence phase in the previous section. Interestingly, Jain *et al.*[56] reported a similar decrease in the dilational elasticity modulus as a consequence of the binding of the polyacrylamide sulfonate polyanion to a

cetyltrimethylammonium bromide monolayer. Hence, now the lower elasticity could be indicating a binding of the DNA to the DPPC/DPPS assisted by Ca^{2+} which results in a whole fluidisation of the surface film.

At higher surface pressures ($\pi > 52$ mN/m) the ε_0-π curve for the DPPC/DPPS 4:1/Ca^{2+}/DNA system displays a sharp increase and a last maximum which precedes collapse. The elasticity of the mixture in this last region is clearly higher and approaches that of the phospholipid mixture on pure water. Accordingly, the DNA is being expelled of the monolayer and the cohesion increases as the non-complexed monolayer is being restored.

We can also appreciate a new local maximum-minimum distribution in the ε_0-π curve for the DPPC/DPPS 4:1/Ca^{2+}/DNA system. This certainly shows that the formation of the monolayer/Ca^{2+}/DNA complex is accompanied by a totally different phase rearrangement from that on water. The minima located at 2, 25 and 40 mN/m in fig. 4.2, were selected for LB-AFM examination with the aim of visualizing the morphology of the coexisting phases in the monolayer/Ca^{2+}/DNA complex.

4.1.1.3. Imaging with AFM

In order to further analyze the origins of the observed changes in surface tension and Gibbs elasticity, we have imaged the changes in the morphology of the DPPC/DPPS 4:1/Ca^{2+}/DNA system by means of AFM. In this way, we assess the effect of Ca^{2+} and DNA on the structure of

DPPC/DPPS 4:1 monolayers with a similar experimental design to that of the monolayer studies. Hence, we analyze first the separate effect of Ca^{2+} and DNA on the DPPC/DPPS 4:1 monolayer to then look into the ternary system. Images were taken in tapping mode so that differences in contrast are caused by a difference in the interaction tip-surface which is ascribed to the local topography, roughness, adhesion or elasticity in each sort of domain. The AFM images have been further analyzed in order to quantify the different morphologies encountered. Table 4 displays a summary of the various systems analyzed including a description of the basic appearance of each system, identification of the different morphologies, the Root mean square roughness (RMS) and the height distribution as an averaged of all the images.

subphase	π (mN/m)	morphology[a]	RMS[b] (nm)	height distribution[c]
H_2O	2.0 ± 0.1	round-shaped domains	0.3 ± 0.3	-
0.1 mg/ml DNA	2.0 ± 0.1	round-shaped domains	0.4 ± 0.1	-
0.1 mg/ml DNA + 5 mMCaCl$_2$	2.0 ± 0.1	a) branched b) net-like	2.1 ± 0.4	-
0.1 mg/ml DNA + 5 mMCaCl$_2$	25.0 ± 0.1	a) granular b) holes and fibers	-	b) trimodal, Δh_1 = 1.59 ± 0.24 nm Δh_2 = 1.1 ± 0.4 nm
0.1 mg/ml DNA + 5 mMCaCl$_2$	40.0 ± 0.1	a) elevations b) holes and fibers	-	b) trimodal, Δh_1 = 1.64 ± 0.23 nm Δh_2 = 1.2 ± 0.4 nm

Table 4. Quantitative analysis of LB-AFM images. [a] When two different mesostructures coexist on the phospholipid/Ca^{2+}/DNA complex film they are separately described as (a) and (b). [b] RMS is calculated to show the contrast between the LB phospholipid monolayer on pure water or on a DNA subphase with respect to the

phospholipid/Ca^{2+}/DNA complex film. RMS is not calculated at 25 or 40 mN/m because the value would not be representative of the two different mesostructures in contact. [c] Height distribution functions. Height differences between the consecutive peaks are shown for trimodal distributions. These height differences allow better characterization of the depth of holes and the height of fibers (Δh_1 and Δh_2, respectively) in the background observed in the phospholipid/Ca^{2+}/DNA complex films at high surface pressures. Reproduced from ref. [77] with permission from the Royal Society of Chemistry.

Consider first the DPPC/DPPS 4:1 on pure water subphase (fig. 4.3A). In order to visualize morphological aspects we chose a surface pressure of 2 mN/m where we have LE and LC phase coexistence according to the surface pressure isotherms (fig. 4.1) and Gibbs elasticity (fig. 4.2) as discussed above. Fig. 4.3 reveals the existence of LE and LC phase coexistence as given by a background (LE) spotted by round-shaped domains (LC). The existence of these domains have been also reported by Ross *et al.* for the same lipid mixture and attributed to lipid demixing and the formation of DPPS-enriched domains[135]. The LE–LC coexistence phase for DPPC takes place at higher π than for DPPS (fig. 4.5). In the mixed system, LC domains are present from the beginning of the compression and possibly act as nucleation sites. The mixed system continuously undergo LE-LC phase transition even at surface pressures well below 4 mN/m leading to a continuous growth of the circular domains as the surface pressure increases (fig. 4.3). Accordingly, the circular domains in fig. 4.3 correspond to DPPS enriched areas. At this surface coverage the round-shaped domains have a diameter of 4 ± 3 µm and the relative domain surface coverage is 72 ± 4 % (fig. 4.3A). The diameter of these domains increases in size as the surface coverage is increased, hence indicating the transition to a

LC phase (fig. 4.4A). Moreover, a very similar morphology was obtained for the AFM images of the binary system DPPC/DPPS 4:1/Ca^{2+} (fig. 4.4B).
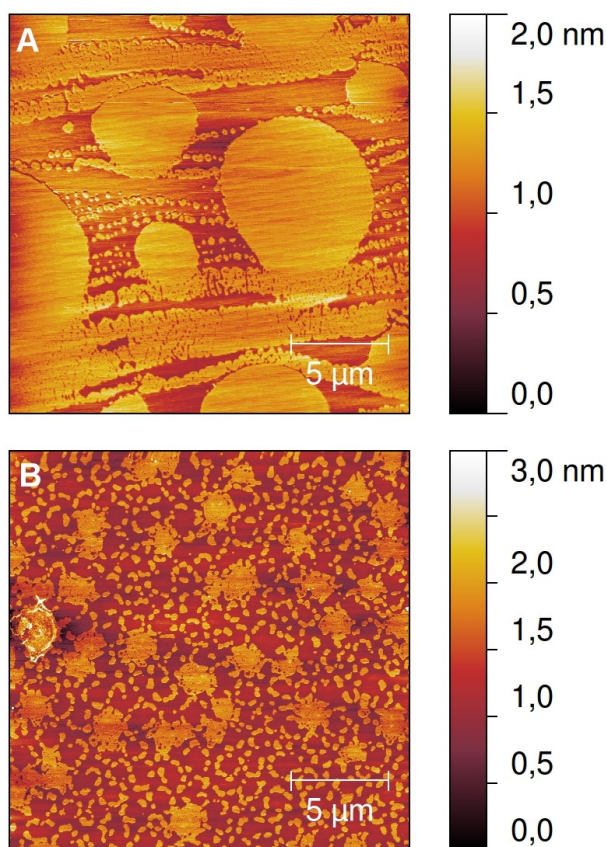

Figure 4.3. AFM topography images of LB transferred spread DPPC/DPPS 4:1 on a pure water subphase (A) and 0.1 mg/ml ctDNA (B) at π = 2 mN/m. In both cases, surface films are heterogeneous showing regions with variable height and circular domains. Reproduced from ref. [77] with permission from the Royal Society of Chemistry.

Fig. 4.3B shows also the AFM image of the binary system DPPC/DPPS 4:1/DNA at the same surface pressure (2 mN/m). Fig. 4.3B reveals again the existence of LE and LC phase coexistence as given

by a background (LE) spotted by round-shaped domains (LC), which should again correspond to DPPS-enriched domains caused by demixing. However, the diameter of such domains seems to be reduced by the presence of DNA in the subphase obtaining now 1.4 ± 0.4 µm. Domain surface coverage is also reduced to 45 ± 3 % suggesting that the demixing process is hindered by the presence of DNA in the subphase. According to Ross *et al.* the formation of DPPS enriched domains formed in fig. 4.3A occurs owing to traces of Ca^{2+} present in water which are essential for the lipid demixing process as measured by TOF-SIMS[135]. In fig. 4.3B, the DNA is likely to complex with the traces of Ca^{2+} in solution, hence playing a purifier role and lowering the residual concentration of Ca^{2+} in pure water, thus hindering the formation of DPPS-enriched domains. This interpretation is in good agreement with the π lift off at the beginning of compression observed in the π-A isotherm for this binary system (DPPC/DPPS 4:1/DNA) in fig. 4.1. Moreover, this effect was also observed by Ross *et al.*[135] for the DPPC/DPPS 4:1/EGTA system and ascribed to the release of DPPS from the more condensed domains to the mixed monolayer. To sum up, the morphology of the DPPC/DPPS 4:1 monolayer spread on a subphase containing 0.1 mg/ml of DNA resembles the monolayer spread on pure water providing no evidence of the DNA complexation in the LB transfer process in the absence of Ca^{2+}.Before continuing the analysis of the AFM images and in order to improve the understanding of the results, it is important to discuss in depth the possible molecular mechanisms underlying the formation of these ternary complexes. Our

results agree with those obtained by Ross *et al.* who already proved that Ca^{2+} preferentially binds to negatively charged DPPS molecules while a hydrated calcium-DPPS complex of larger dimensions is formed[135]. For the case of pure anionic lipid membranes it is also experimentally established that the binding of multivalent cations to negatively charged lipids is endothermic, and thus, entropically driven. This fact strongly suggests that the driving forces for ion binding are due to hydration and solvation effects as well as structural rearrangements in the membrane. Similarly, Sinn *et al.* reported that the presence of anionic phospholipids increased the interaction with Ca^{2+} and Mg^{2+},[143] but they showed by means of calorimetric measurements that the driving force of this interaction is the release of water molecules due to the dehydration of the cations and the phosphate groups, which is an entropically favorable process. Concerning the cation binding, early infrared spectroscopic studies demonstrate the formation of a strong Ca^{2+}-phosphate complex[26]. All-atomistic simulations were used in ref. [88] and [87] to demonstrate that multivalent ions such La^{3+}, Mg^{2+} and Ca^{2+} ions are incorporated deeply in the hydrophilic region of the PS membrane. In particular, adsorbed Ca^{2+} cations tend to be bound to 2 PS^- headgroups in a binding mode which involves both the carboxylic and phosphate moieties of the lipid headgroup. Accordingly, adsorption of Ca^{2+} cations in PS lipid membranes generates a highly inhomogeneous surface with patches of positive charge (both from lipids and ions) directed towards the aqueous phase that induce the DNA adsorption via hydrogen

bonding between the phosphate groups of DNA and the amino groups of PS (see ref. [85] and [36]).
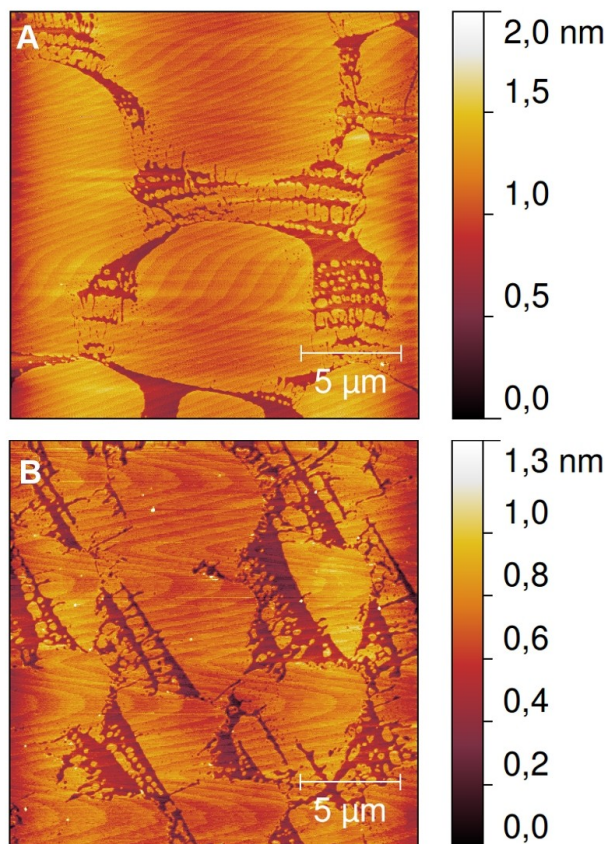
Figure 4.4. (A) AFM topography image of LB transferred spread DPPC/DPPS 4:1 on a pure water subphase at π = 4 mN/m. Circular domains expand over the film. (B) on 5 mM CaCl$_2$ at π = 2 mN/m. Domains strech out and align with the contact line.

Fig. 4.6 shows now the AFM images of the ternary system DPPC/DPPS 4:1/Ca^{2+}/DNA at 2 mN/m. Clearly, now totally different patterns appear in the monolayer, as compared with the pure lipid and the binary systems, with branched and net-like structures (fig. 4.3). Also, the roughness of the monolayer spread on DNA and Ca^{2+} increases

importantly with respect to that spread on DNA without Ca^{2+} as demonstrated by the higher value obtained for the RMS given in table 4. Control AFM images of the DNA adsorbed on mica after LB deposition confirm that the phospholipid monolayer modulates the organization and morphology of the interfacial aggregates (fig. 4.7). Thus, in view of the images and the RMS values, we can conclude that the ternary system lipid/Ca^{2+}/DNA forms interfacial aggregates dispersed on the film. More detailed analysis of the pattern obtained in fig. 4.6 allows distinguishing two different morphologies. Round-shaped areas containing fractal branched structures with an average height of 8 nm (marked with + in fig. 4.6A) and a background (marked with * in fig 4.6A). Moreover, high resolution image 6B allows further identifying a net of fibrils with an average height of 3 nm and width of 0.2 µm in the background. In fact, these fibrilar structures possibly correspond to interfacial aggregates formed as a result of the interaction among the phospholipids, the Ca^{2+} cations and the DNA. These sorts of patterns have been previously observed for other systems containing DNA; namely, Chen *et al.*[14] for the gemini surfactant 18-*s*-18/DNA system and by Antipina *et al.*[1] for the poly-4-vinylpyridine with 16 % cetylpyridinium groups/DNA. However, they have not been reported so far for lipids. The round-shaped areas with larger, branched fibrils in fig. 4.6 are possibly composed of DPPS-enriched domains of the monolayer. DPPS, having higher surface charge density, leads to the complexation of a higher relative amount of DNA with respect to the background (DPPC) and hence, the formation of bigger interfacial aggregates.
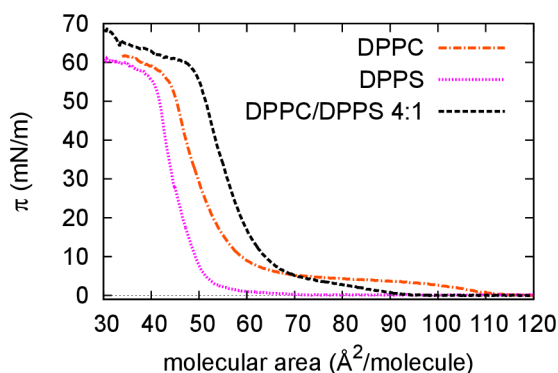
Figure 4.5. π-area isotherms of DPPC (orange dash-dot line), DPPS (pink dotted line) and DPPC/DPPS 4:1 (black dashed line) monolayers. Subphase: pure water. T = 20 ºC. Reproduced from ref. [77] with permission from the Royal Society of Chemistry.

We analyze further the complexity of the interfacial structures of the ternary system DPPC/DPPS 4:1/Ca^{2+}/DNA at higher surface coverage (higher surface pressures). Fig. 4.8 shows the AFM-images recorded from LB films of the ternary system at 25 mN/m. In this case we can also identify two different sorts of domains which can be appreciated, both in the topographic (figs. 4.8A and 4.8C) and in the phase (figs. 4.8B and 4.8D) images. However, the shape and the fine structure of these domains are completely different from those seen at lower surface coverage; 2 mN/m (fig. 4.6). On the one hand, we observe a curved domain with a granular structure (marked with * in fig. 4.8C). These grains have an average diameter of 20 nm. On the other hand, the background presents structures at three well-defined different height levels. There is a discontinuous plane in which holes (depressions, - in fig. 4.8C) and fibers (elevations, + in fig. 4.8C) that tend to border the holes coexist displaying irregular shapes and sizes. This trimodal

morphology is quantified in table 4 where the depth of the holes (depressions) and height of the fibers (elevations) is shown.
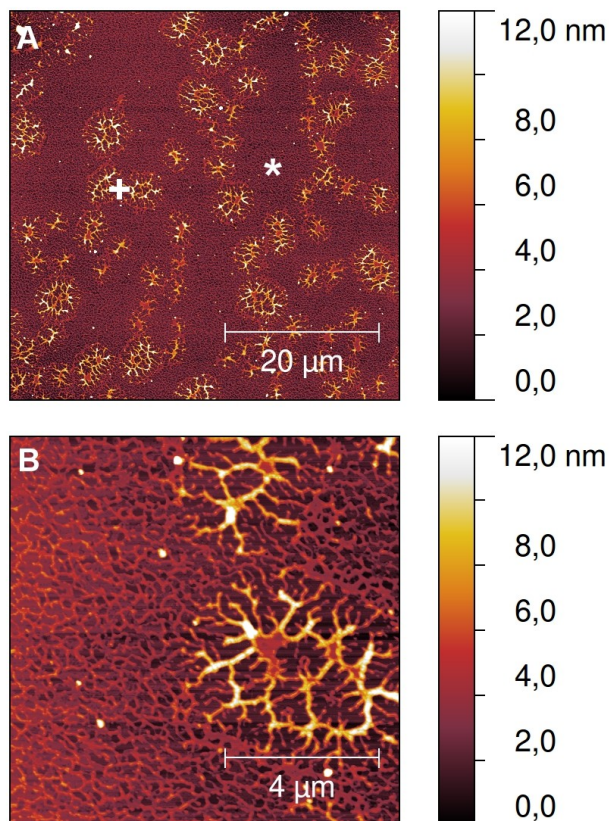

Figure 4.6. (A) AFM topography image of LB transferred spread DPPC/DPPS 4:1 on an aqueous solution subphase containing 5 mM $CaCl_2$ and 0.1 mg/ml ctDNA at π = 2 mN/m. (B) High resolution image. The surface films reveals round-shaped areas containing fractal branched structures (+) and a background (*) The high-resolution image (D) shows a surface network formd by fibrils. Reproduced from ref. [77] with permission from the Royal Society of Chemistry.

Understanding of all the structures observed is not trivial and would require of additional information from other techniques. Anyway, it is possible to interpret the characteristics of the ternary system phospholipid/Ca^{2+}/DNA, considering the size and morphologies of the

interfacial structures visualized in fig. 4.8. Therefore, the fibers (marked with + in fig. 4.8C) possibly correspond to phospholipid/Ca^{2+}/DNA interfacial aggregates considering their dimensions which are clearly greater than one single DNA chain. The removal of phospholipids from the monolayer to form aggregates may explain the appearance of holes (marked with - in fig. 4.8A). Finally, the granular domains (marked with * in fig. 4.8C) constitute a more complex form of interfacial aggregates. Similar granular interfacial aggregates have also been found by Antipina *et al.* for octadecylamine/DNA LB monolayers[1]. This morphology could be caused by DNA strands covered with phospholipid vesicles formed from the monolayer as a result of the interfacial complexation.
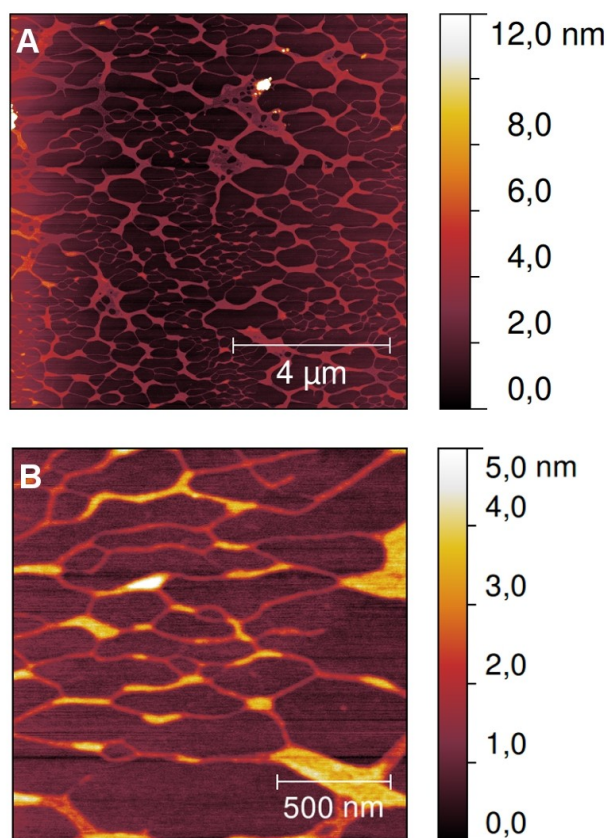
Figure 4.7. (A) AFM topography image of LB transferred from an aqueous solution containing 5 mM CaCl$_2$ and 0.1 mg/ml DNA. (B) High resolution image. Reproduced from ref. [77] with permission from the Royal Society of Chemistry.

Compression up to 40 mN/m resulted mainly in an increase in the area of the background as shown in fig. 4.9A. The structure in the background of fig. 4.9A is very similar to that described at 25 mN/m (fig. 4.8). However, fig. 4.9A reveals the existence of regions significantly thicker than the background of irregular shape and size. These structures appear only at higher interfacial coverage (40 mN/m) and were not seen at 25 mN/m (fig. 4.8). Again, the trimodal morphology is

126

quantified in table 4 where the depth of the holes (depressions) and height of the fibers (elevations) is shown demonstrating the similarities with lower surface coverage.
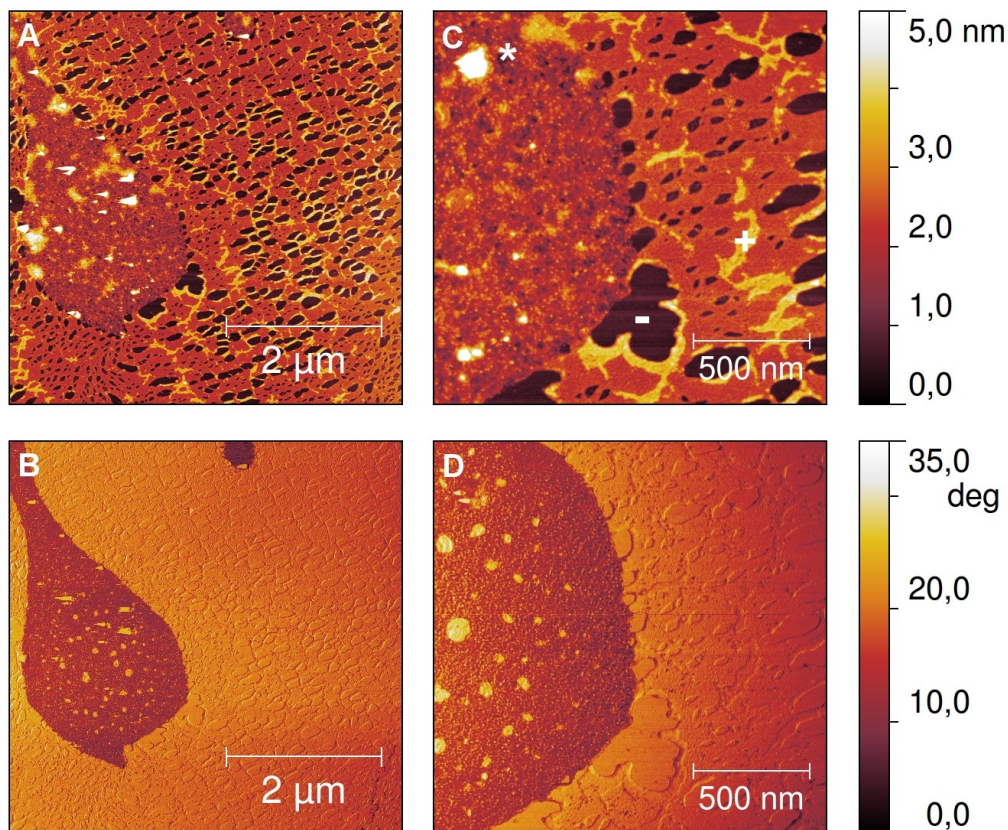

Figure 4.8. AFM topography image of LB transferred spread DPPC/DPPS 4:1 on an aqueous solution subphase containing 5 mM CaCl$_2$ and 0.1 mg/ml ctDNA at π = 25 mN/m. (A) Height image, (B) Phase image, (C) High resolution image (D) Phase from (C). Surface film shows circular domains with granular structure (*). The high-resolution image (C and D) reveals a background composed of a discontinuous plane with holes (-) and fibers (+). Reproduced from ref. [77] with permission from the Royal Society of Chemistry.

In fact, the height distribution profile of the ternary system at higher interfacial coverage (40 mN/m) is plotted in fig. 4.10. This plot

shows three peaks corresponding to the three different height levels commented for the ternary system (figs. 4.8 and 4.9 and table 4). Although fig. 4.10 shows the values corresponding to the system at 40 mN/m, this trimodal morphology is extensive to the ternary system at 25 mN/m as quantified in table 4.
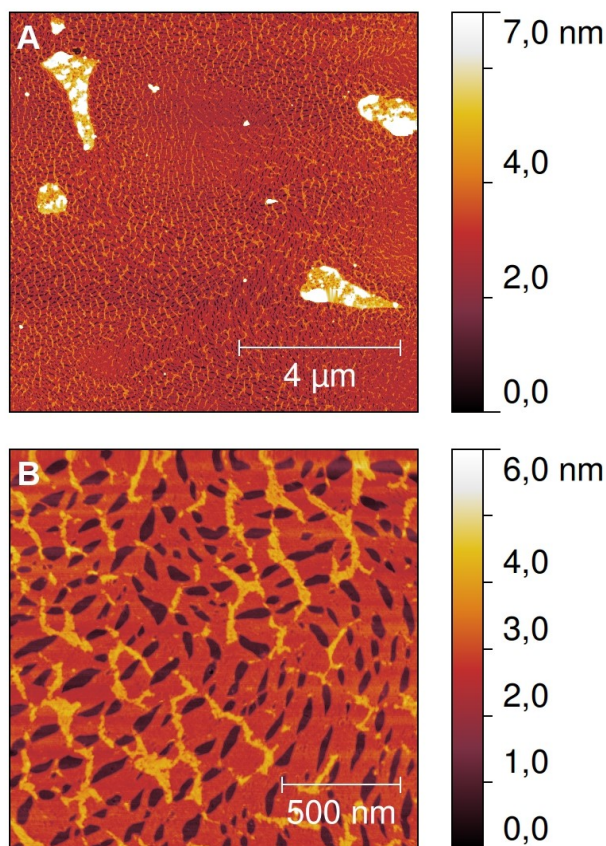
Figure 4.9. (A) AFM topography image of LB transferred spread DPPC/DPPS 4:1 on an aqueous solution subphase containing 5 mM $CaCl_2$ and 0.1 mg/ml ctDNA at π = 40 mN/m. (B) High resolution image. Images show a background composed of a discontinuous plane spotted by regions significantly thicker of irregular shape and size. Reproduced from ref. [77] with permission from the Royal Society of Chemistry.

Hence, the ternary system phospholipid/Ca^{2+}/DNA is formed by a

background composed of a discontinuous plane spotted with holes (depressions) and fibers (elevations). According to this height distribution profile (fig. 4.10), the holes and fibers observed should be located, on average, at -1.8 nm and 1.2 nm with respect to the most abundant height, respectively. The numerical values encountered allow us to identify the morphologies with the composition. The difference in height between the first and the second peak is 1.8 nm (fig. 4.10, table 4). This value reasonably matches the thickness of a DPPC LB monolayer on mica reported in the literature[63]: 2.2 nm. Hence, this allows us concluding from figs. 4.8 and 4.9 that the phospholipid monolayer is discontinuous, being interrupted by the holes. Furthermore, the height of the fibers with respect to the LB phospholipid monolayer according to table 4 is 1.2 nm (fig. 4.10). This value agrees with that reported by Wu *et al*. for the increase in thickness of a lipid/DNA monolayer with respect to pure lipid monolayer of 0.9 nm[164]. Accordingly, the fibers observed in figs. 4.6, 4.8 and 4.9 correspond to phospholipid/Ca^{2+}/DNA interfacial aggregates. The height values obtained from our AFM images mostly agree with those reported in the literature[63,164] for the LB monolayer thickness of lipid and lipid/DNA. Slight differences encountered could be due to different specific system used and also to the surface-tip interactions occurring in the AFM in tapping mode, which are expectable to change when the tip is scanning the different parts or domains in these complex LB monolayers. Therefore, the topographical profile given in fig. 4.10 illustrates the complexation of negatively charged phospholipid monolayer and DNA

mediated by Ca^{2+}.
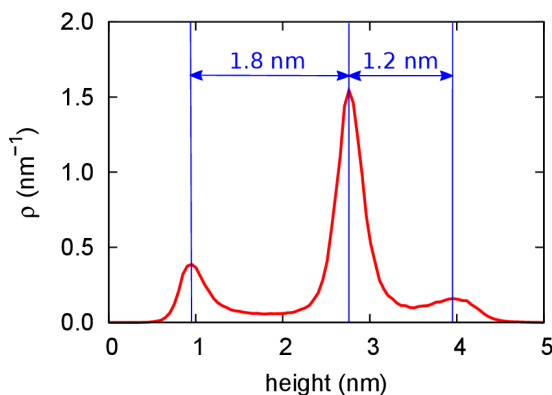
Figure 4.10. Height distribution function obtained from the AFM image in fig. 9B. This curve is representative of the topography obtained at 40 mN/m. Reproduced from ref. [77] with permission from the Royal Society of Chemistry.

A plausible multifunctional scenario can be hypothesized for the complexation of DNA with anionic lipid monolayers. Depending on the lateral packing as quantified by the surface pressure, the complex lipid/DNA can be expected to undergo various conformational transitions. Moreover, the complexation materializes in the form of interfacial aggregates that show a variety of morphologies depending on such lateral packing, as it is sketched in fig. 4.11. The proposed methodological approach combining AFM with monolayers can be productively exploited as a generic tool to explore the molecular mechanism underlying complexation of DNA with negatively charged lipids toward the rational design of biocompatible systems.
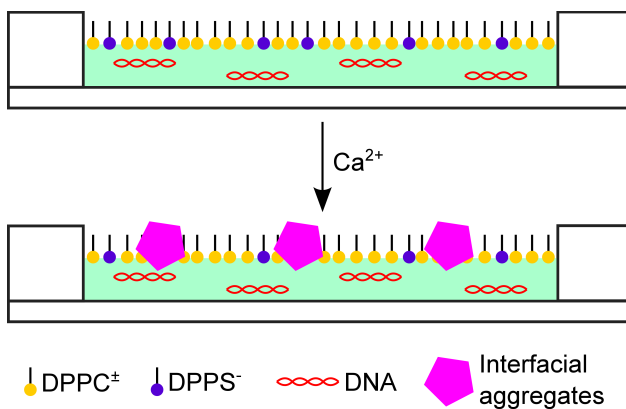
Figure 4.11. Model of formation of interfacial aggregates from Ca^{2+}-mediated DNA binding onto the DPPC/DPPS 4:1 monolayer at the air-solution interface. Reproduced from ref. [77] with permission from the Royal Society of Chemistry.

4.1.2. Response of fluid DOPC/DOPS 1:1 monolayers to Ca^{2+}-mediated DNA binding.

In the previous sections, we have demonstrated the formation of monolayer/Ca^{2+}/DNA complexes and we have characterized the corresponding structures formed at the interface. Accordingly, in this section we search for additional pieces of evidence of complexation at the air-water interface with a negatively-charged monolayer. To this aim, we carry out IRRAS measurements in order to determine the role of Ca^{2+} in mediating the interaction between DNA and the phospholipid monolayer. In addition, we also describe the moieties of lipids involved in the interaction from the analysis of IRRAS bands. In this case, we employ DOPC/DOPS 1:1 as a model of unsaturated phospholipid monolayer due to the previous experience of the group with this system[130].

We performed IRRA spectra during a short stay in the Max Planck Intitute for Colloids and Interfaces in Potsdam (Germany) under the supervision of Prof. Gerald Brezesinski, in order to gain insight into the molecular interaction between DNA and DOPC/DOPS monolayers mediated by Ca^{2+}. We registered the following IRRA spectra: *i)* firstly, lipid monolayer on buffer, *ii)* then, lipid monolayer in the presence of Ca^{2+}, *iii)* lipid monolayer in the presence of DNA, *iv)* finally, the lipid monolayer in the presence of Ca^{2+} and DNA together. The concentration of Ca^{2+} used was 10 mM and the concentration of DNA was 29.5 µg/ml. IRRA spectra provide information about vibration of groups of all the

molecules located at or close to the air-solution interface[25]. Therefore, both the phospholipid monolayer and the molecules interacting with their headgroups can contribute to the measured spectra.

As can be seen in fig. 4.12, the main differences between the spectra recorded on the different subphases are located in the phosphate band region (1300 – 1000 cm^{-1}). Phosphate asymmetric and symmetric stretching bands ($\nu_{as}(PO_2^-)$ and $\nu_s(PO_2^-)$, respectively) were assigned, according to Blume[8]. Let us first describe the spectrum registered on the lipid mixture spread on buffer. $\nu_{as}(PO_2^-)$ and $\nu_s(PO_2^-)$ appear at 1220 and 1088 cm^{-1}, respectively. Asymmetric and symmetric CH_2 stretching bands ($\nu_{as}(CH_2)$ and $\nu_s(CH_2)$) were registered at 2925 and 2855 cm^{-1}, respectively. We obtained the same values for all the subphase compositions used in this work and they match the characteristic values for the LE phase of the lipid monolayer[91] at a surface pressure of 30 mN/m. They also agree with PM-IRRAS measurements reported by Vié *et al.*[157] for this system.

Then, we measured the IRRA spectrum under the same conditions with Ca^{2+} and we observed similar phosphate stretching bands in intensity as those recorded on pure buffer. Differently, the $\nu_{as}(PO_2^-)$ center of gravity ($COG(\nu_{as}(PO_2^-))$) displayed a shift to higher wavenumbers in the presence of Ca^{2+} in the subphase, with respect to that recorded on pure buffer. Similarly, Flach *et al.*[43] reported a shift for the DPPC/DPPS 1:1 (mol/mol) with 5 mM Ca^{2+} added to the subphase. Since the $COG(\nu_{as}(PO_2^-))$ increases to higher wavenumbers with the

hydration degree[26], this shift recorded in the presence of Ca^{2+} and other divalent cations has already been explained in terms of the dehydration of phosphate non-esterified oxygens due to the interaction with the cations[7].
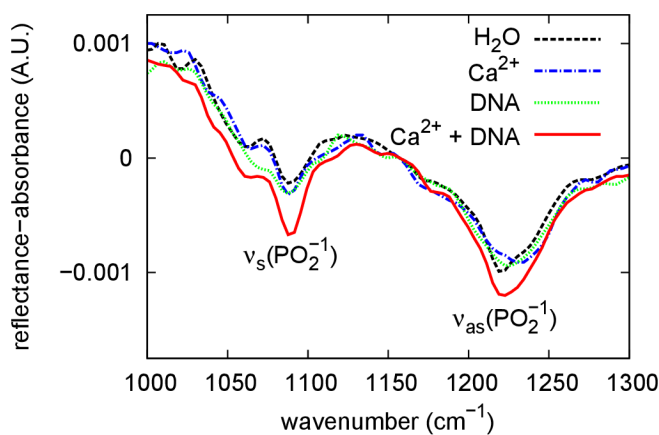
Figure 4.12. IRRAS of DOPC/DOPS monolayers at a surface pressure of 30 mN/m on different subphases consisting on Ca^{2+} 10 mM and 29.5 µg/ml DNA on 40 mM HEPES at pH = 7.4.

The IRRA spectrum in the presence of DNA is also plotted in fig. 4.12. In this case, the phosphate stretching bands are similar to those measured on pure buffer, so we can deduce that there is not any detectable binding of the DNA to the monolayer in the absence of Ca^{2+} cations in the subphase.

Following the procedure already mentioned above, we now analyze the IRRA spectrum of the phospholipid monolayer in the presence of both Ca^{2+} and DNA together. Only when Ca^{2+} cations and DNA are present together in the subphase we observed a significant intensity increase of these two bands indicating that DNA binds to the

phospholipid monolayer only in the presence of Ca^{2+}. This correlates with previous findings, as has already been explained in section 4.1.1. It is also remarkable that the presence of Ca^{2+} and DNA together in the subphase produced a $\nu_{as}(PO_2^-)$ band with the same COG as the one measured on the pure buffer for DOPC/DOPS monolayers. Therefore, this indicates that the water molecules should interact with both, DNA and lipid phosphate groups, in the ternary system monolayer/Ca^{2+}/DNA. Similar results of the phosphate band amplification were previously described by Brezesinski and Gromelski for DMPE zwitterionic monolayers using Ca^{2+} or Mg^{2+} cations to mediate the electrostatic interaction among the phospholipids and DNA[50]. The reason of this increase could be the contribution of DNA phosphate groups which bind to the monolayer under these specific conditions or a change in the phospholipid phosphate group vibrational transition moment (orientation of the headgroup) with respect to the interface plane[92]. Unfortunately, it is not possible to quantify each separate contribution based only on the increase of the phosphate stretching band intensity. At any rate, IRRAS measurements qualitatively confirm that the DNA binding to the DOPC/DOPS monolayer is mediated by Ca^{2+} cations at a molecular level.

4.2. LIPOPLEXES

Once we have determined the phospholipid monolayer/Ca²⁺/DNA complex formation at the air-water interface in section 4.1, we now extend the study to the three dimensions with the preparation of lipoplexes. To this aim, we used PC/PS 1:1 liposomes because our group is skilled in the preparation and characterization of these liposomes in the presence of cations[87,134]. We mixed this negatively charged liposomes with DNA and we induced the formation of lipoplexes by adding Ca²⁺ cations. We then employed a fluorescent probe exclusion assay to characterize the capability of lipoplexes to encapsulate DNA.

4.2.1. PC/PS 1:1/Ca²⁺/DNA characterization

We carried out GelRed® exclusion assays to elucidate the formation of anionic lipoplexes. First, we analyze the formation of PC/PS 1:1/Ca²⁺/DNA complexes as a function of the total phospholipid-DNA bp ratio, L/D:

$$\frac{L}{D} = \frac{n_{PC} + n_{PS}}{n_{DNAbp}} \qquad (25)$$

where n_{PC} and n_{PS} stand for PC and PS mole numbers, respectively and n_{DNAbp} stands for the DNA base pair mole number. We determine the optimal L/D for lipoplex formation and, later on, we characterize the effect of Ca²⁺ concentration.

Fluorescence spectra of the PC/PS 1:1/Ca²⁺/DNA system were

registered and the maximum intensities at λ_{ex} = 264 nm and λ_{em} = 608 nm are shown in fig. 4.13. DNA concentration is kept at 29.5 µg/ml in all the samples and the increasing L/D ratios are obtained by adding the proper amount of PC/PS 1:1 liposomes. The Ca^{2+} concentration was 10 mM in all the samples and they were also buffered with 40 mM HEPES pH = 7.4.
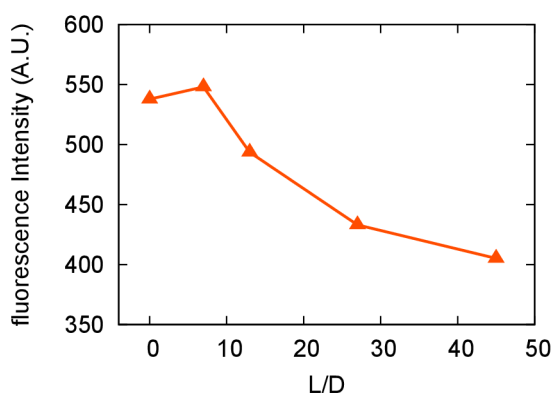
Figure 4.13. Fluorescence intensity at λ_{ex} = 264 nm and λ_{em} = 608 nm for PC/PS 1:1/Ca^{2+}/DNA complexes at different L/D ratios. The $Ca(NO_3)_2$ concentration was 10 mM, the DNA concentration was 29.5 µg/ml and the GelRed® was 15x (supplied at 10000x) in all the samples. All the samples were buffered with 40 mM HEPES pH = 7.4. T = 25 ºC.

L/D = 0 in fig. 4.13 corresponds to a control measurement of the fluorescence intensity of just DNA in these conditions. This fluorescence intensity kept invariant to the liposome addition to L/D = 7, but it fell down when the L/D is further increased. This decrease in fluorescence intensity as compared to the control at L/D = 0 can be understood if we consider DNA is now forming complexes with the liposomes and the Ca^{2+} cations and these complexes are not permeable to the fluorescent probe GelRed® to form the fluorescence emitting DNA-GelRed® pair.

However, the fluorescence intensity decrease at L/D = 27 and L/D = 45 was accompanied by the rapid formation of aggregates, so there could be other reasons for this decrease: on the one hand, the aggregates produce light dispersion, which could diminish the effective excitation and emission radiation intensities and, consequently, a possible fluorescence intensity decrease by inner filter effect[67]. On the other hand, there could be fluorescence quenching[67], if the fluorescent emission were deactivated by other species. Therefore, additional tests were required to assure the formation of lipoplexes from the results in fig. 4.13.

In particular, we designed the following experiment: a sample at L/D = 45 with 10 mM $Ca(NO_3)_2$ and 15x GelRed® was centrifuged at 16000g for 1 min to make the aggregates to fully sediment in the pellet. Then, the supernatant was recovered and EDTA was added at a final concentration of 50 mM. The same procedure was applied to a control sample with the same composition but without liposomes and the fluorescence spectra for both samples were recorded. As can be observed in fig. 4.14, the fluorescence intensity is lower for the sample than the control, proving that part of the DNA has been complexed, either with the aggregates or in a soluble complex in which the GelRed® cannot permeate. As it is going to be commented right after, the DNA-GelRed® fluorescence intensity changes with Ca^{2+} concentration. This concentration can be different for the control and the sample in fig. 4.14, because part of the Ca^{2+} is removed with the aggregates. This is the reason why we added 50 mM EDTA to remove all the Ca^{2+} both in the

control and the sample. In this way, we asssure that the fluorescence intensity differences between them are not due to different Ca^{2+} concentrations. Although aggregates were removed by centrifugation, there could be still soluble light dispersing particles that may produce inner filter effect, thus reducing the fluorescence intensity. In order to discern if the inner filter effect is the cause of the fluorescence intensity decrease observed in fig. 4.14, we registered UV-visible spectra of both the control and the sample (fig. 4.15). Since the resulting absorbance at both λ_{ex} = 264 nm and λ_{em} = 608 nm was the same for both samples, we discard the inner filter effect as a cause of the fluorescence intensity decrease. In conclusion, formation of PC/PS 1:1/Ca^{2+}/DNA complexes that keep DNA isolated from GelRed® is the cause of the decrease in the fluorescence intensity observed at increasing L/D in fig. 4.13.
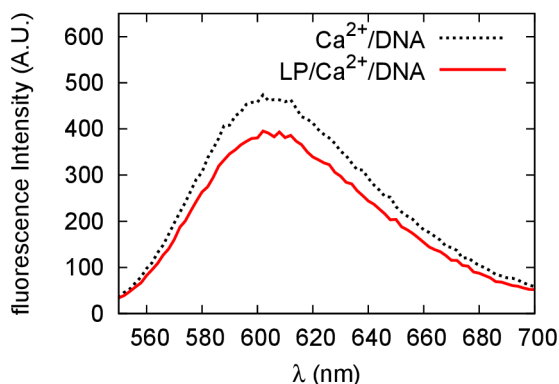
Figure 4.14. Fluorescence spectra of the control (Ca^{2+}/DNA) and the sample (LP/Ca^{2+}/DNA) supernatant. The total phospholipid concentration was 4 mM, the DNA concentration was 29.5 µg/ml (L/D = 45) and the GelRed® was 15x (supplied at 10000x) in both samples. EDTA was added to each supernatant at a final concentration of 50 mM. Both samples were buffered with 40 mM HEPES pH = 7.4. T = 25 ºC.

The results shown in fig. 4.13 are in good agreement with those

reported by Rodríguez-Pulido *et al.*[131], in which the DNA is encapsulated in cationic DODAB/DOPE and DODAB/DLPC liposomes and the fluorescence intensity of EdBr gradually diminishes until it totally vanishes at high enough L/D. Unfortunately, this assymptotical behavior could not be reproduced with PC/PS 1:1 anionic liposomes because at L/D = 45 the total phospholipid concentration is 4 mM, which is technically difficult to increase. Besides, an increase of L/D by diminishing DNA concentration implies a loss in signal-noise ratio.

We now analyze the effect of Ca^{2+} concentration in the formation of lipoplexes. To this aim, we measured the fluorescence intensity of PC/PS 1:1/Ca^{2+}/DNA complexes at different $Ca(NO_3)_2$ concentrations. It is well known that the divalent cations induce structural changes in DNA[31,101,149]. Hence, DNA-probe fluorescence emission is a function of the concentration of Ca^{2+}, as described by other authors[3,113]. Therefore, a control measurement of DNA-GelRed® fluorescence intensity at each Ca^{2+} concentration is necessary to elucidate the role of Ca^{2+} in the lipoplex formation.
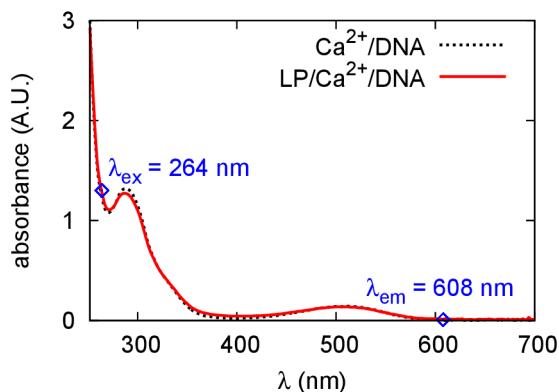
Figure 4.15. UV-visible spectra of the control (Ca^{2+}/DNA) and the sample (LP/Ca^{2+}/DNA) supernatant. The total phospholipid concentration was 4 mM, the DNA concentration was 29.5 µg/ml (L/D = 45) and the GelRed® was 15x (supplied at 10000x) in both samples. EDTA was added to each supernatant at a final concentration of 50 mM. Both samples were buffered with 40 mM HEPES pH = 7.4.

In fig. 4.16 we show the fluorescence intensity of a) liposomes/Ca^{2+}/DNA complexes (LP/Ca^{2+}/DNA) and b) DNA, as a function of Ca^{2+} concentration. Remarkably, LP/Ca^{2+}/DNA complexes reduced their fluorescence intensity as the concentration of Ca^{2+} increases, hence demonstrating the role of Ca^{2+} cations in mediating the anionic liposome-DNA interaction. On the contrary, DNA-GelRed® fluorescence intensity recorded in the absence of liposomes increased with the concentration of Ca^{2+}. Both tendencies saturated at high Ca^{2+} concentrations and were reproducible. Given that the fluorescence intensity does not totally vanish, we deduce that PC/PS 1:1 liposomes only partially complexate DNA in the presence of Ca^{2+} cations at these conditions. Hence, the fluorescence intensity in the liposomes/Ca^{2+}/DNA samples is due to the DNA that remains non-complexed. Taking into account that Ca^{2+} enhances DNA-GelRed® fluorescence (fig. 4.16) when Ca^{2+} is added to the mixture of PC/PS 1:1 liposomes and DNA, the

resulting fluorescence intensity must be influenced by both, the decrease due to the formation of lipoplexes and the increase due to Ca^{2+}-enhancement. Despite these opposite effects, the total fluorescence intensity of the liposomes/Ca^{2+}/DNA decreases when the Ca^{2+} concentration is increased, according to the results shown in fig. 4.16.

Additional information can be inferred from a detailed analysis of the fluorescence intensity curves in fig. 4.16. Let us first discuss the DNA fluorescence intensity as a function of the concentration of Ca^{2+}. We have observed that Ca^{2+} enhances fluorescence intensity and the higher the Ca^{2+} concentration is, the more intense the effect is until the fluorescence intensity saturates at 20 mM Ca^{2+}. This contrasts with the results reported by Patil *et al*.[120] for the plasmid DNA-EdBr, where the addition of Ca^{2+} produced a decrease in the fluorescence intensity. The main differences with our measurements are the use of circular DNA, a different probe and also the order in which the Ca^{2+} is added (they added Ca^{2+} after the probe whereas in our samples the Ca^{2+} was added before the probe). The mentioned factors can influence the DNA-probe intensity as a function of the concentration of Ca^{2+}, because they can affect the DNA-probe binding constant, the DNA-probe complex geometry, the fluorescence quantum yield and the way they all react to Ca^{2+} addition. A detailed analysis about the DNA-probe fluorescence can be found in refs [47] and [6]. However, there are no published results of ctDNA-GelRed® fluorescence as a function of Ca^{2+} concentration so far.

We now analyze the PC/PS 1:1/Ca^{2+}/DNA complex fluorescence

intensity as a function of Ca^{2+} concentration (fig. 4.16). As has been already mentioned, the fluorescence intensity decreases as the Ca^{2+} concentration increases until reaching a saturation at 5 mM Ca^{2+}. Importantly, the liposome/DNA fluorescence intensity in the absence of Ca^{2+} is higher than the one recorded for the DNA-GelRed® alone. This difference in fluorescence intensity is much higher than the one recorded for the liposomes-GelRed®, which suggests that liposomes and DNA somehow interact in the absence of Ca^{2+} cations, thus reinforcing the DNA-GelRed® fluorescence. However, when more Ca^{2+} is added, the fluorescence intensity decreases due to the formation of complexes in which the DNA is not accessible to GelRed® any more. In this way, the PC/PS 1:1/Ca^{2+}/DNA complex fluorescence intensity diminishes as compared to that obtained for DNA at the same Ca^{2+} concentration. The curve saturation at high Ca^{2+} concentrations gives additional insight about the lipoplex formation. As has already been discussed, Ca^{2+} enhances DNA-GelRed® fluorescence, so one could expect some loss of fluorescence intensity when aggregates form at high L/D, as some amount of Ca^{2+} would be retained with the aggregates. In this case, the fluorescence intensity should rise up at high Ca^{2+} concentrations, because the amount of Ca^{2+} in solution should increase. Conversely, the PC/PS 1:1/Ca^{2+}/DNA complex fluorescence intensity saturation at high Ca^{2+} concentrations proves that this premise does not hold. In conclusion, the fluorescence intensity trends observed in fig. 4.16 confirm the Ca^{2+}-mediated lipoplex formation between PC/PS 1:1 liposomes and ctDNA.
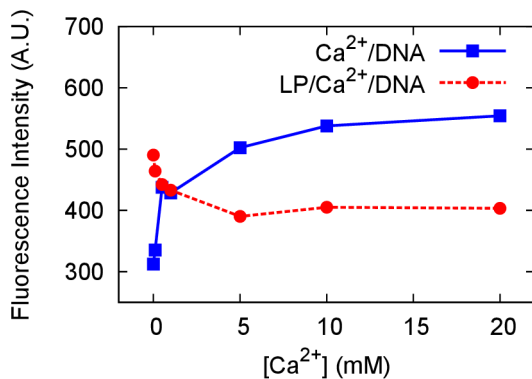
**Figure 4.16**. Fluorescence intensity at λ_{ex} = 264 nm and λ_{em} = 608 nm for PC/PS 1:1/Ca^{2+}/DNA complexes at different Ca(NO$_3$)$_2$ concentrations. The total phospholipid concentration was 4 mM, the DNA concentration was 29.5 µg/ml (L/D = 45) and the GelRed® was 15x (supplied at 10000x) in all the samples. All the samples were buffered with 40 mM HEPES pH = 7.4. T = 25 ºC.

4.3. SIMULATIONS

In the previous sections, we have experimentally characterized the role of Ca^{2+} in mediating the interaction between negatively charged phospholipid mixtures and DNA both at the air-water interface and in bulk. In order to evaluate the role of electrostatic interactions in the formation of this complex as well as to assess the influence of different design variables in the stability of this system, we address a Monte Carlo simulation study on the basis of a coarse grain model to predict the adsorption of a polyanion (PA) onto a like-charged surface. Trivalent cations have been chosen as mediators to develop this simulation tool with the most noticeable effect. In the sections below, the nature of the M^{3+}-mediated PA adsorption onto like-charged surfaces is analyzed and then the influence of the PA charge, the surface charge density, MX_3 concentration and the M^{3+} diameter is discussed. Additionally, estimations of the radius of gyration are used to give insight about the intensity of the adsorption attending to conformational properties.

4.3.1. Trivalent cations induce polyanion adsorption onto like-charged surfaces

In fig. 4.17a, we show $F(z)$ (denoted as F for simplicity) for different numbers of charged monomers in the chain (f). In particular, simulations for f = 5, 10 and 20 were performed with a surface charge density of -0.20 Cm^{-2}, in the presence of 30 mM MX_3 ([3:1] salt). All PAs are formed by 20 monomers. Each monomer holds either -e or 0 electric

charge. Therefore, the PA reduced net charge (Q/e) is equal to f. Charged monomers are homogeneously distributed in the chain. As can be seen, the Helmholtz free energy profiles increase asymptotically at very short distances to the charged plane, display a minimum (denoted as F_{min}) at a short distance and converge to 0 at high distances. Therefore, at very short distances, volume excluded effects dominate the interaction producing a strong repulsion. When the PA separates to avoid contact with the plane at short distance, favorable electrostatic interactions between the PA and the adsorbed trivalent cations attract the PA and promote the adsorption. However, if the distance from the PA to the charged plane keeps increasing, then electrostatic interactions are screened and the charged surface does not influence the PA anymore. Therefore, if the adsorbed PA moves beyond the minimum region, then it does not immediately *readsorb* because there is no a direct attractive force driving it to the well of the potential. In conclusion, these curves give valuable information about PA adsorption behavior onto the like-charged surface. That is the PA adsorbs onto a like-charged surface at these conditions and this adsorption is reversible since desorption is possible with enough thermal agitation.

To give insight into the PA adsorption onto like-charged surfaces, it is quite instructive to analyze the ionic profiles in the simulation cell in the absence of PA. For that reason, ion distribution functions ($g(z)$) for counterions (M^{3+}) and coions (X^-) as well as the charge density profile are shown in fig. 4.17b (inset). M^{3+} adsorption onto the negatively charged surface is evident from its distribution function $g_M(z)$ which

increases several orders of magnitude over the value in bulk at short distances from the charged plane. In addition, the presence of a maximum in the coion profile ($g_X(z)$) together with a minimum in $g_M(z)$ at z = 1.2 nm reveals that there is a considerable accumulation of coions near the adsorbed counterions. Quesada-Pérez *et al*. also reported this kind of electric double layer at similar conditions by both hypernetted-chain/mean-spherical-approximation (HNC/MSA) theory and MC simulations[125]. This characteristic electrolyte organization also suggests that the electric double layer has undergone the phenomenon known as charge inversion in the region near the negatively charged surface. This effect can be more clearly appreciated plotting the integrated surface charge density, $\sigma_{int}(z)$ (see fig. 4.17b), which is calculated integrating the contributions from the negatively charged surface and all the particles enclosed between the charged surface and a parallel plane placed at a distance z. As can be seen, $\sigma_{int}(z)$ is negative at the immediate vicinity of the negatively charged plane but becomes positive where the charge inversion takes place, in the region between z = 0.4 and 3.4 nm, approximately. At higher distances, $\sigma_{int}(z)$ converges to zero, indicating the neutralization of the surface charge in the bulk. Similar profiles of $\sigma_{int}(z)$ were obtained by Wang *et al*. by using the NLDFT model in the presence of PA[158]. Additionally, Turesson *et al*. reproduced this charge inversion profile with MC simulations for linear and branched negatively charged polymers interacting with like-charged surfaces in the presence of Ca^{2+}.[155] Importantly, the charge inversion region marked in fig. 4.17b reasonably matches the previously mentioned F_{min} region. This fact in

conjunction with the M^{3+} adsorption onto the negatively charged surface evidenced by $g_M(z)$, validates the hypothesis formulated above about the essential role of the M^{3+} in the PA adsorption onto a like-charged surface, by creating favorable electrostatic interactions.

In order to study the influence of electrostatic interactions in the PA adsorption onto like-charged surfaces mediated by trivalent cations, we analyze the magnitude of the adsorption (characterized by the depth of the well of the Helmholtz free energy) as a function of the electric charge of the interacting objects: on the one hand we study the adsorption of different net charge PAs onto the same like-charged surface in this section. On the other hand, we study the adsorption of the same PA onto different like-charged surfaces with different charge density in the next section.

4.3.2. Influence of the polyanion charge

The role of the total PA charge f is also investigated from the F profiles in fig. 4.17a. Observing the F_{min} region, we can conclude that the more charged the PA is, the deeper the F well is. In other words, the higher f is, the greater the F minimum absolute value ($|F_{min}|$) is. $|F_{min}|$ values for the three PAs studied as a function of the total PA charge ($f = 5$, $f = 10$ and $f = 20$) are shown in fig. 4.17a (inset). These results highlight the role of electrostatic interactions in the PA adsorption onto like-charged surfaces, because it has been proven that the adsorption is stronger when the PA is more charged. This means that, once the PA

adsorption has taken place, desorption is more difficult when the PA charge is higher. In agreement with the results shown in fig. 4.17a, Messina *et al*. observed that M^{3+}-mediated PA adsorption onto a like-charged sphere was favored by the total PA charge and a poorly charged PA was strongly repelled from the particle in aqueous solution[95]. Additionally, Turesson *et al*. simulations with increasing polymerization degree PAs produced an increase in the surface excess of PA monomers, what confirms that the Ca^{2+}-mediated PA adsorption is enhanced by the total PA charge[155]. In conclusion, total PA charge modulates the adsorption onto a like-charge surface.

We have also obtained additional information about the intensity of the adsorption from the number of mean adsorbed monomers (N_{ad}) and the standard deviation (s) of this magnitude were computed as measurements of the adsorption intensity and dispersion, respectively ($N_{ad} \pm s$). We performed these calculations within simulations where the CM of the PA is restricted to the interval between $z = 0$ and $z = 5$ nm, because the F minimum is located in this interval in all the cases. The results for N_{ad} represented in fig. 4.17a are 8 ± 4, 11 ± 3 and 12 ± 3 for the PAs with $f = 5$, $f = 10$ and $f = 20$, respectively. That is to say, there is a direct correlation between the number of adsorbed monomers and the PA charge. Accordingly, Dias *et al*. observed $N_{ad} = 20$ in a simulation for a 50-monomer PA interacting with a negatively charged responsive surface[24], being the mean adsorbed monomers-total PA monomers ratio similar to the results reported here.
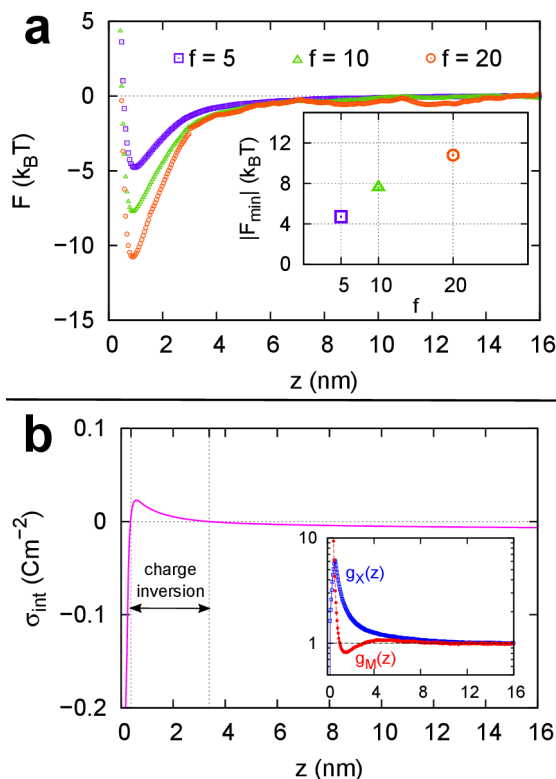
Figure 4.17. A) Helmholtz free energy (*F*) as a function of the distance of the center of mass of the PA to the charged surface (*z*), for 20-monomer PAs with different number of charged monomers *f* = 5 (squares, purple), *f* = 10 (triangles, green), *f* = 20 (circles, orange). The monomer charge is -*e*. The surface charge density is -0.20 Cm^{-2} and the MX$_3$ concentration is 30 mM. Reprinted with permission from ref. [76]. Copyright (2014) AIP publishing LLC.

4.3.3. Influence of the surface charge density

In this section, we explore the role of the surface charge density in the PA adsorption onto like-charge surfaces. To this aim, we performed simulations at the charge densities σ_0 = -0.04, -0.12 and -0.20 Cm^{-2} whereas other parameters were kept constant. In fig. 4.18a

we show the results for the system Helmholtz free energy F as a function of the distance of the PA to the charged plane z, for the three different surface charge densities studied. As we have already explained in the previous section, the minimum in the F profile evidences the PA adsorption onto the like-charged surface. The absolute value of this minimum $|F_{min}|$ increases when the surface is more negatively charged (see fig. 4.18a, inset). In this way, the most intense adsorption takes place at the charge density of σ_0 = -0.20 Cm^{-2}; the adsorption is lower at σ_0 = -0.12 Cm^{-2} and it is negligible at σ_0 = -0.04 Cm^{-2}. In agreement with the results shown in fig. 4.18a, Wang *et al*. observed that M^{3+}-mediated PA adsorption onto like-charged surfaces enhanced when increasing the surface charge density[158]. Furthermore, Turesson *et al*. observed an increase in the adsorption excess of PA monomers when they increased the surface charge density in absolute value in the presence of Ca^{2+}.[155] In this regard, we have also quantified the magnitude of the adsorption with the number of mean adsorbed monomers ($N_{ad} \pm s$), being 4 ± 4, 9 ± 4 and 12 ± 3 for σ_0 = -0.04, -0.12 and -0.20 Cm^{-2}, respectively. The tendency of these values is the same as $|F_{min}|$ (fig. 4.18a, inset) and, since $N_{ad} = s$ for σ_0 = -0.04 Cm^{-2}, there is no evidence of adsorption at this surface charge density. Dias *et al*. characterized N_{ad} in simulations with positively charged responsive surfaces and they also found that the more charged the surface was, the more intense the PA adsorption onto oppositely-charged surfaces was[24].

Integrated charge density profiles $\sigma_{int}(z)$ for these systems in the absence of PA are shown in fig. 4.18b. The comparison of $\sigma_{int}(z)$ for the

three different surface charge densities provides an additional interpretation from the Helmholtz free energy curves shown in fig. 4.18a. Charge inversion is evident when σ_0 is -0.20 or -0.12 Cm^{-2}. Moreover, $\sigma_{int}(z)$ becomes more positive when $\sigma_0 = -0.20$ Cm^{-2} than $\sigma_0 = -0.12$ Cm^{-2}, what means the charge inversion is stronger in the former case. Hence, the attractive surface-PA interaction and the adsorption should be more intense at $\sigma_0 = -0.20$ Cm^{-2} than $\sigma_0 = -0.12$ Cm^{-2}, in good agreement with the results shown in fig. 4.18a. Importantly, there is no charge inversion at $\sigma_0 = -0.04$ Cm^{-2}, as can be appreciated in the corresponding integrated charge density $\sigma_{int}(z) \leq 0$ at any distance to the charged plane. These results agree with a previous work in which the effect of the surface charge density on the charge inversion was studied by means of electrophoresis experiments as well as MC simulations[89]. Accordingly, this feature confirms the role of ionic correlations in promoting the M^{3+}-mediated PA adsorption onto like-charged surfaces via surface charge inversion. Wang *et al*. also observed that the magnitude of this charge inversion increased when the magnitude of the surface charge density, $|\sigma_0|$, was increased[158]. However, they used much higher values of $|\sigma_0|$ and they did not explore the lack of charge inversion at low $|\sigma_0|$.

We also represent the counterion and coion distribution functions, $g_M(z)$ and $g_X(z)$, respectively (fig. 4.18b, inset) for $\sigma_0 = -0.04$ Cm^{-2}. In this case, $g_M(z) \geq g_X(z)$ at all distances from the charged plane z, that is to say, trivalent counterions M^{3+} are adsorbed onto the negatively charged

surface while coions X^- interpenetrate the counterion diffuse layer to compensate the charge. This is in contrast with the ion correlations calculated at $\sigma_0 = -0.20$ Cm^{-2} (fig. 4.17b, inset), where the $g_M(z)$ decreases under $g_X(z)$ and displays a minimum, revealing charge inversion.
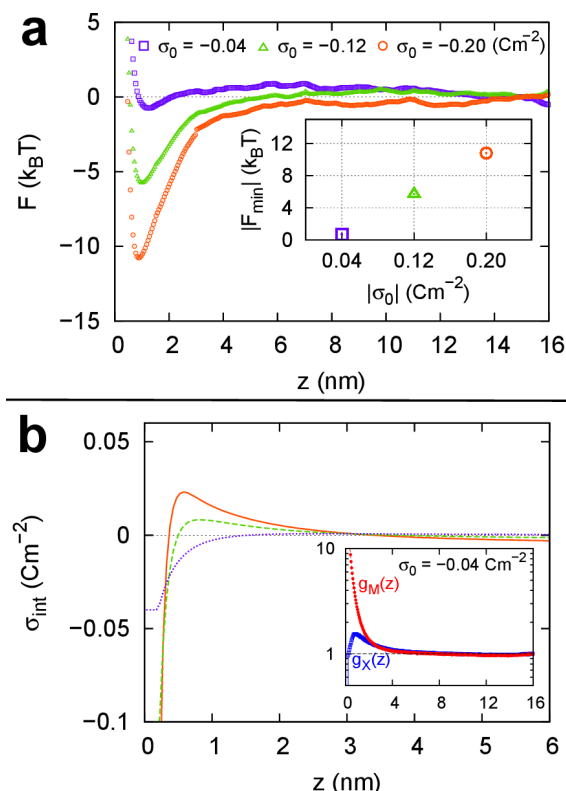
Figure 4.18. (A) Helmholtz free energy F as a function of the distance of the center of mass of the PA to the charged surface (z) for PAs interacting with like-charged surfaces of surface charge density $\sigma_0 = -0.04$ Cm^{-2} (squares, purple), $\sigma_0 = -0.12$ Cm^{-2} (triangles, green), $\sigma_0 = -0.20$ Cm^{-2} (circles, orange). All simulations are carried out with a 20 charged monomer PA in the presence of 30 mM MX$_3$. Inset: Absolute value of the minimum of F ($|F_{min}|$) as a function of the absolute value of σ_0. (B) Integrated charge densities σ_{int} as a function of z for $\sigma_0 = -0.04$ Cm^{-2} (dotted, purple), $\sigma_0 = -0.12$ Cm^{-2} (dashed, green), $\sigma_0 = -0.20$ Cm^{-2} (solid, orange). Inset: Counterion and coion distribution functions $g_M(z)$ (red) and $g_X(z)$ (blue), respectively for $\sigma_0 = -0.04$ Cm^{-2}. Reprinted with permission from ref. [76]. Copyright (2014) AIP publishing LLC.

4.3.4. Radius of gyration

In this section, we extend the characterization of the adsorption from chain conformation analysis. To this aim, we have calculated the radius-of-gyration projections parallel and perpendicular to the charged surface (eqs. 23 and 24). Fig. 4.19 shows the results obtained for different surface charge densities (and a MX_3 concentration of 30 mM). As can be seen, both projections are considerably smaller than the end-to-end distance that would correspond to a highly extended chain, which means that the PA chain is partly collapsed in the presence of trivalent cations. Our results also show the projection of the radius of gyration onto the *xy*-plane increases with the absolute value of the surface charge density and the degree of adsorption whereas the projection in the *z*-direction decreases. In other words, the chain shrinks in the direction perpendicular to the surface but it expands in the parallel directions. In addition, $\langle R_{Gxy}^2 \rangle^{1/2} < \sqrt{2} \langle R_{Gz}^2 \rangle^{1/2}$ for $\sigma_0 = -0.04$ C/m^2 but $\langle R_{Gxy}^2 \rangle^{1/2} > \sqrt{2} \langle R_{Gz}^2 \rangle^{1/2}$ for $\sigma_0 = -0.20$ C/m^2, which implies that the chain is more expanded in the direction perpendicular to the surface for low surface charge density but becomes more expanded in the parallel directions when this parameter grows. In any case, this behavior allows the chain to increase the number of beads near the surface and the degree of adsorption when the charge of the surface increases.
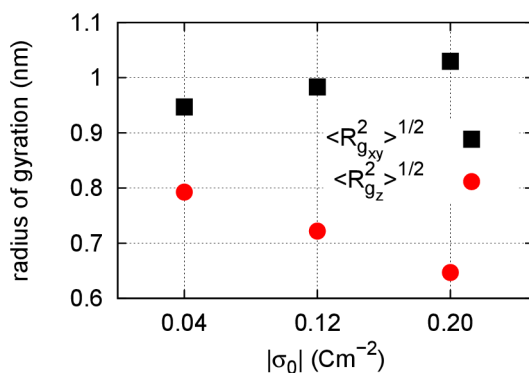
Figure 4.19. Projections of the radius of gyration onto the *xy*-plane (squares) and the *z*-axis (circles) as a function of the surface charge density. Simulations are carried out with a 20 monomer PA in the presence of 30 mM MX_3. Reprinted with permission from ref. [76]. Copyright (2014) AIP publishing LLC.

4.3.5. Influence of the multivalent salt concentration

In section 1 we have shown that PAs are adsorbed onto like-charged surfaces in the presence of M^{3+} due to the ionic correlations, which reverse the charge surface leading to the adsorption. Taking into account that the ionic correlations depend on the MX_3 concentration c, one could expect that M^{3+}-mediated PA adsorption onto like-charged surfaces is modulated by this concentration. To this aim, we have performed simulations at different c and the results are shown in fig. 4.20.

We first present the system Helmholtz free energy F as a function of z for a set of increasing concentrations of MX_3, c = 10, 20, 30, 40 and 90 mM (fig. 4.20a). Although 90 mM is commonly a high concentration

for trivalent ions, osmotic stress experiments on DNA in the presence of Co^{3+} solutions up to 100 mM have been performed in the literature[128]. In addition, high calcium (and sometimes magnesium) concentrations have been also used to mediate PA adsorption onto like-charged surfaces in many other systems[155]. In any case, we have analyzed this high concentration for theoretical purposes: To find out if the attraction between the PA and the surface displays a non-monotonic behavior with c. The magnitude of $|F_{min}|$ is plotted as a function of c in fig. 4.20a (inset). As can be seen, the depth of the minimum hardly changes when the concentration is increased from 10 to 40 mM but drops when c is increased to 90 mM. These results for the surface-PA electrostatic interaction (in the presence of trivalent cations) agree with those obtained by Turesson *et al*. for adsorption onto like-charged surfaces in the presence of Ca^{2+}.[155] Ulrich *et al*. also reported a similar behavior for PA adsorption onto an oppositely-charged sphere[156]. It should be also mentioned that Wang *et al.* predicted trivalent-cation-mediated adsorption onto a like-charged planar surface at salt-free solutions and high salt concentrations of the order of 0.5 M, even larger than the values studied in this work, although they did not explore intermediate concentrations[158].

Integrated charge distributions represented in fig. 4.20b permit us to elucidate the role of charge inversion in the PA adsorption onto like-charged surfaces at different M^{3+} concentrations. As can be seen, σ_{int} reverses its sign at the charged surface vicinity displaying a maximum that increases with c. Conversely, this c-enhanced charge inversion is

not correlated with the PA-adsorption onto the like-charged surface, because at c = 90 mM the adsorption diminishes while the magnitude of the charge inversion is the highest. Examining $g_M(z)$ and $g_X(z)$ at this M^{3+} concentration (fig. 4.20b, inset), we find that counterions and coions form the electric double layer but, unlike the simulations at c = 30 mM (fig. 4.17b, inset), the counterions display a pronounced maximum after the minimum. As a consequence, the effect of the charge inversion is totally screened at short distances to the negatively charged plane. In fact, it can be appreciated in the integrated charge distribution at c = 90 mM in fig. 4.20b, that the charge density drops to zero at shorter distances than the ones at more diluted regimes. In conclusion, the balance between the charge inversion and the screening produced at different MX_3 concentrations determine the magnitude of the PA-adsorption onto like-charged surfaces, being the adsorption optimal at intermediate MX_3 concentrations.
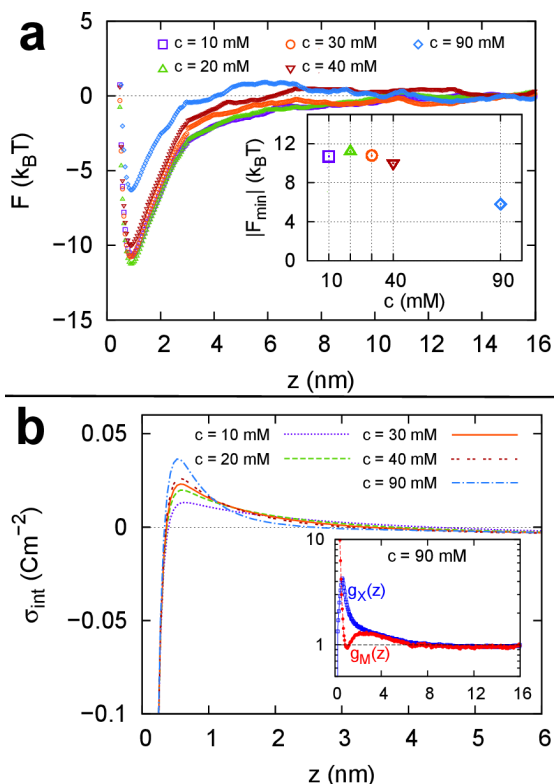
Figure 4.20. (A) Helmholtz free energy F as a function of the distance of the center of mass of the PA to the charged surface (z), for a 20 charged monomer PA interacting with a like-charged surface of surface charge density σ_0 = -0.20 Cm^{-2} in the presence of different MX_3 concentrations: c = 10 mM (squares, purple), 20 mM (up triangles, green), 30 mM (circles, orange), 30 mM (down tringes, brown) and 90 mM (inverted squares, blue). Inset: Absolute value of the minimum of F ($|F_{min}|$) as a function of c. (B) Integrated charge density σ_{int} as a function of z. Inset: Counterion and coion distribution functions, $g_M(z)$ (red) and $g_X(z)$ (blue), respectively for c = 90 mM. Reprinted with permission from ref. [76]. Copyright (2014) AIP publishing LLC.

4.3.6. Influence of the counterion diameter

In the sections above, we have discussed the role of trivalent cations in promoting the PA adsorption onto like-charged surfaces. The

high valence of trivalent cations facilitates the surface charge inversion and creates strong attractive interactions that stabilize the system during the adsorption. Nevertheless, beside the electrostatic interactions, volume excluded effects modulate the surface-PA interaction as well. Furthermore, trivalent cations in solution are covered by a hydration shell that may interfere the direct contact with negatively charged objects. Therefore, simulations with M^{3+} of different diameter allows us to characterize the strength of steric repulsions in the surface/M^{3+}/PA complex formed upon adsorption.

Helmholtz free energy profiles for PAs interacting with like-charged surfaces in the presence of either 0.4 or 0.8 nm diameter trivalent cations are shown in fig. 4.21. Both curves display a minimum near the surface. Hence, the PA adsorption onto the like-charge surface takes place when it is mediated by trivalent cations of the studied diameters. However, the adsorption is weaker in the case the M^{3+} diameter d_M = 0.8 nm, since F profile displays a minimum of less absolute value. In other words, doubling the M^{3+} diameter results in a loss of stability in the surface/M^{3+}/PA complex. Steric repulsion, which is accounted for in these simulations through the hard sphere potential, keeps every pair of particles separated at a distance of at least the sum of their radii. As a consequence, when the M^{3+} diameter is increased, the distance between M^{3+} and the PA monomers and the distance between M^{3+} and the negatively charge plane turns larger and this weakens the electrostatic interactions that stabilize the surface/M^{3+}/PA complex. In conclusion, the M^{3+}-mediated PA adsorption onto like-charged surfaces

is less intense when the M^{3+} diameter is increased.

Remarkably, the results shown in fig. 4.21 give insight about the role of electrostatic interactions in the PA adsorption onto like-charged surfaces in the presence of hydrated trivalent cations. In this way, the increase in the effective ion radius because of the solvation produces a reduction in the pairwise Coulomb potential between M^{3+} and the negatively charged objects. In fact, the value of d_M = 0.8 nm used in this simulation is close to the hydrated ion diameter of some trivalent metals (Al^{3+} - 0.96 nm)[55]. However, the CG model presented here cannot predict the role of water molecules as the solvent is treated as continuum. In this way, all-atomistic simulations could provide valuable information about the effect of the water molecules in the M^{3+}-mediated PA adsorption onto like-charged surfaces, in terms of interaction potential and entropy. The first results in this line with MD simulations have been recently published[36,85]. According to these results, the Ca^{2+} plays an essential role in the DNA adsorption onto a negatively charged PS monolayer by either directly bridging the interaction between negatively charged groups or inducing a rearrangement in the monolayer configuration and exposing positively charged groups as DNA binding sites. Future simulations with cations of different nature and valences would be useful to compare the results reported here about the effect of volume excluded effects through the hydrated cation diameter.
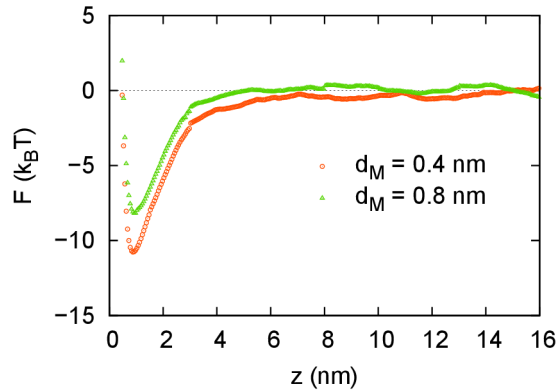
Figure 4.21. Helmholtz free energy *F* as a function of the distance of the center of mass of the PA to the charged surface (*z*) for a 20 charged monomer PA interacting with a like-charged surface of surface charge density σ_0 = -0.20 Cm^{-2} in the presence of 30 mM MX_3 for two different trivalent cation diameters: d_M = 0.4 nm (circles, orange) and d_M = 0.8 nm (triangles, green). Reprinted with permission from ref. [76]. Copyright (2014) AIP publishing LLC.

CHAPTER 5: CONCLUSIONS AND REMARKS

The experimental and theoretical results discussed in section 4 clearly evidence the spontaneous formation of a ternary complex anionic membrane/cation/polyanion. Thus, we have extended the biophysical characterization of these systems, describing a variety of features such as their capability to encapsulate DNA, the influence of lateral packing in their morphology at the interface or the role of electrostatic interactions in their formation/destabilization mechanism. The main conclusions of this thesis are summarized here:

- Ca^{2+} mediates complexation of anionic phospholipid films with DNA in solution and at the air-water interface.

- Anionic lipoplexes form spontaneously from PC/PS 1:1 negatively charged liposomes and DNA in the presence of Ca^{2+}. Complexation increases with both the lipid-DNA ratio and the concentration of Ca^{2+}. The binding saturates at high concentrations of cations, as predicted by coarse-grain models.

- The surface pressure modulates the complexation of anionic saturated phospholipid monolayers at the air-water interface. Complexation takes places at lower lateral packing (i.e. surface coverage, surface pressure), while DNA molecules are expelled from the monolayer at high lateral compression.

- DPPC/DPPS 4:1 monolayer/Ca^{2+}/DNA interaction results in film fluidisation and formation of interfacial aggregates, whose morphology and size depends on the lateral packing and hence could be potentially modulated by the surface pressure. At low

surface pressures, DNA complexates mainly at DPPS-enriched domains forming fractal net-like structures. At higher surface pressure, phospholipid/DNA complexation adopts the form of fibers lying on a discontinuous monolayer.

- Phosphate groups have been experimentally identified as functional groups involved in Ca^{2+}-mediated DNA binding to unsaturated DOPC/DOPS 1:1 monolayers. These moieties keep hydrated upon formation of the ternary complex at the air-water interface.

- Although different sorts of interactions are involved in anionic lipoplex formation, the trivalent-cation-mediated attraction between a negatively charged surface and a polyanion can be predicted considering purely electrostatic interactions. The range of the interaction is limited to a few nanometers. Beyond this point, electrostatic attractive forces are so weak that they do not lead to adsorption.

- Electrostatic polyanion adsorption onto like-charged surfaces mediated by trivalent cations increases with the electric charge of either the polyanion or the surface. Since the magnitude of the interaction, in terms of the shift in the π-A isotherm, is the same between zwitterionic and anionic monolayers in real systems, a more detailed model, taking into account surface effects and hydration, is requiered to fully describe the formation, stability and

function of anionic lipoplexes.

- Surface charge inversion promotes electrostatic polyanion adsorption onto like-charged surfaces mediated by trivalent cations. This adsorption is weakened at high electrolyte concentrations due to electrostatic screening. Therefore, a delicate balance between charge inversion and electrostatic screening determines the strength of the attraction.

To sum up, an innovative application of complementary experimental and theoretical approaches have allowed to improve current knowledge about the formation/stablisation mechanisms of anionic lipoplexes. In this study, we present new results that extend the physicochemical characterization of the anionic membrane-cation-polyanion ternary system. In this way, we have analyzed in detail the role of lateral packing in the resulting structures at the interface and the role of electrostatic interactions in the formation/destabilization of complexes. At this point, further research is needed to evaluate the influence of the different sorts of interactions concerning anionic lipoplexes. From the results presented here, a wider characterization with other systems should help to understand better the formation, stability and function of anionic lipoplexes. To this aim, refinement of the different experimental and theoretical approaches used in this work and others is desireable. Only in this way, we may achieve a rational design and production of anionic lipopolex for a biomedical purpose in the future.

REFERENCES

(1) Antipina MN, Gainutdinov RV, Rachnyanskaya AA, Tolstikhina AL, Yurova TV, Khomutov GB. Studies of Nanoscale Structural Ordering in Planar DNA Complexes with Amphiphilic Mono- and Polycations. *Surf Sci*. **2003**; *532-535*, 1025-33.

(2) Antipina MN, Schulze I, Heinze M, Dobner B, Langner A, Brezesinski G. Physical–Chemical Properties and Transfection Activity of Cationic Lipid/DNA Complexes. *ChemPhysChem*. **2009**; *10*, 2471-9.

(3) Avitabile M, Sciacca G, Raciti G. Influence of Different Counterions on the Fluorescent Probe-DNA Complex. *Ital J Biochem*. **1992**; *41*, 1-8.

(4) Barrán-Berdón AL, Muñoz-Úbeda M, Aicart-Ramos C, Pérez L, Infante M, Castro-Hartmann P, Martín-Molina A, Aicart E, Junquera E. Ribbon-type and Cluster-type Lipoplexes Constituted by a Chiral Lysine Based Cationic Gemini Lipid and Plasmid DNA. *Soft Matter*. **2012**; *8*, 7368-80.

(5) Behroozi F. Theory of Elasticity inTwo Dimensions and its Application to Langmuir-Blodgett Films. *Langmuir*. **1996**; *12*, 2289-91.

(6) Bhattacharya S, Mandal SS. Interaction of surfactants with DNA. Role of Hydrophobicity and Surface Charge on Intercalation and DNA Melting. *Biochim Biophys Acta*. **1997**; *1323*, 29-44.

(7) Binder H, Zschornig O. The Effect of Metal Cations on the Phase Behavior and Hydration Characteristics of Phospholipid Membranes. *Chem Phys Lipids*. **2002**; *115*, 39-61.

(8) Blume A. Properties of Lipid Vesicles: FT-IR Spectroscopy and Fluorescence Probe Studies. *Curr Opin Colloid Interface Sci*. **1996**; *1*, 64-77.

(9) Boda D, Chan K, Henderson D. Monte Carlo Simulation of an Ion-dipole Mixture as a Model of an Electrical Double Layer. *J Chem Phys*. **1998**; *109*, 7362-71.

(10) Bohinc K, Brezesinski G, May S. Modeling the Influence of Adsorbed DNA on the Lateral Pressure and Tilt Transition of a Zwitterionic Lipid Monolayer. *Phys Chem Chem Phys*. **2012**; *14*, 10613-21.

(11) Boroudjerdi H, Kim YW, Naji A, Netz RR, Schlagberger X, Serr A. Statics and Dynamics of Strongly Charged Soft Matter. *Phys Rep*. **2005**; *416*, 129-99.

(12) Carnal F, Stoll S. Adsorption of Weak Polyelectrolytes on Charged Nanoparticles. Impact of Salt Valency, pH, and Nanoparticle Charge Density. Monte Carlo Simulations. *J Phys Chem B*. **2011**; *115*, 12007-18.

(13) Chandler D. *Introduction to Modern Statistical Mechanics*. Oxford University Press, **1987**.

(14) Chen Q, Kang X, Li R, Du X, Shang Y, Liu H, Hu Y. Structure of the complex monolayer of gemini surfactant and DNA at the air/water interface. *Langmuir*. **2012**; *28*, 3429-38.

(15) Chen XD, Li L, Liu MH. Assembly and Characterization of Ternary SV-DNA-TMPyP Complex Langmuir-Blodgett Films. *Langmuir*. **2002**; *18*, 4449-54.

(16) Chesnoy S, Huang L. Structure and Function of Lipid-DNA Complexes for Gene

Delivery. *Annu Rev Biophys Biomol Struct*. **2000**; *29*, 27-47.

(17) Chodanowski P, Stoll S. Monte Carlo Simulations of Hydrophobic Polyelectrolytes: Evidence of Complex Configurational Transitions. *J Chem Phys*. **1999**; *111*, 6069-81.

(18) Chodanowski P, Stoll S. Polyelectrolyte Adsorption on Charged Particles: Ionic Concentration and Particle Size Effects—A Monte Carlo Approach. *J Chem Phys*. **2001**; *115*, 4951-60.

(19) Cristofolini L, Berzina T, Erokhina S, Konovalov O, Erokhin V. Structural Study of the DNA Dipalmitoylphosphatidylcholine Complex at the Air-Water Interface. *Biomacromolecules*. **2007**; *8*, 2270-5.

(20) Crozier PS, Stevens MJ. Simulations of Single Grafted Polyelectrolyte Chains: ssDNA and dsDNA. *J Chem Phys*. **2003**; *118*, 3855-60.

(21) Dias R, Lindman B. *DNA Interactions with Polymers and Surfactants*. Wiley, **2008**.

(22) Dias RS, Pais AACC. Polyelectrolyte Condensation in Bulk, at Surfaces, and under Confinement. *Adv Colloid Interface Sci*. **2010**; *158*, 48-62.

(23) Dias RS, Pais AACC. Effect of the Architecture on Polyelectrolyte Adsorption and Condensation at Responsive Surfaces. *J Phys Chem B*. **2012**; *116*, 9246-54.

(24) Dias RS, Pais AACC, Linse P, Miguel MG, Lindman B. Polyion Adsorption onto Catanionic Surfaces. A Monte Carlo study. *J Phys Chem B*. **2005**; *109*, 11781-8.

(25) Dittrich M, Bottcher M, Oliveira JSL, Dobner B, Mohwald H, Brezesinski G. Physical-chemical Characterization of Novel Cationic Transfection Lipids and the Binding of Model DNA at the Air-Water Interface. *Soft Matter*. **2011**; *7*, 10162-73.

(26) Dluhy RA, Cameron DG, Mantsch HH, Mendelsohn R. Fourier-Transform Infrared Spectroscopic Studies of the Effect of Calcium-Ions on Phosphatidylserine. *Biochemistry*. **1983**; *22*, 6318-25.

(27) Dobrynin AV. Theory and Simulations of Charged Polymers: From Solution Properties to Polymeric Nanomaterials. *Curr Opin Colloid Interface Sci*. **2008**; *13*, 376-88.

(28) Doi K, Haga T, Shintaku H, Kawano S. Development of Coarse-Graining DNA Models for Single-Nucleotide Resolution Analysis. *Philos Trans R Soc Lond A*. **2010**; *368*, 2615-28.

(29) Dokka S, Toledo D, Shi XG, Castranova V, Rojanasakul Y. Oxygen Radical-Mediated Pulmonary Toxicity Induced by Some Cationic Liposomes. *Pharm Res*. **2000**; *17*, 521-5.

(30) Dubrovin EV, Staritsyn SN, Yakovenko SA, Yaminsky IV. Self-Assembly Effect During the Adsorption of Polynucleotides on Stearic Acid Langmuir-Blodgett Monolayer. *Biomacromolecules*. **2007**; *8*, 2258-61.

(31) Duguid J, Bloomfield VA, Benevides J, Thomas GJJ. Raman Spectroscopy of DNA-Metal Complexes. I. Interactions and Conformational Effects of the Divalent

Cations: Mg, Ca, Sr, Ba, Mn, Co, Ni, Cu, Pd, and Cd. *Biophys J*. **1993**; *65*, 1916-28.

(32) Erdmann M, David R, Fornof A, Gaub HE. Electrically Controlled DNA Adhesion. *Nat Nanotechnol*. **2010**; *5*, 154-9.

(33) Evans DF, Wennerström H. *The Colloidal Domain: Where Physics, Chemistry, Biology and Technology Meet*. Wiley, **1999**.

(34) Farago O, Grønbech-Jensen N. Simulation of Self-Assembly of Cationic Lipids and DNA into Structured Complexes. *J Am Chem Soc*. **2009**; *131*, 2875-81.

(35) Farago O, Grønbech-Jensen N, Pincus P. Mesoscale Computer Modeling of Lipid-DNA Complexes for Gene Therapy. *Phys Rev Lett*. **2006**; *96*, 018102.

(36) Faraudo J, Martín-Molina A. Competing Forces in the Interaction of Polyelectrolytes with Charged Interfaces. *Curr Opin Colloid Interface Sci*. **2013**; *18*, 517-23.

(37) Faraudo J, Travesset A. Phosphatidic Acid Domains in Membranes: Effect of Divalent Counterions. *Biophys J*. **2007**; *92*, 2806-18.

(38) Faraudo J, Travesset A. The Many Origins of Charge Inversion in Electrolyte Solutions: Effects of Discrete Interfacial Charges. *J Phys Chem C Nanomater Interfaces*. **2007**; *111*, 987-94.

(39) Felgner PL. Nonviral Strategies for Gene Therapy. *Sci Am*. **1997**; *276*, 102-6.

(40) Felgner PL, Gadek TR, Holm M, Roman R, Chan HW, Wenz M, Northrop JP, Ringold GM, Danielsen M. Lipofection: a Highly Efficient, Lipid-Mediated DNA-Transfection Procedure. *Proc Natl Acad Sci U S A*. **1987**; *84*, 7413-7.

(41) Filion MC, Phillips NC. Toxicity and Immunomodulatory Activity of Liposomal Vectors Formulated with Cationic Lipids toward Immune Effector Cells. *Biochim Biophys Acta*. **1997**; *1329*, 345-56.

(42) Filion MC, Phillips NC. Major limitations in the use of cationic liposomes for DNA delivery. *Int J Pharm*. **1998**; *162*, 159-70.

(43) Flach CR, Brauner JW, Mendelsohn R. Calcium Ion Interactions with Insoluble Phospholipid Monolayer Films at the A/W Interface. External Reflection-Absorption IR Studies. *Biophys J*. **1993**; *65*, 1994-2001.

(44) Frantescu A, Tonsing K, Neumann E. Interfacial Ternary Complex DNA/Ca/Lipids at Anionic Vesicle Surfaces. *Bioelectrochemistry*. **2006**; *68*, 158-70.

(45) Frenkel D, Smit B. *Understanding Molecular Simulation, From Algorithms to Applications*. Academic Press, **2002**.

(46) Friedmann T. Overcoming the Obstacles to Gene Therapy. *Sci Am*. **1997**; *276*, 96-101.

(47) Geall AJ, Blagbrough IS. Rapid and Sensitive Ethidium Bromide Fluorescence Quenching Assay of Polyamine Conjugate-DNA Interactions for the Analysis of

Lipoplex Formation in Gene Therapy. *J Pharm Biomed Anal*. **2000**; *22*, 849-59.

(48) Gelbart WM, Bruinsma RF, Pincus PA, Parsegian VA. DNA-Inspired Electrostatics. *Phys Today*. **2000**; *53*, 38-44.

(49) Gromelski S, Brezesinski G. Adsorption of DNA to Zwitterionic DMPE Monolayers Mediated by Magnesium Ions. *Phys Chem Chem Phys*. **2004**; *6*, 5551-6.

(50) Gromelski S, Brezesinski G. DNA Condensation and Interaction with Zwitterionic Phospholipids Mediated by Divalent Cations. *Langmuir*. **2006**; *22*, 6293-301.

(51) Guo W, Lee R. Efficient Gene Delivery Using Anionic Liposome-Complexed Polyplexes (LPDII). *Biosience Reports*. **2000**; *20*, 419-32.

(52) Hacein-Bey-Abina S, von Kalle C, Schmidt M, Le Deist F, Wulffraat N, McIntyre E, Radford I, Villeval JL, Fraser CC, Cavazzana-Calvo M, Fischer A. A Serious Adverse Event after Successful Gene Therapy for X-linked Severe Combined Immunodeficiency. *New Engl J Med*. **2003**; *348*, 255-6.

(53) Harrington JJ, Van Bokkelen G, Mays RW, Gustashaw K, Willard HF. Formation of De Novo Centromeres and Construction of First-generation Human Artificial Microchromosomes. *Nat Genet*. **1997**; *15*, 345-55.

(54) Humphrey W, Dalke A, Schulten K. VMD: Visual Molecular Dynamics. *J Mol Graph*. **1996**; *14*, 33-38, 27.

(55) Israelachvili J. *Intermolecular and Surface Forces*. Academic Press, **2010**.

(56) Jain NJ, Albouy PA, Langevin D. Study of Adsorbed Monolayers of a Cationic Surfactant and an Anionic Polyelectrolyte at the Air-Water Interface. *Langmuir*. **2003**; *19*, 5680-90.

(57) Jendrejack RM, de Pablo JJ, Graham MD. Stochastic Simulations of DNA in Flow: Dynamics and the Effects of Hydrodynamic Interactions. *J Chem Phys*. **2002**; *116*, 7752-9.

(58) Jiménez-Ángeles F, Odriozola G, Lozada-Cassou M. Electrolyte Distribution around Two Like-charged Rods: Their Effective Attractive Interaction and Angular Dependent Charge Reversal. *J Chem Phys*. **2006**; *124*, 134902.

(59) Jorge AF, Pereira RFP, Nunes SCC, Valente AJM, Dias RS, Pais AACC. Interpreting the Rich Behavior of Ternary DNA-PEI-Fe(III) Complexes. *Biomacromolecules*. **2014**; *15*, 478-91.

(60) Kapoor M, Burgess DJ. Physicochemical Characterization of Anionic Lipid-based Ternary siRNA Complexes. *Biochimica et Biophysica Acta - Biomembranes*. **2012**; *1818*, 1603-12.

(61) Khiati S, Pierre N, Andriamanarivo S, Grinstaff MW, Arazam N, Nallet F, Navailles L, Barthelemy P. Anionic Nucleotide-Lipids for In Vitro DNA Transfection. *Bioconjugate Chem*. **2009**; *20*, 1765-72.

(62) Kim JH, Yim SY, Oh MK, Phan MD, Shin K. Adsorption Behaviors and Structural

Transitions of Organic Cations on an Anionic Lipid Monolayer at the Air-Water Interface. *Soft Matter*. **2012**; *8*, 6504-11.

(63) Kim K, Kim C, Byun Y. Preparation of a Dipalmitoylphosphatidylcholine/Cholesterol Langmuir-Blodgett Monolayer that Suppresses Protein Adsorption. *Langmuir*. **2001**; *17*, 5066-70.

(64) Koltover I, Salditt T, Rädler JO, Safinya CR. An Inverted Hexagonal Phase of Cationic Liposome-DNA Complexes Related to DNA Release and Delivery. *Science*. **1998**; *281*, 78-81.

(65) Kulkarni VI, Shenoy VS, Dodiya SS, Rajyaguru TH, Murthy RR. Role of Calcium in Gene Delivery. *Expert Opin Drug Deliv*. **2006**; *3*, 235-45.

(66) Kundu S, Langevin D, Lee LT. Neutron Reflectivity Study of the Complexation of DNA with Lipids and Surfactants at the Surface of Water. *Langmuir*. **2008**; *24*, 12347-53.

(67) Lakowicz JR. *Principles of Fluorescence Spectroscopy*. Springer, **2006**.

(68) Lappalainen K, Jääskeläinen I, Syrjänen K, Urtti A, Syrjänen S. Comparison of Cell Proliferation and Toxicity Assays Using Two Cationic Liposomes. *Pharm Res*. **1994**; *11*, 1127-31.

(69) Larguinho M, Santos HM, Doria G, Scholz H, Baptista PV, Capelo JL. Development of a Fast and Efficient Ultrasonic-based Strategy for DNA Fragmentation. *Talanta*. **2010**; *81*, 881-6.

(70) Lasic DD. *Liposomes in Gene Delivery*. CRC Press, **1997**.

(71) Lehrmann R, Seelig J. Adsorption of Ca^{2+} and La^{3+} to Bilayer-membranes - Measurement of the Adsorption Enthalpy and Binding Constant with Titration Calorimetry. *Biochim Biophys Acta*. **1994**; *1189*, 89-95.

(72) Li S, Huang L. Nonviral gene therapy: promises and challenges. *Gene Ther*. **2000**; *7*, 31-4.

(73) Li XM, Smaby JM, Momsen MM, Brockman HL, Brown RE. Sphingomyelin Interfacial Behavior: the Impact of Changing Acyl Chain Composition. *Biophys J*. **2000**; *78*, 1921-31.

(74) Liang HJ, Harries D, Wong GCL. Polymorphism of DNA-anionic Liposome Complexes Reveals Hierarchy of Ion-Mediated Interactions. *P Natl Acad Sci Usa*. **2005**; *102*, 11173-8.

(75) Lorenz CD, Faraudo J, Travesset A. Hydrogen Bonding and Binding of Polybasic Residues with Negatively Charged Mixed Lipid Monolayers. *Langmuir*. **2008**; *24*, 1654-8.

(76) Luque-Caballero G, Martín-Molina A, Quesada-Pérez M. Polyelectrolyte Adsorption onto Like-charged Surfaces Mediated by Trivalent Counterions: A Monte Carlo Simulation Study. *J Chem Phys*. **2014**; *140*, 174701.

(77) Luque-Caballero G, Martín-Molina A, Sánchez-Treviño AY, Rodríguez-Valverde MA, Cabrerizo-Vílchez MA, Maldonado-Valderrama J. Using AFM to Probe the Complexation of DNA with Anionic Lipids Mediated by Ca^{2+}: the Role of Surface Pressure. *Soft Matter*. **2014**; *10*, 2805-15.

(78) Lv H, Zhang S, Wang B, Cui S, Yan J. Toxicity of Cationic Lipids and Cationic Polymers in Gene Delivery. *J Control Release*. **2006**; *114*, 100-9.

(79) Ma G, Allen HC. DPPC Langmuir Monolayer at the Air-Water Interface: Probing the Tail and Head Groups by Vibrational Sum Frequency Generation Spectroscopy. *Langmuir*. **2006**; *22*, 5341-9.

(80) MacDonald RC, Gorbonos A, Mornsen MM, Brockman HL. Surface Properties of Dioleoyl-sn-glycerol-3-ethylphosphocholine, a Cationic Phosphatidylcholine Transfection Agent, Alone and in Combination with Lipids or DNA. *Langmuir*. **2006**; *22*, 2770-9.

(81) Maldonado-Valderrama J, Fainerman VB, Gálvez-Ruiz MJ, Martín-Rodríguez A, Cabrerizo-Vílchez MA, Miller R. Dilatational Rheology of Beta-casein Adsorbed Layers at Liquid-Fluid Interfaces. *J Phys Chem B*. **2005**; *109*, 17608-16.

(82) Maldonado-Valderrama J, Gunning AP, Wilde PJ, Morris VJ. In Vitro Gastric Digestion of Interfacial Protein Structures: Visualisation by AFM. *Soft Matter*. **2010**; *6*, 4908-15.

(83) Marsh D. Elastic Curvature Constants of Lipid Monolayers and Bilayers. *Chem Phys Lipids*. **2006**; *144*, 146-59.

(84) Marshall J, Yew NS, Eastman SJ, Jiang C, Scheule RK, Cheng SH. Cationic Lipid-Mediated Gene Delivery to the Airways, in *Non-viral Vectors for Gene Therapy*. Academic Press, **1999**.

(85) Martín-Molina A, Luque-Caballero G, Faraudo J, Quesada-Pérez M, Maldonado-Valderrama J. Adsorption of DNA onto Anionic Lipid Surfaces. *Adv Colloid Interface Sci*. **2014**; *206*, 172-5.

(86) Martín-Molina A, Maroto-Centeno JA, Hidalgo-Álvarez R, Quesada-Pérez M. Charge Reversal in Real Colloids: Experiments, Theory and Simulations. *Colloids Surf A Physicochem Eng Asp*. **2008**; *319*, 103-8.

(87) Martín-Molina A, Rodríguez-Beas C, Faraudo J. Charge Reversal in Anionic Liposomes: Experimental Demonstration and Molecular Origin. *Phys Rev Lett*. **2010**; *104*, 168103.

(88) Martín-Molina A, Rodríguez-Beas C, Faraudo J. Effect of Calcium and Magnesium on Phosphatidylserine Membranes: Experiments and All-Atomic Simulations. *Biophys J*. **2012**; *102*, 2095-103.

(89) Martín-Molina A, Rodríguez-Beas C, Hidalgo-Álvarez R, Quesada-Pérez M. Effect of Surface Charge on Colloidal Charge Reversal. *J Phys Chem B*. **2009**; *113*, 6834-9.

(90) McLoughlin D, Dias R, Lindman B, Cardenas M, Nylander T, Dawson K, Miguel M,

Langevin D. Surface Complexation of DNA with Insoluble Monolayers. Influence of Divalent Counterions. *Langmuir*. **2005**; *21*, 1900-7.

(91) Mendelsohn R, Flach CR. Infrared Reflection–Absorption Spectrometry of Monolayer Films at the Air–Water Interface, in *The Handbook of Vibrational Spectroscopy*. Wiley, **2002**.

(92) Mendelsohn R, Mao G, Flach CR. Infrared Reflection-Absorption Spectroscopy: Principles and Applications to Lipid-Protein Interaction in Langmuir Films. *Biochim Biophys Acta*. **2010**; *1798*, 788-800.

(93) Mengistu DH, Bohinc K, May S. Binding of DNA to Zwitterionic Lipid Layers Mediated by Divalent Cations. *J Phys Chem B*. **2009**; *113*, 12277-82.

(94) Messina R. Electrostatics in Soft Matter. *J Phys Condens Matter*. **2009**; *21*, 113102.

(95) Messina R, Holm C, Kremer K. Like-charge Colloid–Polyelectrolyte Complexation. *J Chem Phys*. **2002**; *117*, 2947-60.

(96) Messina R, Holm C, Kremer K. Conformation of a Polyelectrolyte Complexed to a Like-charged Colloid. *Phys Rev E*. **2002**; *65*, 041805.

(97) Michanek A, Kristen N, Höök F, Nylander T, Sparr E. RNA and DNA Interactions with Zwitterionic and Charged Lipid Membranes — A DSC and QCM-D Study. *Biochim Biophys Acta*. **2010**; *1798*, 829-38.

(98) Michanek A, Yanez M, Wacklin H, Hughes A, Nylander T, Sparr E. RNA and DNA Association to Zwitterionic and Charged Monolayers at the Air–Liquid Interface. *Langmuir*. **2012**; *28*, 9621-33.

(99) Milani S, Bombelli FB, Berti D, Baglioni P. Nucleolipoplexes: A New Paradigm for Phospholipid Bilayer-Nucleic Acid Interactions. *J Am Chem Soc*. **2007**; *129*, 11664-5.

(100) Milani S, Karlsson G, Edwards K, Baglioni P, Berti D. Association of Polynucleotides with Nucleolipid Bilayers Driven by Molecular Recognition. *J Colloid Interface Sci*. **2011**; *363*, 232-40.

(101) Minasov G, Tereshko V, Egli M. Atomic-Resolution Crystal Structures of B-DNA Reveal Specific Influences of Divalent Metal Ions on Conformation and Packing. *J Mol Biol*. **1999**; *291*, 83-99.

(102) Morris VJ, Gunning AP. Microscopy, Microstructure and Displacement of Proteins from Interfaces: Implications for Food Quality and Digestion. *Soft Matter*. **2008**; *4*, 943-51.

(103) Mortazavi SM, Mohammadabadi MR, Khosravi-Darani K, Mozafari MR. Preparation of Liposomal Gene Therapy Vectors by a Scalable Method without Using Volatile Solvents or Detergents. *J Biotechnol*. **2007**; *129*, 604-13.

(104) Mozafari MR, Hasirci V. Mechanism of Calcium Ion Induced Multilamellar Vesicle DNA Interaction. *J Microencapsul*. **1998**; *15*, 55-65.

(105) Mozafari MR, Omri A. Importance of Divalent Cations in Nanolipoplex Gene Delivery. *J Pharm Sci*. **2007**; *96*, 1955-66.

(106) Mozafari MR, Reed CJ, Rostron C. Prospects of Anionic Nanolipoplexes in Nanotherapy: Transmission Electron Microscopy and Light Scattering Studies. *Micron*. **2007**; *38*, 787-95.

(107) Mozafari MR, Reed CJ, Rostron C. Cytotoxicity Evaluation of Anionic Nanoliposomes and Nanolipoplexes Prepared by the Heating Method without Employing Volatile Solvents and Detergents. *Pharmazie*. **2007**; *62*, 205-9.

(108) Mozafari MR, Reed CJ, Rostron C, Hasirci V. A Review of Scanning Probe Microscopy Investigations of Liposome-DNA Complexes. *J Liposome Res*. **2005**; *15*, 93-107.

(109) Mozafari MR, Zareie MH, Piskin E, Hasirci V. Formation of Supramolecular Structures by Negatively Charged Liposomes in the Presence of Nucleic Acids and Divalent Cations. *Drug Deliv*. **1998**; *5*, 135-41.

(110) Muñoz-Úbeda M, Rodríguez-Pulido A, Nogales A, Llorca O, Quesada-Pérez M, Martín-Molina A, Aicart E, Junquera E. Gene Vectors Based on DOEPC/DOPE Mixed Cationic Liposomes: A Physicochemical Study. *Soft Matter*. **2011**; *7*, 5991-6004.

(111) Muñoz-Úbeda M, Rodríguez-Pulido A, Nogales A, Martín-Molina A, Aicart E, Junquera E. Effect of Lipid Composition on the Structure and Theoretical Phase Diagrams of DC-Chol/DOPE-DNA Lipoplexes. *Biomacromolecules*. **2010**; *11*, 3332-40.

(112) Naji A, Kanduč M, Forsman J, Podgornik R. Perspective: Coulomb Fluids—Weak Coupling, Strong Coupling, in between and beyond. *J Chem Phys*. **2013**; *139*, 150901.

(113) Nandi R, Chaudhuri K, Maiti M. Effects of Ionic Strength and pH on the Binding of Sanguinarine to Deoxyribonucleic Acid. *Photochem Photobiol*. **1985**; *42*, 497-503.

(114) Netz RR. Electrostatistics of Counter-ions at and between Planar Charged Walls: From Poisson-Boltzmann to the Strong-Coupling Theory. *Eur Phys J E*. **2001**; *5*, 557-74.

(115) Nguyen TT, Shklovskii BI. Complexation of a Polyelectrolyte with Oppositely Charged Spherical Macroions: Giant Inversion of Charge. *J Chem Phys*. **2001**; *114*, 5905-16.

(116) Ohki S, Düzgünes N. Divalent Cation-Induced Interaction of Phospholipid Vesicle and Monolayer Membranes. *Biochim Biophys Acta*. **1979**; *552*, 438-49.

(117) Paiva D, Martín-Molina A, Cardoso I, Quesada-Pérez M, do Carmo Pereira M, Rocha S. The Effect of a Fluorinated Cholesterol Derivative on the Stability and Physical Properties of Cationic DNA Vectors. *Soft Matter*. **2013**; *9*, 401-9.

(118) Patil SD, Rhodes DG, Burgess DJ. Anionic Liposomal Delivery System for DNA Transfection. *AAPS J*. **2004**; *6*, 13-22.

(119) Patil SD, Rhodes DG, Burgess DJ. DNA-Based Therapeutics and DNA Delivery

Systems: A Comprehensive Review. *AAPS J*. **2005**; *7*, E61-E77.

(120) Patil SD, Rhodes DG, Burgess DJ. Biophysical Characterization of Anionic Lipoplexes. *Biochim Biophys Acta*. **2005**; *1711*, 1-11.

(121) Phillips JC, Braun R, Wang W, Gumbart J, Tajkhorshid E, Villa E, Chipot C, Skeel RD, Kale L, Schulten K. Scalable Molecular Dynamics with NAMD. *J Comput Chem*. **2005**; *26*, 1781-802.

(122) Qiao BF, Olvera de la Cruz M. Driving Force for Crystallization of Anionic Lipid Membranes Revealed by Atomistic Simulations. *J Phys Chem B*. **2013**; *117*, 5073-80.

(123) Quesada-Pérez M, Ibarra-Armenta JG, Martín-Molina A. Computer Simulations of Thermo-shrinking Polyelectrolyte Gels. *J Chem Phys*. **2011**; *135*, 094109.

(124) Quesada-Pérez M, Martín-Molina A. Monte Carlo Simulation of Thermo-responsive Charged Nanogels in Salt-Free Solutions. *Soft Matter*. **2013**; *9*, 7086-94.

(125) Quesada-Pérez M, Martín-Molina A, Hidalgo-Álvarez R. Simulation of Electric Double Layers with Multivalent Counterions: Ion Size Effect. *J Chem Phys*. **2004**; *121*, 8618-8626.

(126) Quesada-Pérez M, Ramos J, Forcada J, Martín-Molina A. Computer Simulations of Thermo-sensitive Microgels: Quantitative Comparison with Experimental Swelling Data. *J Chem Phys*. **2012**; *136*, 244903.

(127) Rädler JO, Koltover I, Salditt T, Safinya CR. Structure of DNA-Cationic Liposome Complexes: DNA Intercalation in Multilamellar Membranes in Distinct Interhelical Packing Regimes. *Science*. **1997**; *275*, 810-4.

(128) Rau DC, Parsegian VA. Direct Measurement of the Intermolecular Forces between Counterion-Condensed DNA Double Helices. Evidence for Long Range Attractive Hydration Forces. *Biophys J*. **1992**; *61*, 246-59.

(129) Reviakine I, Simon A, Brisson A. Effect of Ca^{2+} on the Morphology of Mixed DPPC-DOPS Supported Phospholipid Bilayers. *Langmuir*. **2000**; *16*, 1473-7.

(130) Rodríguez-Beas C. Propiedades físicoquímicas de complejos mesoscópicos formados por fosfolípidos y macroiones multivalentes [PhD thesis]. Universidad de Granada, **2012**.

(131) Rodríguez-Pulido A, Martín-Molina A, Rodríguez-Beas C, Llorca O, Aicart E, Junquera E. A Theoretical and Experimental Approach to the Compaction Process of DNA by Dioctadecyldimethylammonium Bromide/Zwitterionic Mixed Liposomes. *J Phys Chem B*. **2009**; *113*, 15648-61.

(132) Rodríguez-Pulido A, Ortega F, Llorca O, Aicart E, Junquera E. A Physicochemical Characterization of the Interaction between DC-Chol/DOPE Cationic Liposomes and DNA. *J Phys Chem B*. **2008**; *112*, 12555-65.

(133) Roldán-Vargas S, Barnadas-Rodriguez R, Martín-Molina A, Quesada-Pérez M, Estelrich J, Callejas-Fernandez J. Growth of Lipid Vesicle Structures: From Surface

Fractals to Mass Fractals. *Phys Rev E*. **2008**; *78*, 010902.

(134) Roldán-Vargas S, Martín-Molina A, Quesada-Pérez M, Barnadas-Rodríguez R, Estelrich J, Callejas-Fernández J. Aggregation of Liposomes Induced by Calcium: A Structural and Kinetic Study. *Phys Rev E*. **2007**; *75*, 021912.

(135) Ross M, Steinem C, Galla HJ, Janshoff A. Visualization of Chemical and Physical Properties of Calcium-Induced Domains in DPPC/DPPS Langmuir-Blodgett Layers. *Langmuir*. **2001**; *17*, 2437-45.

(136) Rzepiela AJ, Louhivuori M, Peter C, Marrink SJ. Hybrid Simulations: Combining Atomistic and Coarse-Grained Force Fields Using Virtual Sites. *Phys Chem Chem Phys*. **2011**; *13*, 10437-48.

(137) Safinya CR. Structures of Lipid–DNA Complexes: Supramolecular Assembly and Gene Delivery. *Curr Opin Struct Biol*. **2001**; *11*, 440-8.

(138) Sambrook J, Russell DW. *Molecular Cloning: A Laboratory Manual*. Cold Spring Harbor Laboratory Press, **2001**.

(139) Seijo M, Pohl M, Ulrich S, Stoll S. Dielectric Discontinuity Effects on the Adsorption of a Linear Polyelectrolyte at the Surface of a Neutral Nanoparticle. *J Chem Phys*. **2009**; *131*, 174704.

(140) Shangguan T, Cabral-Lilly D, Purandare U, Godin N, Ahl P, Janoff A, Meers P. A Novel N-acyl Phosphatidylethanolamine-Containing Delivery Vehicle for Spermine-Condensed Plasmid DNA. *Gene Ther*. **2000**; *7*, 769-83.

(141) Silva SML, Coelho LN, Malachias Â, Perez CA, Pesquero JL, Magalhães-Paniago R, de Oliveira MC. Study of the Structural Organization of Cyclodextrin–DNA Complex Loaded Anionic and pH-Sensitive Liposomes. *Chem Phys Lett*. **2011**; *506*, 66-70.

(142) Simões S, Filipe A, Faneca H, Mano M, Penacho N, Düzgünes N, Pedroso de Lima M. Cationic Liposomes for Gene Delivery. *Expert Opin Drug Deliv*. **2005**; *2*, 237-54.

(143) Sinn CG, Antonietti M, Dimova R. Binding of Calcium to Phosphatidylcholine-Phosphatidylserine Membranes. *Colloid Surface A Physicochem Eng Asp*. **2006**; *282*, 410-9.

(144) Sovago M, Wurpel GWH, Smits M, Muller M, Bonn M. Calcium-Induced Phospholipid Ordering Depends on Surface Pressure. *J Am Chem Soc*. **2007**; *129*, 11079-84.

(145) Srinivasan C, Burgess DJ. Optimization and Characterization of Anionic Lipoplexes for Gene Delivery. *J Control Release*. **2009**; *136*, 62-70.

(146) Steve ON, Carlos FL, Goundla S, Michael LK. Coarse Grain Models and the Computer Simulation of Soft Materials. *J Phys Condens Matter*. **2004**; *16*, R481-R512.

(147) Stevens MJ. Simple Simulations of DNA Condensation. *Biophys J*. **2001**; *80*,

130-9.

(148) Suga K, Tanabe T, Tomita H, Shimanouchi T, Umakoshi H. Conformational Change of Single-Stranded RNAs Induced by Liposome Binding. *Nucleic Acids Res*. **2011**; *39*, 8891-900.

(149) Sun XG, Cao EH, Zhang XY, Liu DG, Bai CL. The Divalent Cation-Induced DNA Condensation Studied by Atomic Force Microscopy and Spectra Analysis. *Inorg Chem Commun*. **2002**; *5*, 181-6.

(150) Torrie GM, Valleau JP. Electrical Double Layers. I. Monte Carlo Study of a Uniformly Charged Surface. *J Chem Phys*. **1980**; *73*, 5807-16.

(151) Tresset G, Cheong WCD, Lam YM. Role of Multivalent Cations in the Self-Assembly of Phosphiolipid-DNA Complexes. *J Phys Chem B*. **2007**; *111*, 14233-8.

(152) Tresset G, Cheong WCD, Tan YLS, Boulaire J, Lam YM. Phospholipid-Based Artificial Viruses Assembled by Multivalent Cations. *Biophys J*. **2007**; *93*, 637-44.

(153) Tresset G, Lansac Y. Long-Range Architecture of Single Lipid-Based Complex Nanoparticles with Local Hexagonal Packing. *J Phys Chem Lett*. **2011**; *2*, 41-6.

(154) Tresset G, Lansac Y, Romet-Lemonne G. Supramolecular Assemblies of Lipid-Coated Polyelectrolytes. *Langmuir*. **2012**; *28*, 5743-52.

(155) Turesson M, Labbez C, Nonat A. Calcium Mediated Polyelectrolyte Adsorption on Like-Charged Surfaces. *Langmuir*. **2011**; *27*, 13572-81.

(156) Ulrich S, Laguecir A, Stoll S. Complexation of a Weak Polyelectrolyte with a Charged Nanoparticle. Solution Properties and Polyelectrolyte Stiffness Influences. *Macromolecules*. **2005**; *38*, 8939-49.

(157) Vié V, Legardinier S, Chieze L, Le Bihan O, Qin Y, Sarkis J, Hubert JF, Renault A, Desbat B, Le Rumeur E. Specific Anchoring Modes of Two Distinct Dystrophin Rod Sub-domains Interacting in Phospholipid Langmuir Films Studied by Atomic Force Microscopy and PM-IRRAS. *Biochim Biophys Acta*. **2010**; *1798*, 1503-11.

(158) Wang L, Liang HJ, Wu JZ. Electrostatic Origins of Polyelectrolyte Adsorption: Theory and Monte Carlo Simulations. *J Chem Phys*. **2010**; *133*, 044906.

(159) Wang R, Wang ZG. Effects of Image Charges on Double Layer Structure and Forces. *J Chem Phys*. **2013**; *139*, 124702.

(160) Wang WJ, Park RY, Travesset A, Vaknin D. Ion-Specific Induced Charges at Aqueous Soft Interfaces. *Phys Rev Lett*. **2011**; *106*, 056102.

(161) Watkins HM, Vallee-Belisle A, Ricci F, Makarov DE, Paxco KW. Entropic and Electrostatic Effects on the Folding Free Energy of a Surface-Attached Biomolecule: An Experimental and Theoretical Study. *J Am Chem Soc*. **2012**; *134*, 2120-6.

(162) Willard HF. Genomics and Gene Therapy. Artificial Chromosomes Coming to Life. *Science*. **2000**; *290*, 1308-9.

(163) Woodle MC, Scaria P. Cationic Liposomes and Nucleic Acids. *Curr Opin Colloid Interface Sci*. **2001**; *6*, 78-84.

(164) Wu JC, Lin TL, Jeng US, Torikai N. Neutron Reflectivity Studies on the DNA Adsorption on Lipid Monolayers at the Air-Liquid Interface. *Physica B Condens Matter*. **2006**; *385-86*, 838-40.

(165) http://www.gwyddion.net

(166) http://cellbiology.med.unsw.edu.au/units/science/lecture0803.htm

(167) Zhong ZR, Han JF, Wan Y, Zhang ZR, Sun X. Anionic Liposomes Enhance and Prolong Adenovirus-Mediated Gene Expression in Airway Epithelia in Vitro and in Vivo. *Mol Pharm*. **2011**; *8*, 673-82.

(168) Ziebarth J, Wang YM. Coarse-Grained Molecular Dynamics Simulations of DNA Condensation by Block Copolymer and Formation of Core-Corona Structures. *J Phys Chem B*. **2010**; *114*, 6225-32.

(169) Zuzzi S, Cametti C, Onori G, Sennato S. Liposome-Induced DNA Compaction and Reentrant Condensation Investigated by Dielectric Relaxation Spectroscopy and Dynamic Light Scattering Techniques. *Phys Rev E*. **2007**; *76*, 011925.

ANNEX: LIST OF PUBLISHED PAPERS

The most of the results presented in this manuscript have already been published and we provide here the list of publications. Paper 1 is a review article about the state of the art about biophysical characterization of anionic lipoplexes, summarizing both experimental evidences and theoretical insights. This information can be found in the introduction of this thesis. Paper 2 is about the experimental characterization of the DNA complexation onto anionic phospholipid monolayers mediated by Ca^{2+}, discussed in section 4.1.1. Paper 3 tells of coarse-grain simulations about polyanion adsorption onto like-charged surfaces mediated by trivalent cations, discussed in section 4.3. Full text of the published articles must be accessed through the editorial website.

Paper 1

Title: Adsorption of DNA onto anionic lipid surfaces.

Authors: Alberto Martín Molina, Germán Luque Caballero, Jordi Faraudo, Manuel Quesada Pérez and Julia Maldonado Valderrama.

Journal: Advances in Colloid and Interface Science. **2014**, *206*, 172-185.

Abstract: Currently self-assembled DNA delivery systems composed of DNA multivalent cations and anionic lipids are considered to be promising tools for gene therapy. These systems become an alternative to traditional cationic lipid–DNA complexes because of their low cytotoxicity lipids. However, currently these nonviral gene delivery methods exhibit low transfection efficiencies. This feature is in large part

due to the poorly understood DNA complexation mechanisms at the molecular level. It is well-known that the adsorption of DNA onto likely charged lipid surfaces requires the presence of multivalent cations that act as bridges between DNA and anionic lipids. Unfortunately, the molecular mechanisms behind such adsorption phenomenon still remain unclear. Accordingly a historical background of experimental evidences related to adsorption and complexation of DNA onto anionic lipid surfaces mediated by different multivalent cations is firstly reviewed. Next, recent experiments aimed to characterise the interfacial adsorption of DNA onto a model anionic phospholipid monolayer mediated by Ca^{2+} (including AFM images) are discussed. Afterwards, modelling studies of DNA adsorption onto charged surfaces are summarized before presenting preliminary results obtained from both CG and all-atomic MD computer simulations. Our results allow us to establish the optimal conditions for cation-mediated adsorption of DNA onto negatively charged surfaces. Moreover, atomistic simulations provide an excellent framework to understand the interaction between DNA and anionic lipids in the presence of multivalent divalent cations. Accordingly, our simulation results in conjunction go beyond the macroscopic picture in which DNA is stuck to anionic membranes by using multivalent cations that forms a glue layers between them. Structural aspects of the DNA adsorption and molecular binding between the different charged groups from DNA and lipids in the presence of divalent cations are reported in the last part of the study. Although this research work is far from biomedical applications, we truly

believe that scientific advances in this line will assist, at least in part, in the rational design and development of optimal carrier systems for genes and applicable to other drugs.

Paper 2

Title: Using AFM to probe the complexation of DNA with anionic lipids mediated by Ca^{2+}: the role of surface pressure.

Authors: Germán Luque Caballero, Alberto Martín Molina, Alda Yadira Sánchez Treviño, Miguel Ángel Rodríguez Valverde, Miguel Ángel Cabrerizo Vílchez and Julia Maldonado Valderrama.

Journal: Soft Matter. **2014**, *10*, 2805-2815.

Abstract: Complexation of DNA with lipids appears currently as an alternative to classical vectors based on viruses. Still, most of the research to date, focuses on cationic lipids owing to their spontaneous complexation with DNA. Nonetheless, recent investigations have revealed that cationic lipids induce a large number of adverse effects for DNA delivery. Precisely, the lower cytotoxicity of anionic lipids accounts for their use as a promising alternative. However, the complexation of DNA with anionic lipids (mediated by cations) is still in early stages and is not yet well understood. In order to explore the molecular mechanisms underlying the complexation of anionic lipid and DNA we propose a combined methodology based on the surface pressure-area isotherms, Gibbs elasticity and AFM. These techniques allow elucidating the role of the surface pressure in the complexation and visualizing the

interfacial aggregates for the first time. We demonstrate that the DNA complexes with negatively charged model monolayers (DPPC/DPPS 4:1) only in the presence of Ca^{2+}, but is expelled at very high surface pressures. Also, according to the Gibbs elasticity plot, the complexation of lipids and DNA implies a whole fluidisation of the monolayer and a completely different phase transition map in the presence of DNA and Ca^{2+}. AFM imaging allows identification for the first time of specific morphologies associated with different packing densities. At low surface coverage, a branched net like structure is observed whereas at high surface pressure fibers formed of interfacial aggregates appear. In summary, Ca^{2+} mediates the interaction between DNA and negatively charged lipids but also the conformation of the ternary system depends on the surface pressure. Such observations are important new generic features of the interaction between DNA and anionic lipids.

Paper 3

Title: Polyelectrolyte adsorption onto like-charged surfaces mediated by trivalent counterions. A Monte Carlo simulation study.

Authors: Germán Luque Caballero, Alberto Martín Molina, and Manuel Quesada Pérez.

Abstract: Both experiments and theory have evidenced that multivalent cations can mediate the interaction between negatively charged polyelectrolytes and like-charged objects, such as anionic lipoplexes

(DNA-cation-anionic liposome complexes). In this paper, we use Monte Carlo simulations to study the electrostatic interaction responsible for the trivalent-counterion-mediated adsorption of polyelectrolytes onto a like-charged planar surface. The evaluation of the Helmholtz free energy allows us to characterize both the magnitude and the range of the interaction as a function of the polyelectrolyte charge, surface charge density, [3:1] electrolyte concentration and cation size. Both polyelectrolyte and surface charge favor the adsorption. It should be stressed, however, that the adsorption will be negligible if the surface charge density does not exceed a threshold value. The effect of the [3:1] electrolyte concentration has also been analyzed. In certain range of concentrations, the counterion-mediated attraction seems to be independent of this parameter whereas very high concentrations of salt weaken the adsorption. If the trivalent cation diameter is doubled the adsorption moderates due to the excluded volume effects. The analysis of the integrated charge density and ionic distributions suggests that a delicate balance between charge inversion and screening effects governs the polyelectrolyte adsorption onto like-charged surfaces mediated by trivalent cations.